UNIVERSITY OF CALIFORNIA, SAN DIEGO

Spinocerebellar Ataxia Type 7 is Characterized by Defects in Mitochondrial and Metabolic Function

A dissertation submitted in partial satisfaction of the requirements for the degree Doctor of Philosophy

in

Biomedical Sciences

by

Jacqueline Marie Ward

Committee in charge:

Professor Albert La Spada, Chair
Professor Eric Bennett
Professor Lawrence Goldstein
Professor Alysson Muotri
Professor Miles Wilkinson

2016

The Dissertation of Jacqueline Marie Ward is approved, and it is acceptable in quality and form for publication on microfilm and electronically:

_____

_____

_____

_____

_____

Chair

University of California, San Diego

2016

DEDICATION

This work is dedicated to my grandfather,

Dr. Wayne Ward,

the kindest person I've ever known.

His memory inspires me to be a better person daily.

TABLE OF CONTENTS

LIST OF FIGURES

LIST OF TABLES

LIST OF SUPPLEMENTAL FILES

ACKNOWLEDGEMENTS

I would like to thank my advisor, Dr. Al La Spada, for his support and guidance throughout this work and for supporting me in all of my pursuits. He welcomed me into his lab, has encouraged me in tough times, and I'm grateful for the opportunity to learn from him. Among the many skills I have honed and acquired in graduate school, I have learned the most from him about patience, persistence, and communication. I am grateful to the rest of my thesis committee too, for their encouragement and feedback. I am proud to consider myself an honorary member of Dr. Alysson Muotri's lab, without whom, this project would have been nearly impossible. I want to thank him for training me in the stem cell field and treating me as one of your own students. I would also like to thank Dr. Larry Goldstein whose role as a scientist, an advocate, and a communicator to the public has been an inspiration to me. Dr. Miles Wilkinson was the first professor I ever met at UCSD, and has been a constant source of support and encouragement for the entirety of my time here. Dr. Eric Bennett has been a great collaborator whose feedback has made me a better scientist.

I would like to thank all of the past and present members of the La Spada lab. There are too many to name, but I would especially like to thank Colleen Stoyas for her help with all of the mouse work in this project. Her collaboration in the past year has been integral in bringing this work to fruition.

Bryce Sopher has been a constant source of wisdom throughout the entirety of this work, and helped with the lentiviral system for the stem cell model. I would also like to acknowledge Helen Miranda, Amanda Mason, and Hary Frankowski for their close friendship and support both in the lab and out. Within the Muotri lab, I would like to acknowledge Earl Chailangkarn and Charlie Thomas, who taught me reprogramming and gene editing techniques, respectively. Along with Allan Acab, Cleber Trujillo, and Priscilla Negraes, they gave their time willingly to advise and assist me with the stem cell portion of this work. I am grateful to John Steele, from the Goldstein lab, who advised me in the use of flow cytometry, among many other things. I am also grateful to Ron Evans and his lab at the Salk Institute, for their efforts throughout our collaboration. The Salk Biophotonics Core was also integral in assisting with the electron microscopy portion of these studies. All of these people were not just colleagues, but friends, and helped me through everything from failed experiments to a ruptured appendix. I am forever grateful.

I have been very fortunate during my time here to have the support of a close community of friends and family. The faculty, staff, and students of the Biomedical Sciences graduate program have provided a home for me here in California. I was fortunate to start graduate school with 36 of the weirdest, smartest, best people I could imagine. My best friends and classmates, Laura Shaw, Lauren Fong, and Chris Abdullah, have become my family. On top of being fun and whip-smart, they have brought me (mostly) up to speed in my deficits of pop culture knowledge and millennial technology.

Lastly, I wouldn't be here today without the support of my 'biological' family. I was fortunate to have my aunt, Becky Blanche, nearby for many years to serve as a stand-in mom. On top of their love and support, my uncle and aunt, Larry Ward and Peggy Atwell, have given me free use of their Mammoth condo, the value of which cannot be overstated. Learning to love skiing may be my biggest accomplishment of graduate school. Lastly, I'd like to thank my mom and dad, Mimi and David Ward, and my brother, Thomas Ward, for their unwavering love. There is still no one who knows me better than my little brother. My dad (begrudgingly) supported me in moving 2000 miles across the country and loves me steadfastly. And apart from working hard in her career and for her family, my mother has taught me to pursue the things I love, even if those things are crazy 10-mile swim races. Thank you for your love and support forever and always.

Chapters 2 and 3 are original documents describing scientific work that, in part, will form the basis of a forthcoming manuscript being prepared for submission. Ward JM, Stoyas CA, Fan W, Evans R, Muotri AR, and La Spada AR. "Spinocerebellar ataxia type 7 is characterized by mitochondrial dysfunction." The dissertation author is the principal author of this work.

VITA

Education

2016 Ph.D., Biomedical Sciences
University of California, San Diego

2010 B.S., Biochemistry and Molecular Biology
Rhodes College, Memphis, TN

Publications

Ward JM, La Spada AR. Ataxin-3, DNA damage repair, and SCA3 cerebellar degeneration: on the path to parsimony? *PLoS Genet*. 11, e1004937 (2015).

Rao MK, Matsumoto Y, Richardson ME, Panneerdoss S, Bhardwaj A, **Ward JM**, Shanker S, Bettegowda A, Wilkinson MF. Hormone- and DNA demethylation-induced relief of a tissue-specific and developmentally regulated block in transcriptional elongation. *J Biol Chem*. 289(51), 35087–35101 (2014).

Ward JM, La Spada AR. Identification of the SCA21 disease gene: remaining challenges and promising opportunities. *Brain*. 137, 2626-2628 (2014).

Ward JM, La Spada AR. The expanding world of stem cell modeling of Huntington's disease: creating tools with a promising future. *Genome Med*. 4, 68 (2012).

ABSTRACT OF THE DISSERTATION

Spinocerebellar Ataxia Type 7 is Characterized by Defects in Mitochondrial and Metabolic Function

by

Jacqueline Marie Ward
Doctor of Philosophy in Biomedical Sciences
University of California, San Diego, 2016
Professor Albert La Spada, Chair

Spinocerebellar ataxia type 7 (SCA7) is an inherited neurodegenerative disease caused by a CAG/polyglutamine (polyQ) repeat expansion in the ataxin-7 gene. Adult patient clinical features include cerebellar ataxia, which leads to problems with movement and speech, and retinal degeneration, which leads to blindness. Infants and children with SCA7 present with a much more progressive and severe form of the disease that affects non-neuronal

tissues and can lead to multi-organ failure. Mitochondrial dysfunction has been implicated in the pathogenesis and progression of neurodegenerative diseases, but this is yet to be explored in SCA7. SCA7 patients, both adult and juvenile, have similar clinical features to patients with mitochondrial disease. I explored these connections in a mouse model of infantile-onset SCA7 and a novel isogenic stem cell model. I find that SCA7 exhibits mitochondrial dysfunction in both models through mitochondrial fragmentation and decreased metabolic respiration. Purkinje cells in SCA7 mice also have larger individual mitochondria when assessed at an ultrastructural level. These mice exhibit decreases in metabolic substrates, as well, but stem cell-derived neural progenitor cells (NPCs) expressing mutant ataxin-7 do not exhibit any defects in mitochondrial membrane potential (MMP), levels of reactive oxygen species (ROS), or levels of mitochondrial proteins. Ataxin-7 is an integral part of the STAGA transcriptional co-activator complex. Thus, I hypothesized that this dysfunction was caused by transcriptional dysregulation of nuclear genes important to mitochondrial function. Through an assessment of gene expression in SCA7 mice, I did not find evidence for global transcriptional dysregulation of gene sets encoding mitochondrial proteins, but I did identify a decrease in the expression of the gene encoding nicotinamide nucleotide adenylyltransferase 1 (NMNAT1), an enzyme critical for the synthesis of nicotinamide adenine dinucleotide (NAD+). Mass spectrometry analysis of NAD+ in SCA7 mice revealed a significant reduction in NAD+ levels in the cerebellum. While further studies are needed to ascertain the mechanistic

implications of these findings, this work establishes mitochondrial dysfunction as a key feature of the molecular pathology of SCA7.

Chapter 1:

Introduction

Clinical description of SCA7

Spinocerebellar ataxia type 7 (SCA7) is an inherited neurological disorder characterized by cerebellar ataxia, dysarthria, ophthalmoplegia, hyperreflexia, spasticity, and retinal degeneration[1]. Although the disease is rare, affecting ~1/500,000 individuals, SCA7 exhibits a wide geographic distribution, occurring in all major racial groups, and various ethnic populations[2,3]. SCA7 is caused by a CAG/polyglutamine (polyQ) repeat expansion in the *ATXN7* gene, and is therefore one of nine polyQ disorders. In addition, it is a member of a larger category of neurodegenerative diseases caused by toxic misfolded proteins, including the more common neurodegenerative diseases: Alzheimer's disease (AD), Parkinson's disease (PD), and amyotrophic lateral sclerosis (ALS). Adult SCA7 patients usually present with cerebellar ataxia that manifests as problems with walking, speaking, and manual dexterity. A unique feature of SCA7 that allows it to be distinguished from other ataxias is retinal degeneration. This occurs in the form of a cone-rod dystrophy, which leads to loss of visual acuity and eventually total blindness. Infant and juvenile SCA7 patients present with a much more severe form of the disease, which is discussed further below.

Polyglutamine Diseases

SCA7 is one of nine inherited disorders caused by CAG/polyQ repeats, including spinobulbar muscular atrophy (SBMA), Huntington’s disease (HD), dentatorubral-pallidoluysian atrophy (DRPLA), and five other forms of

spinocerebellar ataxia (SCA1, 2, 3, 6, & 17). One common feature of these diseases is protein misfolding due to the expanded polyQ tract. Ataxin-7, the causal disease protein in SCA7, contains an amino-terminus polyQ tract that normally ranges in size from 4 to 35 glutamines, but expands from 37 to greater than 300 glutamines in affected patients[4,5]. SCA7 is dominantly inherited and like the other polyQ repeat diseases shows genetic instability, with a tendency to large expansion of the CAG repeat tract during germ line transmission and in somatic tissues[6]. PolyQ repeat disorders, such as SCA7, thus exhibit “anticipation”, as successive generations with the disease become symptomatic at earlier ages. This is due to expansion of the repeat when transmitted from affected parent to affected child. In SCA7, this effect is more pronounced when the mutation is paternally transmitted[7].

Ataxin-7 function

Mammalian ataxin-7 is a component of the human Spt3-Taf9-Ada-Gcn5 acetyltransferase (STAGA) complex[8,9]. This is a transcriptional co-activator complex with histone acetyltransferase (HAT) and deubiquitinase (DUB) modules. Transcriptional co-activators do not bind DNA, but are recruited by other transcription factors to perform a variety of functions for target gene transcription, including chromatin remodeling[10]. Ataxin-7 plays an important role in the DUB module of STAGA by physically anchoring the ubiquitin protease subunit, Usp22, to the STAGA complex[11]. PolyQ expansions in ataxin-7 result in both increases of histone H2B ubiquitination at target

genes[12] (unpublished data, La Spada lab), and a global increase of ubiquitinated histone H2B[13]. In addition to its role in the DUB module, ataxin-7 is important for SAGA's HAT activity, which is mediated by Gcn5, the catalytic subunit of STAGA's HAT module. The La Spada lab and others have shown that there is decreased histone H3 acetylation, leading to transcriptional dysregulation, at certain genes important to photoreceptor function in SCA7 mouse models[9,14]. Taken together, STAGA functions to promote transcription through histone H2B deubiquitination and histone H3 acetylation, and ataxin-7 is a critical component of both of these activities. When ataxin-7 contains a polyQ expansion, both of these effects are diminished.

Infantile-onset SCA7

SCA7 has a very broad phenotypic spectrum. Disease progression is variable and severity correlates with the length of the polyQ expansion. The presentation can range from infants, who succumb to the disease in infancy, to adults, who display a very slow progression of symptoms. In infantile-onset forms of the disease, progression is very rapid and presents a much broader spectrum of clinical phenotypes than the adult version of the disease. Hypotonia, muscle wasting, developmental delay, and congestive heart failure have all been observed with SCA7 CAG repeats ranging from 180 to 460 (reviewed in Whitney, et al. [15]). These cases invariably result in fatal multi-organ failure[15-17].

Mouse SCA7 models

Different mouse models of SCA7 have provided better insight into the progression and pathogenesis of this disease. Previous work in the La Spada lab has generated several mouse models in which 92Q ataxin-7 is expressed throughout the entire CNS, as well as specifically in different types of cerebellar neurons and glia[18-20]. These are all varieties of transgenic expression systems with heterologous promoters. Another lab has generated a knock-in model of infantile-onset SCA7 that the La Spada lab has obtained for study[14]. These mice were generated by introducing 266 CAG repeats into the endogenous mouse *Sca7* locus, which normally contains just 5 CAG repeats. In this system, ataxin-7 is expressed at endogenous levels and in the appropriate spatiotemporal manner. Sca7$^{266Q/5Q}$ mice exhibit many of the common infantile-onset clinical features with symptom onset at 5 weeks and death at 4-5 months[14]. Though severe, these mice serve as a useful model to understand the physiological features of infantile-onset SCA7 and a key to better understand the molecular basis of the disease overall.

Induced pluripotent stem cells

In 2007, a group led by Shinya Yamanaka demonstrated that adult human somatic cells could be reprogrammed to a pluripotent state by introduction of four defined transcription factors[21]. These induced pluripotent stem cells (iPSCs) were reprogrammed from human fibroblasts and possess a differentiation potential similar to that of embryonic stem cells (ESCs)[22]. These

cells are collectively referred to as human pluripotent stem cells (hPSCs). This technology created a new way to study human, especially neurological, diseases in which the affected tissue may be prohibitive to sample. Though rodent models of neurological diseases have produced many important advances, this 'disease in a dish' provides another option to study human cells directly.

Isogenic disease models

One of the challenges of iPSC disease modeling is the sheer variability between different iPSC lines. This variability stems from several factors. When modeling genetic diseases, researchers often obtain healthy control cells from first-degree relatives of the patients so as to limit genetic variability when comparing the cells. These individuals share 50% of their DNA, but there remain substantial genetic differences between them. Additionally, there is genetic and epigenetic variability that can result from the reprogramming process. There are somatic mutations that can develop between individual fibroblast cells, either before sampling or during culturing. Moreover, the act of reprogramming fibroblasts necessitates an overhaul of the chromatin state[23]. This process leads to clonal cell line differences through the process of iPSC derivation. Lastly, the differences mentioned can lead to variable differentiation capacities of each clonal line—thereby making it difficult to compare equivalent cell types in culture without stressful purification steps. It is best to compare several clones of several individuals to ensure *bona fide*

results, but the sheer variability that results from all of these differences can cause subtle phenotypes to get lost in the noise[24]. Another option that has become popular recently due to the advent of new technology is to create isogenic gene-edited cell lines. Isogenic disease models contain identical genomes except that they differ at the edited gene of interest.

CRISPR gene editing

In response to the challenges presented by the variability described above, the advent of gene editing has been a boon for the field. Zinc finger nucleases (ZFNs) and transcription activator–like effector nucleases (TALENs) had previously been used to target specific changes to genes. But the advent of Clustered Regularly Interspaced Short Palindromic Repeats (CRISPR) technology has made it inexpensive and straightforward to perform this gene editing in a broad range of systems. CRISPRs are repetitive sequences that serve as genomic anchors for foreign DNA and thus provide adaptive immunity for many forms of bacteria and archaea[25]. The RNA generated from the CRISPR gene serves to guide CRISPR-associated (Cas) proteins to complementary DNA that then induce double strand breaks (DSBs) at that site. Recently, engineered versions of the CRISPR system that utilize a guide RNA complementary to a specific genomic site, have been used in mammalian systems to induce targeted genome editing[26,27]. Targeted gene editing can lead to several outcomes. If a donor template is provided in the editing process, the DSB can be resolved through homologous recombination

(HR) with a change of a single or a small tract of nucleotide(s). However, the simplest way of utilizing this technology is to induce DSBs and rely on non-homologous end joining (NHEJ) for repair. In these cases, the DSB is repaired, but often with minor mistakes in the form of small insertions or deletions (indels) in the DNA. When these indels lead to frame shifts in the open reading frame, this frequently results in premature stop codons further downstream in the transcript. When these indels occur in both alleles, they lead to a functional knockout of the protein. In the field of iPSC genetic disease modeling, DSB resolution by either HR or NHEJ may be useful depending on the application.

Neural progenitor cells as a model of neurodegeneration

Already iPSC-derived cells have been used to model many neurological diseases, and even complex diseases such as schizophrenia exhibit disease-relevant phenotypes[28]. An important step in all of these studies is differentiating the iPSCs into the cell type of interest. Differentiation protocols have been developed for a number of specific neural cell types[29]. Neural progenitor cells (NPCs) are multipotent stem cells that are able to differentiate into any cell of the neural lineage *in vivo*. These cells were first isolated from the mouse brain[30,31], but have more recently been derived from hPSCs[32]. hPSC-derived neural cells grown *in vitro* exhibit gene expression patterns and functionality similar to cells in the early stage of fetal development[33]. This has sometimes made it challenging to model diseases of aging in a dish[34]. Despite

these challenges, NPCs have been shown to recapitulate disease-specific phenotypes associated with a number of adult-onset neurodegenerative diseases[35-37]. There are several contributing factors that could lead to these observations. Detrimental effects may occur throughout a lifetime, but do not become pathogenic until there are enough other critical hits encountered through the process of aging. Furthermore, growing these cells in culture is inherently quite different from their native environment, and could serve as an artificial acceleration of aging *in vitro.* Whereas adult-onset SCA7 has a clinical progression more typical of a neurodegenerative disease, infantile- and juvenile-onset SCA7 is so severe that it could be considered a neurodevelopmental disorder. These patients present with symptoms very early, and in a wide variety of cell and tissue types. Thus I hypothesize that NPCs will be a particularly relevant cell model for understanding more about this class of SCA7 pathology in a human neural system.

Polyglutamine diseases and mitochondrial dysfunction

Mitochondria have been implicated in a vast array of neurodegenerative diseases[38]. The cellular energy demand of neurons is very high, and they rely almost exclusively on oxidative phosphorylation, as glycolytic ability is limited. Specifically in the polyQ field, the bulk of research connecting mitochondrial dysfunction to these diseases has focused on Huntington's disease (HD). Mitochondrial dysfunction, including increased lactate[39], decreased activity of electron transport chain (ETC) complexes II and III[40], and mitochondrial

depolarization[41] has been observed in HD cell culture models, animal models, and patient samples (reviewed in Lin and Beal [38]). The La Spada lab and others have linked this dysfunction to PPAR-γ coactivator-1α (PGC-1α)[42-44]. PGC-1α is a master regulator of transcriptional programs that promote mitochondrial biogenesis and function. The disruption of the PGC-1α transcriptional program thereby connects mitochondrial dysfunction to nuclear transcriptional dysregulation in HD. In SBMA as well, mitochondrial dysfunction has been associated with the disease in different model systems[35,45]. In fact, there is evidence that the androgen receptor protein interacts with PGC-1α in the nucleus, as well as localizes to the mitochondria[45]. Many of the proteins affected by polyQ expansion are localized to the nucleus and play a role in transcriptional regulation[46]. It makes sense then that disruption in mitochondrial function might be linked directly to nuclear transcription in these diseases.

Ataxia and mitochondrial dysfunction

Of the inherited forms of spinocerebellar ataxia, mitochondrial impairment has been implicated in several. SCA3, also known as Machado-Joseph disease, has been the mostly widely characterized in respect to mitochondrial dysfunction. Models of SCA3 have reduced activity of ETC complex II, similar to HD, as well as increased mutations in mitochondrial DNA (mtDNA)[47,48]. Mitochondrial impairments in morphology and function have also recently been reported to contribute to SCA1 progression[49]. In SCA12, the

underlying mutation has been shown to increase expression of the gene *Pp2r2b,* which is associated with mitochondrial dysfunction and increased oxidative stress[50]. And lastly, earlier age of onset in SCA2 has been associated with the presence of a single nucleotide polymorphism (SNP) in the gene for mitochondrial complex I (10398G)[51]. Of other types of ataxia, Freidreich's ataxia (FA) is the most common. FA is considered a mitochondrial disease in its own right due to the inherited mutation leading to reduced expression of the frataxin protein. Frataxin localizes to the mitochondria and is thought to function in mitochondria iron transport and respiration[52,53].

SCA7 similarity to mitochondrial disease

Mitochondrial diseases are a heterogeneous group of genetic diseases. They are caused by mutations in nuclear- or mitochondrial-encoded genes whose protein products function in the mitochondria. Despite the fact that this set of diseases is caused by a variety of mutations in many genes, there is a similarity in clinical presentation as the overall dysfunction of mitochondria is more evident in some tissues than others[54]. Muscle and brain dysfunction are common, as those tissues tend to have the highest energy demands for oxidative metabolism. Ataxia itself is a common trait[55]. Hypotonia, muscle weakness, ophthalmoplegia, and ptosis are also highly prevalent clinical traits[55]. All of these phenotypes are also present in infantile-onset, or in some cases, adult-onset SCA7. Furthermore, there have been several clinical reports of mitochondrial abnormalities in liver and skeletal muscle biopsies

from SCA7 patients[56-59]. Surprisingly, other than these small descriptive studies, there has been little indication in the literature that mitochondria are involved in SCA7 pathogenesis.

Questions and goals of the thesis

The hypothesis that led to the work herein is that mitochondrial dysfunction is a key feature of SCA7 pathogenesis. Despite the lack of studies connecting these dots, I felt that the overwhelming prevalence of mitochondrial dysfunction in other neurodegenerative disease, in conjunction with the similarity of SCA7 clinical features to other mitochondrial diseases was worthy of investigation. I was most interested in pursuing this hypothesis in models of the infantile-onset form of SCA7, as this multisystem disease would likely yield the most obvious connection to mitochondrial dysfunction. My first line of investigation was a characterization of mitochondrial structure and metabolic deficits in the infantile-onset SCA7$^{266Q/5Q}$ knock-in mouse model, described in chapter 2. I followed this with generation and characterization of a novel stem cell model of SCA7, and an analysis of mitochondrial structure and metabolic respiration, described in chapter 3. One of my other goals was to investigate the mechanism of how mutant ataxin-7 might be related to mitochondrial dysfunction. My hypothesis was that, similar to HD, mitochondrial genes would be downregulated in the cerebellum of SCA7 mice. I addressed this through a bioinformatics approach, described in chapter 4, but this will ultimately be the goal of follow up studies. With this work, I establish and characterize the

connection between SCA7 and mitochondrial dysfunction. My findings have opened the door to further detailed studies of the mechanism behind this link.

Chapter 2:

Mitochondrial Dysfunction in an Infantile-onset SCA7 Mouse Model

Abstract

I used a knock-in mouse model to characterize mitochondrial dysfunction that occurs in infantile-onset spinocerebellar ataxia type 7 (SCA7). SCA7 exhibits similar clinical features to mitochondrial diseases and infantile-onset SCA7 patients suffer from major deficits in energetically demanding tissues. I found that these mice have decreased mitochondrial content and fragmented mitochondrial networks in their cerebellar Purkinje cells (PCs). At an ultrastructural level, the individual mitochondria are increased in size, likely as compensation for decreased network length. These mice have a significant decrease in oxygen consumption and indicators of reduced metabolic substrates. Lastly, adenosine triphosphate (ATP), the energetic output of metabolic respiration, may be reduced in the cerebellum of SCA7 mice. These data demonstrate that mitochondrial dysfunction is a novel feature associated with SCA7 pathogenesis.

2.1 Introduction

Spinocerebellar ataxia type 7 (SCA7) is an inherited neurological disorder characterized by cerebellar ataxia, dysarthria, ophthalmoplegia, hyperreflexia, spasticity, and retinal degeneration[1]. SCA7 is caused by a CAG/polyglutamine (polyQ) repeat expansion in the *ATXN7* gene. It belongs to a family of 8 other neurodegenerative disorders caused by this type of dynamic mutation. SCA7 has a very broad phenotypic spectrum. Disease progression is highly variable and

based on the length of the polyQ expansion. Ataxin-7 is expressed ubiquitously[60], but the adult-onset form of SCA7 specifically causes dysfunction in certain neuronal populations, including Purkinje cells (PCs) and retinal photoreceptors.

In infantile-onset SCA7, progression is very rapid and presents a much broader spectrum of clinical phenotypes than the adult version of the disease. Hypotonia, muscle wasting, developmental delay, and congestive heart failure have all been observed in patients with CAG repeats larger than 180 (reviewed in Whitney, et al. [15]). These cases invariably result in fatal multi-organ failure[15-17]. Due to clinical similarities, metabolic disorders or lipid storage diseases are often suspected in cases of infantile SCA7[16,61]. In fact, mitochondrial disorders that have a high prevalence of muscle and brain dysfunction due to their high energy demands share many features with infantile SCA7. Even the adult form of SCA7 can phenocopy mitochondrial encephalopathies, as these diseases often affect similar cell types[61]. Apart from small-scale case reports indicating abnormal mitochondria in SCA7 patient skeletal muscle or liver tissue[56-59], there has not been a thorough investigation of mitochondrial involvement in SCA7.

The La Spada lab has obtained a knock-in mouse model of infantile-onset SCA7[14]. In this system, ataxin-7 is expressed at endogenous levels and in the appropriate spatio-temporal manner. These mice were generated by introducing 266 CAG repeats into the endogenous mouse *Sca7* locus, which normally contains just 5 CAG repeats. Sca7$^{266Q/5Q}$ mice exhibit many of the common infantile-onset clinical features, including weight loss, ptosis, and muscle wasting,

among others[14]. Due to the severity and multi-system effects modeled in these mice, they are the most suitable physiological model for studying the connection between SCA7 and metabolic and mitochondrial dysfunction.

To get a broad view of mitochondrial defects, I evaluated mitochondrial structure morphology in PCs of SCA7 mice. I found that these mitochondrial networks are more fragmented, an effect that has been associated with bioenergetic defects. Through ultrastructure analysis, I also evaluated the morphology of individual mitochondria. Interestingly, it seems like there are larger mitochondria in SCA7 PCs, which I hypothesize is a compensatory mechanism for an overall decrease in the total mitochondrial content. Furthermore, I find that these SCA7 mice have a dramatically reduced oxygen consumption rate. To my knowledge, this is a novel assessment in the field of ataxia. I also found that there is a decrease in levels of metabolic substrates as these mice have diminished fat content and lower blood glucose levels. These are all novel phenotypes associated with SCA7. While this work establishes the connection between SCA7 and mitochondrial dysfunction, I complement this with studies performed in a human model of the disease, as described in chapter 3.

2.2 Results

SCA7 shares clinical features with mitochondrial disease

Recently, the clinical commonalities observed amongst genetically different mitochondrial diseases have been aggregated into a novel database and bioinformatics tool that ranks the prevalence of certain symptoms[55]. The most common mitochondrial disease traits include features that are often observed in patients with SCA7, especially infantile-onset forms of the disease (Figure 2.1a). This bioinformatics tool uses a machine-learning algorithm to cluster diseases together based on clinical features. SCA7 clusters very closely with 3-methylglutaconic aciduria type III (MGCA3) (Figure 2.1b), which is caused by a mutation in OPA3, an integral component of the mitochondrial outer membrane[62]. Other optic atrophies caused by mitochondrial mutations (autosomal dominant optic atrophy; Leber's optic atrophy) also cluster very closely with SCA7 (Figure 2.1b). Additionally, this tool assigns a "mito-score" on a scale of 0-100, with a score above 50 indicating more overlap with mitochondrial diseases than non-mitochondrial diseases[55]. SCA7 scores 93.

SCA7 KI mice characterization

To understand more about overall metabolic and mitochondrial defects in SCA7, the La Spada lab obtained SCA7$^{266Q/5Q}$ mice, a model of infantile SCA7[14]. These mice were reported to contain a 266 CAG repeat expansion in the mouse *Sca7* locus[14]. Upon receipt in the lab, these mice exhibited a more severe phenotype than reported. The lifespan of these mice was 10-12 weeks, as opposed to the 16-20 weeks reported[14] (Figure 2.2a). Symptom onset was

consistent at 5-6 weeks (35-45 days), based on body weight (Figure 2.2b). Through extensive genotyping efforts by others in the lab, it is estimated that the mutation expanded (or originated in an alternate mouse line) to ~350 CAGs (data not shown). Hereafter, I will refer to these mice simply as “SCA7 mice” and the mice reported previously as $SCA7^{266Q/5Q}$ mice.

Mitochondrial content and network length is reduced in SCA7 PCs

Within the cerebellum, PCs are highly vulnerable to dysfunction and degeneration in SCA7. PCs are some of the largest neurons in the CNS and have highly branching dendrites. Due to this unique cellular morphology, PCs have also been shown to be highly susceptible to mitochondrial defects[63]. Thus, they are the ideal starting point to assess SCA7-associated mitochondrial dysfunction. I began by analyzing total mitochondrial content in the soma of PCs from SCA7 mice (example image shown in Figure 2.3a). Using an ImageJ morphometry plugin, I quantified the mitochondrial content within the soma, as well as skeletonized the Tom20 immunofluorescence signal to quantify mitochondrial network morphology[64]. I found that there was a significant decrease in total mitochondria based on the percentage of Tom20 immunofluorescence to the overall cell body (Figure 2.3b). There was also a slight, albeit significant, decrease in average length in the mitochondrial network length in the SCA7 PCs (Figure 2.3c). Example skeletonized images of both extremes: high average length (14 um) and low average length (5 um) are shown

in Figure 2.3d, although the average difference between the WT and SCA7 was considerably more subtle. This decrease in average length reflected a more fragmented mitochondrial network, which has been associated with lower respiratory activity and bioenergetic defects[65,66].

SCA7 PCs have larger mitochondria

The analysis of the structure of the mitochondrial network indicated differences in morphology on a network-level scale. I was also interested in analyzing the morphology of individual mitochondria on a smaller, organelle-level scale. I performed transmission electron microscopy (TEM) analysis on ultrathin sections of cerebellum from SCA7 and WT mice. I was easily able to identify mitochondria in PC soma (Figure 2.4a and 2.4b) and dendrites (Figure 2.4c and 2.4d). TEM analysis is best utilized for interrogating organelle morphology and structure, but I also noticed during analysis that the images of SCA7 soma seemed to contain fewer total individual mitochondria (indicated by arrowheads in Figure 2.4). This qualitative observation agrees with the decrease in mitochondrial content observed through the immunofluorescence imaging experiments. I quantified parameters of size (perimeter, area, and feret diameter) and shape (circularity and aspect ratio) for mitochondria separately from the soma and dendrites. I found that the mitochondria from both SCA7 PC soma and dendrites were overall larger in size (Figures 2.5a-2.5f), though the dendritic mitochondria seemed to exhibit a bigger, albeit more variable, difference.

Mitochondria were equivalent between WT and SCA7 in shape measurements both in PC soma and dendrites (Figure 2.5g-2.5j).

SCA7 mice have reduced metabolic rate

Since fragmented mitochondrial networks have been associated with low respiratory activity and bioenergetic defects[65,66], I sought to assess the overall metabolic physiology of these mice. I began with the broadest evaluation of metabolic dysfunction by submitting the SCA7 mice to indirect calorimetric measurement to assess oxygen consumption rate (OCR), as oxygen is a necessary component of aerobic respiration. I found that the SCA7 mice exhibited an overall reduction in OCR (Figure 2.6a), which is significantly reduced during both active (dark) and inactive (light) periods (Figure 2.6b). With this analysis, I also monitored CO_2 output to assess the respiratory exchange ratio (RER [VCO_2/VO_2]). The RER reflects the preference for carbohydrates or fat as a metabolic substrate. The SCA7 mice had a reduced RER (Figure 2.6c and 2.6d) indicating more fat being metabolized in addition to an overall reduction in metabolic rate.

SCA7 mice have reduced glucose levels and fat content

With a reduced metabolic rate, I investigated other indicators of abnormal metabolism in the SCA7 mice. I noticed in the process of dissection that the

SCA7 mice had diminished fat depots compared to their wild type littermates (Figure 2.7a). The inguinal white adipose tissue (iWAT) of the SCA7 mice was significantly decreased in proportion to overall body weight (BW) throughout the disease course (Figure 2.7a and 2.7b). I also assessed fasting blood glucose levels through tail venipuncture to determine utilization of carbohydrates. The SCA7 mice had significantly decreased blood glucose levels (Figure 2.7c). Taken together, the decrease in adipose tissue and blood glucose indicate an increased utilization of metabolic substrates. Coupled with the indirect calorimetry experiments, these results indicate an overall disruption of metabolic respiration. The overall goal of metabolic respiration is to catabolize substrates in the form of carbohydrates, fats, and proteins into adenosine triphosphate (ATP), a usable form of cellular energy. I next evaluated whether there was a coordinate reduction in energy output in the form of ATP.

SCA7 have slightly reduced ATP content in cerebellum

To see if there was a coordinate defect in metabolic output, I measured ATP levels from cerebellar extract of SCA7 and control mice. The cerebellum is both the primary region of degeneration in SCA7 and a highly metabolically active tissue, making this a prime target tissue for uncovering defects in energy metabolism. I observed a decrease in the ATP/ADP ratio as well as total ATP content, though neither was statistically significant ($p=0.15$, 0.08, respectively) (Figure 2.7d and 2.7e). I am in the process of refining and continuing these

studies to determine whether ATP content is reduced more significantly in other tissues. After all, while these mice suffer from neuronal deficits, they also have marked dysfunction in other tissues, so reduced ATP may be more evident in other metabolic tissues. If this is the case, as my initial studies in the cerebellum indicate, it reflects an overall defect in efficient energy metabolism.

2.3 Discussion

Mitochondrial dysfunction has emerged as a salient feature of many neurodegenerative diseases[38,67]. In fact, the human central nervous system alone accounts for 20% of energy metabolized[68]. Outside of their main function of energy production, mitochondria also play a role in apoptosis, calcium storage, and metabolism of hormones and neurotransmitters. It logically follows then that their maintenance and normal function would be intricately intertwined with normal neuronal function. Despite this emerging importance, the role of mitochondria in SCA7 had not been investigated. I chose to initiate this line of investigation in a mouse model of infantile-onset SCA7.

I assessed mitochondrial structure as an indication of mitochondrial health. While mitochondria are dynamic organelles that constantly undergo fission and fusion, a tip on the balance one way or the other can result in bioenergetic defects[65,69]. I examined both the overall structure of the cellular mitochondrial network, and the morphology of individual mitochondrial

ultrastructure. I found a decrease in total mitochondrial content, along with more fragmented mitochondrial networks in SCA7 PCs. This was coupled with an overall increase in size of individual mitochondria as assessed by their ultrastructure. If the mitochondria are not able to fuse properly (or alternatively, too much fission is occurring), the individual mitochondria may compensate by growing larger in an attempt to increase the capability for metabolic respiration. TEM, by necessity, only represents a cross section of the cell. Scanning electron microscopy (SEM) would give a better picture of the 3D nature of the individual mitochondria, which I plan to perform in future experiments.

I did not pursue experiments aimed to specifically interrogate or rescue excessive fission or impaired fusion, so at this point I cannot definitively argue a defect in one over another. The components of mitochondrial fission and fusion have been well characterized. Fusion is mediated by Mfn1, Mfn2 (outer membrane), and Opa1 (inner membrane), while fission is mediated primarily by Drp1. It would be very interesting to cross the SCA7 mice with Opa1 overexpressing mice[70], or alternatively Drp1 heterozygote knockout mice[71] (homozygotes are embryonic lethal) to further understand the effects of these processes and potentially rescue SCA7-associated mitochondrial deficits.

It is evident from this work that these mice have a gross defect in energy metabolism. They consume less oxygen and rely more on fat as a metabolic substrate than carbohydrates. I have not seen reports of this effect occurring in any other mouse models of ataxia. To my knowledge, this type of defect has only

been observed in a handful of neurodegenerative disease models. Two mouse models that have shown exacerbated Alzheimer's disease phenotypes (PITRM deficiency; DNA Pol β deficiency) have also shown decreased metabolic rates[72,73]. Interestingly, HD mouse models have either shown no difference in basal metabolic rate or an increase in oxygen consumption under fasting conditions[42,74]. Studies on the effects of aged mice have also indicated that there was a trend towards a decrease in metabolic rate in old age, but not significantly[75]. While impaired energy metabolism may not be wholly unique to SCA7, the effect is dramatic in these mice—justifying a continued analysis of mitochondrial dysfunction.

The entire purpose of metabolic respiration is the breakdown of substrates to produce ATP, the energetic currency of the cell. I found trends towards decreased total amounts of ATP and decreased ATP/ADP ratio. Though not statistically significant, this result could indicate impairment in metabolic respiration specifically in the brain whereas the metabolic rate and glucose/fat content observations provide a picture of whole body metabolism.

Recently, evidence has mounted that mitochondrial dysfunction may be a cause of neurodegeneration, not just an effect[65]. Assaults on mitochondria, either through treatment with mitochondrial toxins such as rotenone or 3-nitroproprionic acid (3-NP), or through genetic mutation of mitochondrial genes results in neurodegenerative effects[76-79]. Since the mitochondrial content and morphology experiments in cerebellar PCs were all performed in symptomatic mice, I cannot

decouple the observed mitochondrial defects from the neurodegenerative process. By assessing other non-neuronal metabolic defects I hoped to determine whether these mitochondrial effects were specific to the affected cells in the brain, or were part of a larger picture of mitochondrial dysfunction. Since the mice have an overall decreased metabolic rate, and a reduction in other metabolic parameters, concomitant with neurodegenerative symptoms, I believe that the mitochondrial deficit is either an independent effect or could potentially even lead to the neuronal dysfunction.

The cerebellum (especially the PCs within) and retina have high energy demands so it could be that these cells are the most vulnerable in suffering from mitochondrial dysfunction in adult SCA7 patients. It is very telling that the infantile-onset SCA7 patients also suffer from deficits in other energetically demanding tissues (heart, skeletal muscle). In MRIs or post-mortem studies of brains from these infantile SCA7 cases, some reports indicate cerebellar atrophy[15,17], while others have indicated largely normal brain structure[80]. The ataxin-7 protein is expressed ubiquitously throughout the brain, but also widely in peripheral tissues as well[60]. It is possible that the multisystem effects observed in these infantile-onset cases of SCA7 are independent of the neurological dysfunction, and instead due to toxicity of the mutant protein in non-neuronal tissue. I hope to further investigate these defects more definitively by looking at mitochondrial structure in more tissue types and younger mice.

With these results, I have taken the first step towards assessing mitochondrial dysfunction in SCA7. Further work will be necessary to establish the cause and effect dynamic of neurodegeneration vs. mitochondrial dysfunction. I also hope to broaden our understanding of the defect in mitochondrial dynamics by augmenting and/or depleting the fission and fusion machinery. In the next chapter I will describe my efforts to establish a novel human stem cell model of SCA7 and interrogate these effects in another system.

2.4 Experimental procedures

MitoDB analysis

SCA7 was queried against the MitoDB database[55] (www.mitodb.com) with incidence of 100% ataxia, 83% visual acuity, 30% visual impairment, 69% optic atrophy, 43% pigmentary retinopathy, 70% ophthalmoplegia, 50% pyramidal signs, 50% extrapyramidal symptoms, 50% spasticity, and 25% hearing loss.

Immunohistochemistry

SCA7 knock-in mice were obtained from the Zoghbi lab. All animal experimentation adhered to NIH guidelines and was approved by and performed in accordance with the University of California San Diego Institutional Animal Care and Use Committee. Ten-week-old mice were deeply anesthetized with isoflurane and perfused with 4% PFA. Brains were dissected, immersed in 30% sucrose, and cut on a vibrating microtome into 30 um sagittal sections. These

free floating sections were incubated in blocking solution containing 10% goat serum, 1% BSA, and 0.3% Triton X-100 for 1 hour at room temperature. Primary antibodies, anti-Calbindin antibody (Sigma-Aldrich, C9848) and anti-Tom20 (Santa Cruz, sc11415), were diluted 1:500 in blocking solution and sections were incubated overnight at 4°C. After 2 washes with PBS, sections were incubated with anti-mouse superclonal AlexaFluor 488 and anti-rabbit AlexaFluor 555 (Fisher) at 1:500 and 1:250 dilutions, respectively, for 1 hour at room temperature. Sections were then washed one time in PBS, incubated in PBS supplemented with 1:5000 Hoechst 33342 for 10 minutes at room temperature, and washed again before mounting on glass slides with Prolong Gold anti-fade reagent (Life Technologies). Images were taken on a fluorescence microscope (Z1 Axio Observer Apotome, Zeiss) at 40x magnification in a single plane. Equivalent numbers of fields were captured for each condition. Each PC soma was manually encircled based on Calbindin staining and morphometry parameters were quantified by an ImageJ plugin, as described previously[64]. Mitochondrial area was calculated as a percentage of the soma area. Average mitochondrial length was quantified in microns.

Electron microscopy and mitochondrial ultrastructure

Eight and half-week-old mice were deeply anesthetized with isoflurane and perfused with a fixative solution made of 2% PFA and 2.5% glutaraldehyde in PBS. Brains were dissected and placed in fixative solution overnight at 4°C.

The brains were then cut into 50 um sagittal sections on a vibratome. Ultrathin sections were prepared from equivalent regions within the cerebellum and imaged at 4000x on a Carl Zeiss Libra 120kV PLUS Energy Filtered Transmission Electron Microscope at the Salk Institute Biophotonics Core. Images from soma and dendrites were grouped together and intact mitochondria within each structure were identified by double membrane and presence of cristae. Individual mitochondria were traced in ImageJ and measured for area, perimeter, feret diameter (caliper length), circularity ($4\pi A/p^2$), and aspect ratio (major axis/minor axis).

Indirect calorimetry in metabolic cages

Female 8-week-old mice were housed in the Oxymax/CLAMS metabolic cage system from Columbus Instruments for 4 days with ad libitum access to food and water on a 12-hour light/dark cycle. VO2 and RER were measured by the Oxymax system after a 24-hour acclimation period.

Glucose and iWAT dissection

Glucose was measured using the NovaMAX glucometer system via tail venipuncture after 6 hours of fasting. Mice were sacrificed either by exposure to a lethal dose of CO_2 or isoflurane anesthesia followed by decapitation. The iWAT

from the right side of each mouse was surgically excised and weighed as described previously[81].

ATP analysis

Cerebella from eight and a half-week-old female mice was dissected and homogenized in 450 uL PBS with 2 mM ethylenediaminetetraacetic acid (EDTA) with a handheld pellet pestle motor. Fifty uL of 50% trichloroacetic acid (TCA) was added to each sample and incubated on ice for 15 minutes. Lysate was then centrifuged at 10000 x *g* for 30 minutes at 4°C and the TCA extract (supernatant) was transferred to a 13-mm glass test tube. Six volumes of diethyl ether were added to each sample, vortexed, and the upper ether phase was aspirated. This process was repeated 3 more times. The aqueous sample was transferred to an eppendorf tube and left in the fume hood for 30 minutes for ether evaporation. The ATP and ADP present in TCA extracts from the cerebellum of 8.5-week-old female mice were then quantitatively converted to fluorescent 1,N^6-ethenoadenine derivatives as previously described[82].

Acknowledgements

Chapter 2, in part, will be part of a forthcoming manuscript being prepared for submission. Ward JM, Stoyas CA, Fan W, Evans R, Muotri AR, and La Spada AR. The dissertation author is the principal author of this work.

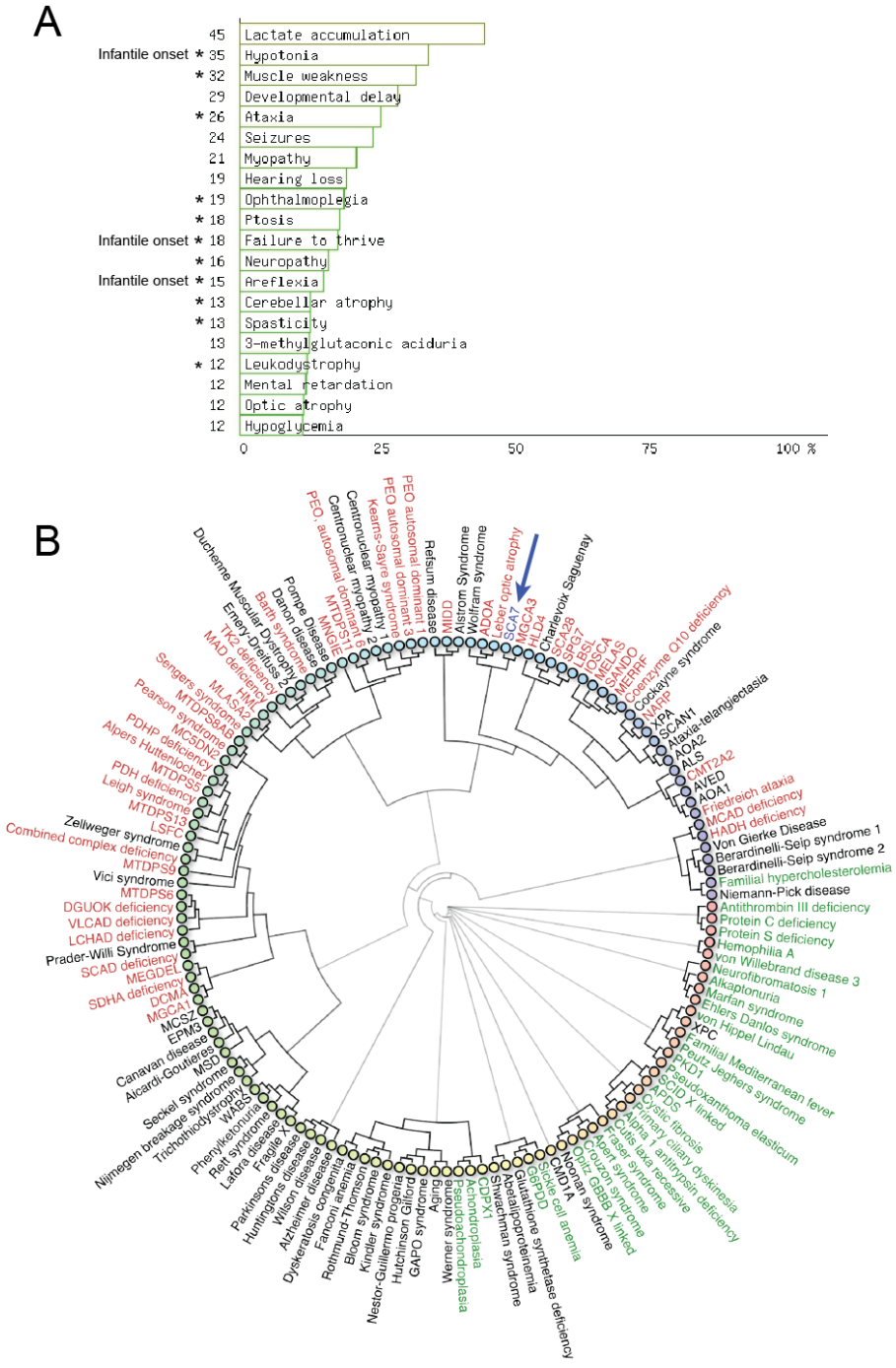

Figure 2.1 SCA7 has clinical features similar to mitochondrial diseases. A The top 20 traits seen in mitochondrial diseases from www.mitodb.com out of more than 600 total traits. Overlapping symptoms with SCA7 are marked with an asterisk. Symptoms prominent in infantile-onset SCA7 are indicated. **B** Circular hierarchical dendrogram indicates diseases with similar symptoms. Diseases in red are known to have mitochondrial cause or involvement, green is non-mitochondrial, black is unknown, and blue with arrow is SCA7.

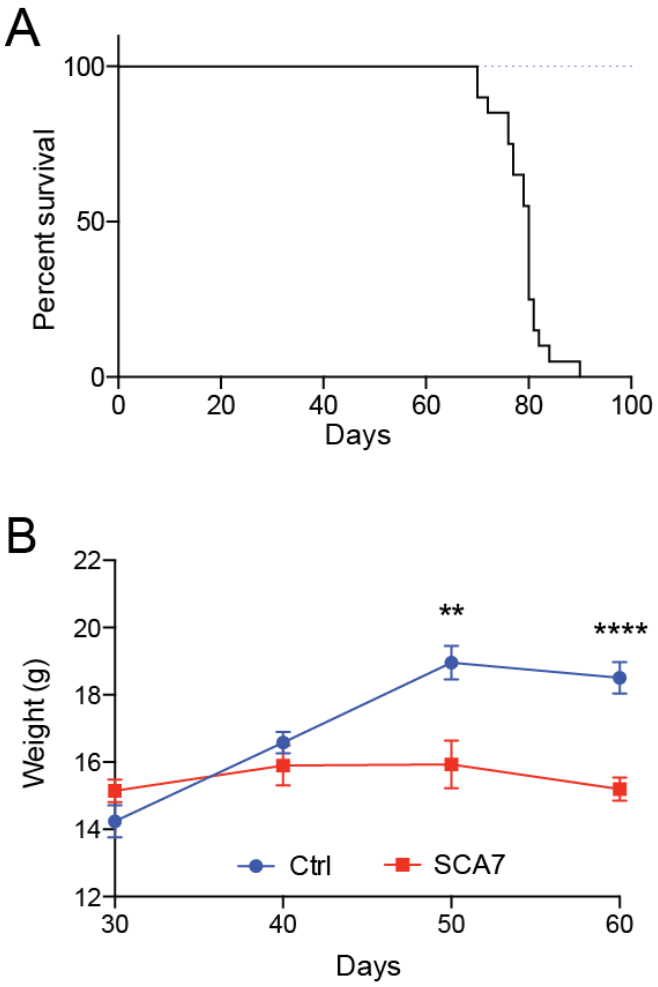

Figure 2.2 SCA7 mice have decreased survival and body weight. A Kaplan-Meier survival curve indicates a median survival time of 80 days for SCA7 KI mice. Dotted line indicates survival of WT mice. n = 20. **B** Body weights of SCA7 and WT mice at different time points. Data are represented as mean ± SEM, *n* ≥ 5 mice per genotype, **P≤0.001, ****P≤0.0001.

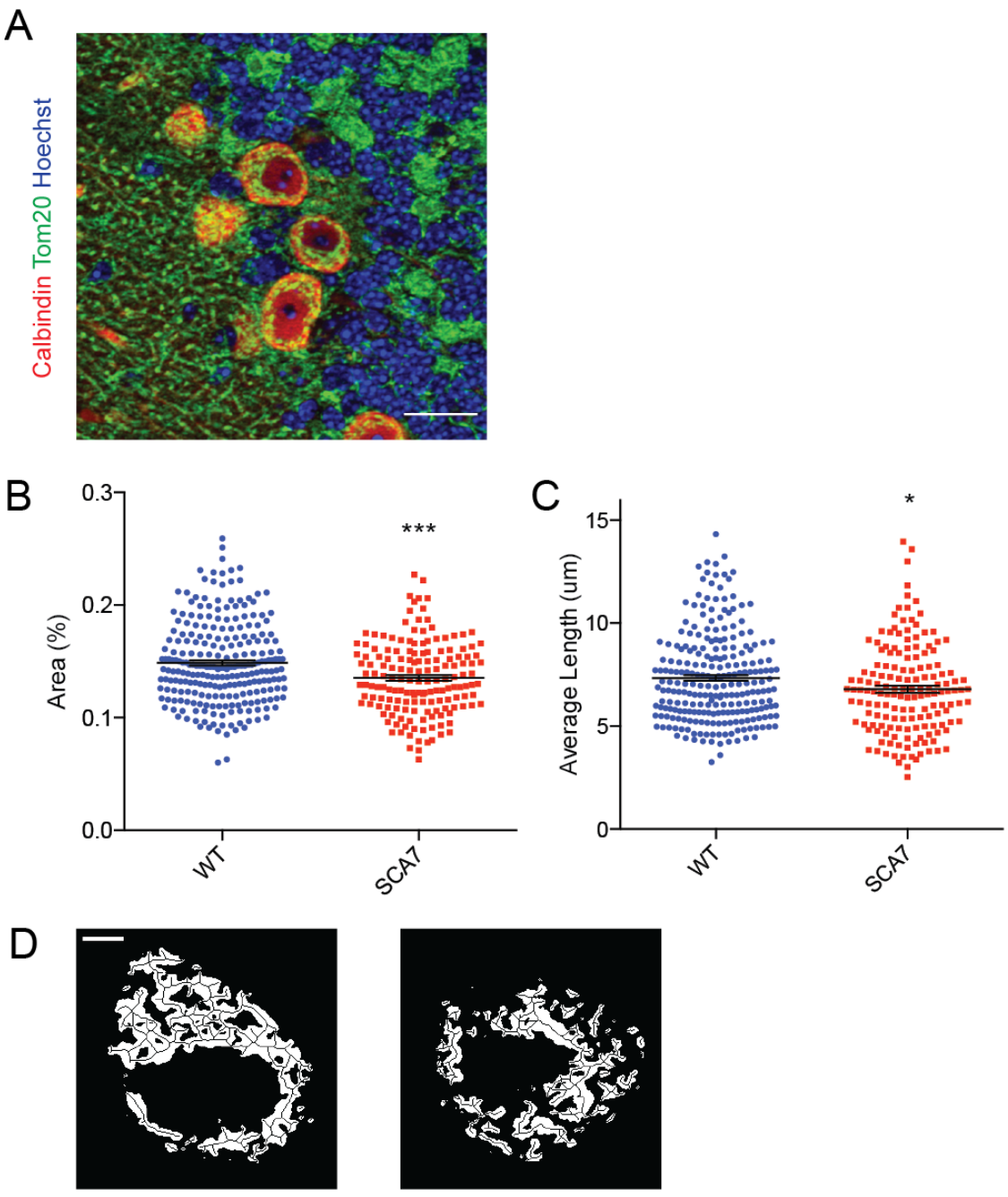

Figure 2.3 SCA7 Purkinje cells have decreased mitochondrial content and length. A Representative merged image of stained Purkinje cells (Calbindin, red) and mitochondria (Tom20, green) with nuclei (Hoechst, blue) from a cerebellar section. Scale bar, 20 um. **B** Tom20 immunofluorescence signal as a percentage of selected area of Calbindin immunofluorescence. **C** Average length of skeletonized mitochondria network. **D** Example images of skeletonized Tom20 signal to exhibit extremes of length measurement. The average lengths of the mitochondria in the image on left and right are 14 um and 5 um, respectively. Scale bar, 5 um. Data are represented as mean ± SEM, $n \geq 100$ cells per genotype, *P≤0.05, ***P≤0.001.

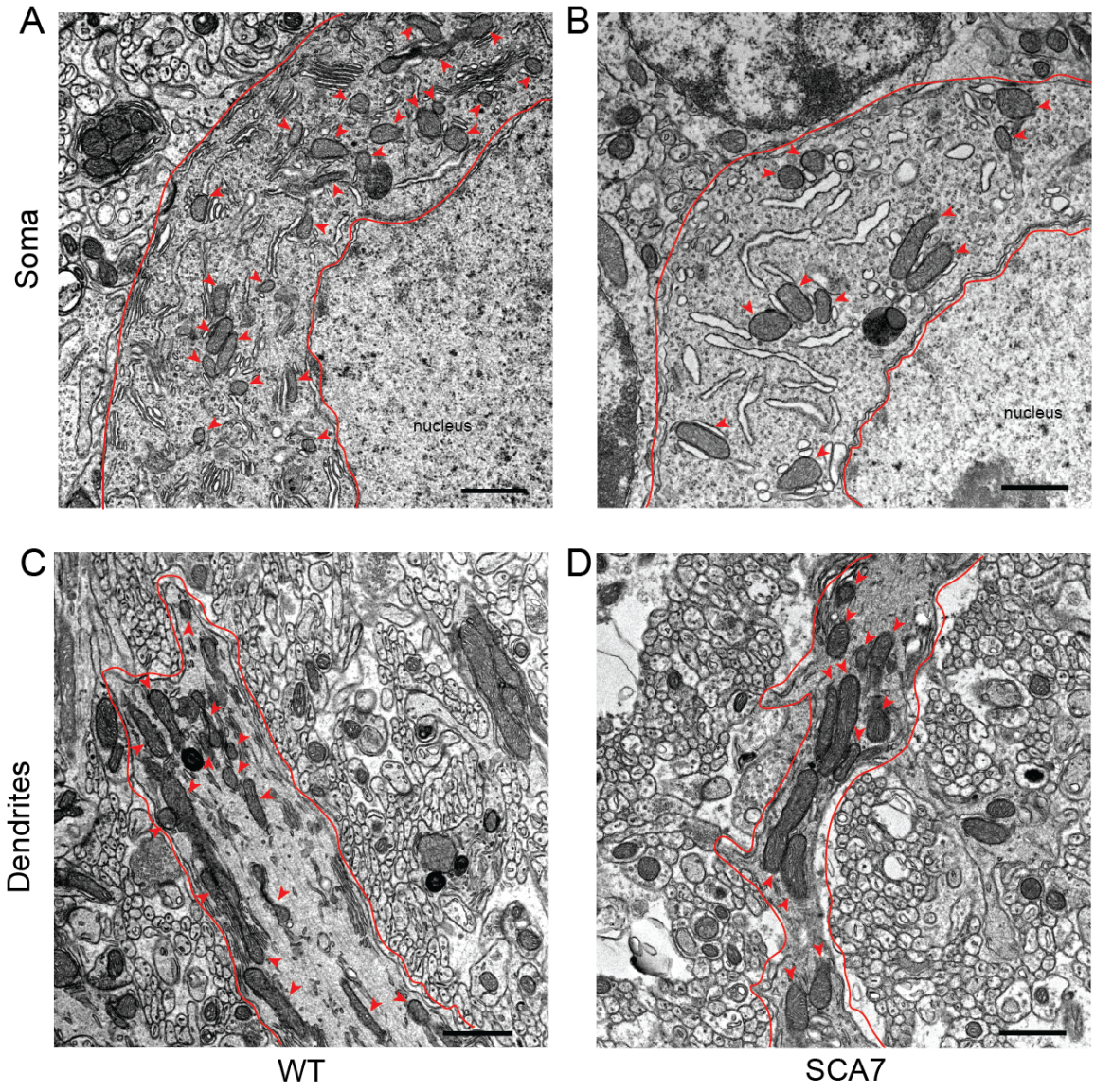

Figure 2.4 SCA7 Purkinje cells display fewer mitochondria that are increased in size. Representative images of WT (**A**) and SCA7 (**B**) PC soma and WT (**C**) and SCA7 (**D**) PC dendrites. Red arrowheads indicate mitochondria. Red outlines indicate either the cytoplasm of a PC soma or a dendrite to clearly show analyzed area from extracellular space or other cells. Scale bar, 1 um.

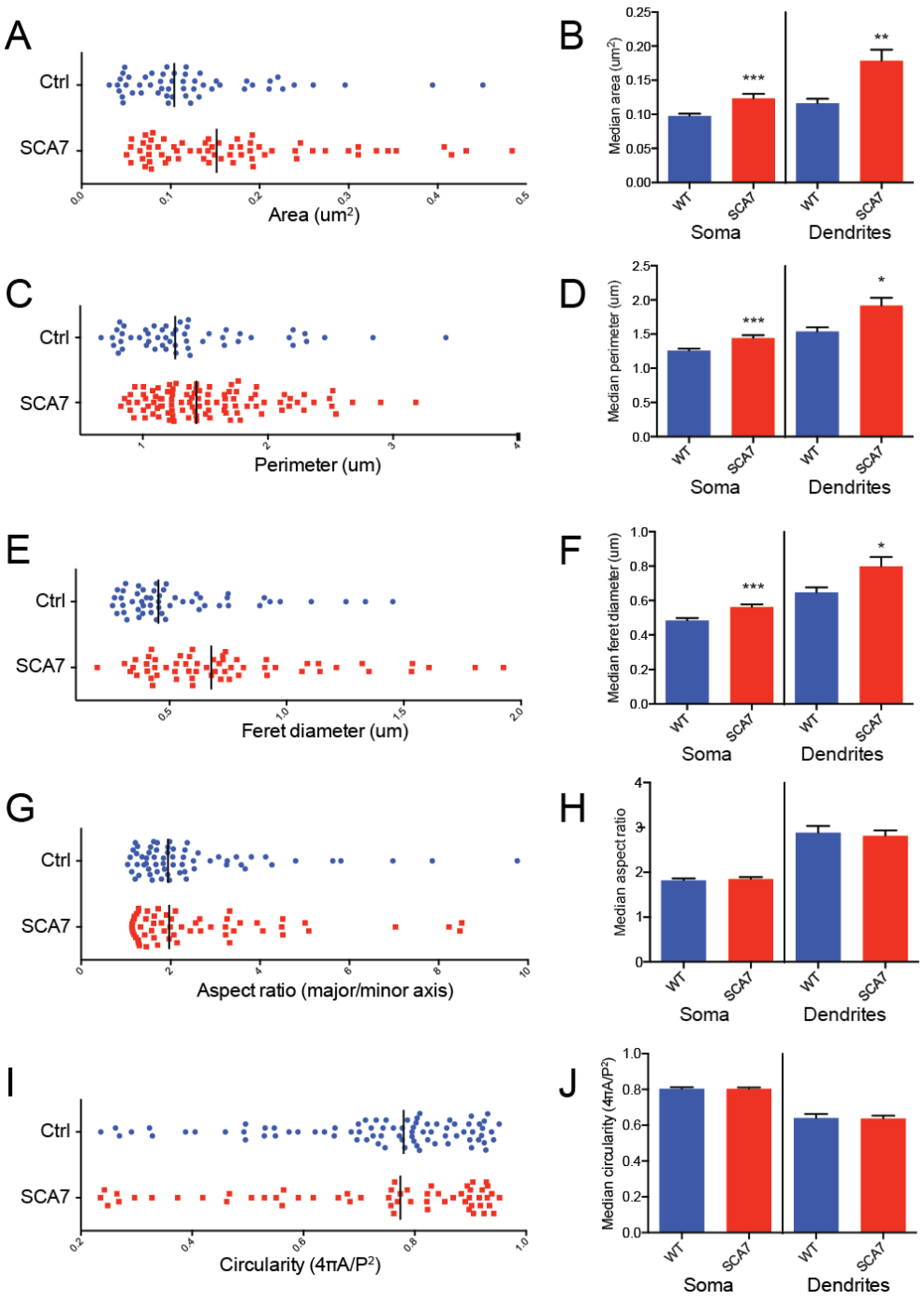

Figure 2.5 Quantification of ultrastructural analysis indicates increased SCA7 mitochondrial size. Representative graph of mitochondrial area (**A**) and quantification (**B**), representative perimeter (**C**) and quantification (**D**), representative Feret diameter (**E**) and quantification (**F**), representative aspect ratio (**G**) and quantification (**H**), and representative circularity (**I**) and quantification (**J**) from WT and SCA7 soma. Each dot represents an individual mitochondrion from a single PC soma. Black bars in dot plots are the median. Bar graphs are represented as mean ± SEM, $n \geq 21$ cells from 2 different mice per genotype.

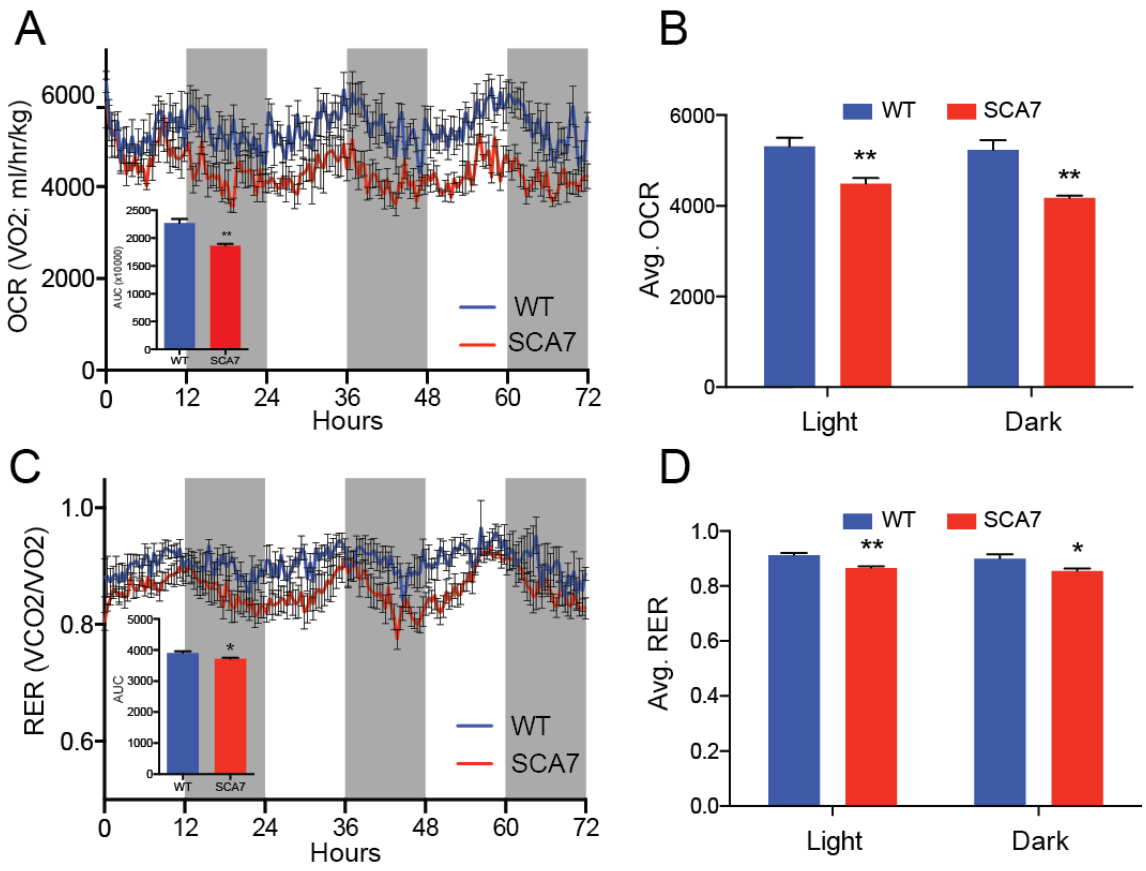

Figure 2.6 SCA7 mice exhibit decreased metabolic respiration. A Metabolic cage measurement of the oxygen consumption rate (VO2, mL/kg/hr) quantified by area under the curve (AUC) in inset, over the course of 72 hrs. **B** Quantification of average measurements of OCR during light and dark intervals. **C** Respiratory exchange ratio (RER) (CO2 emission/O2 consumption), quantified by area under the curve (AUC) in inset, over the course of 72 hours. **D** Quantification of average measurements of RER during light and dark intervals. White panels in **A** and **C** indicate 12 hrs of light, and gray panels indicate 12 hrs of dark. Data are represented as mean ± SEM, n = 5 mice per genotype, *P≤0.05, **P≤0.01.

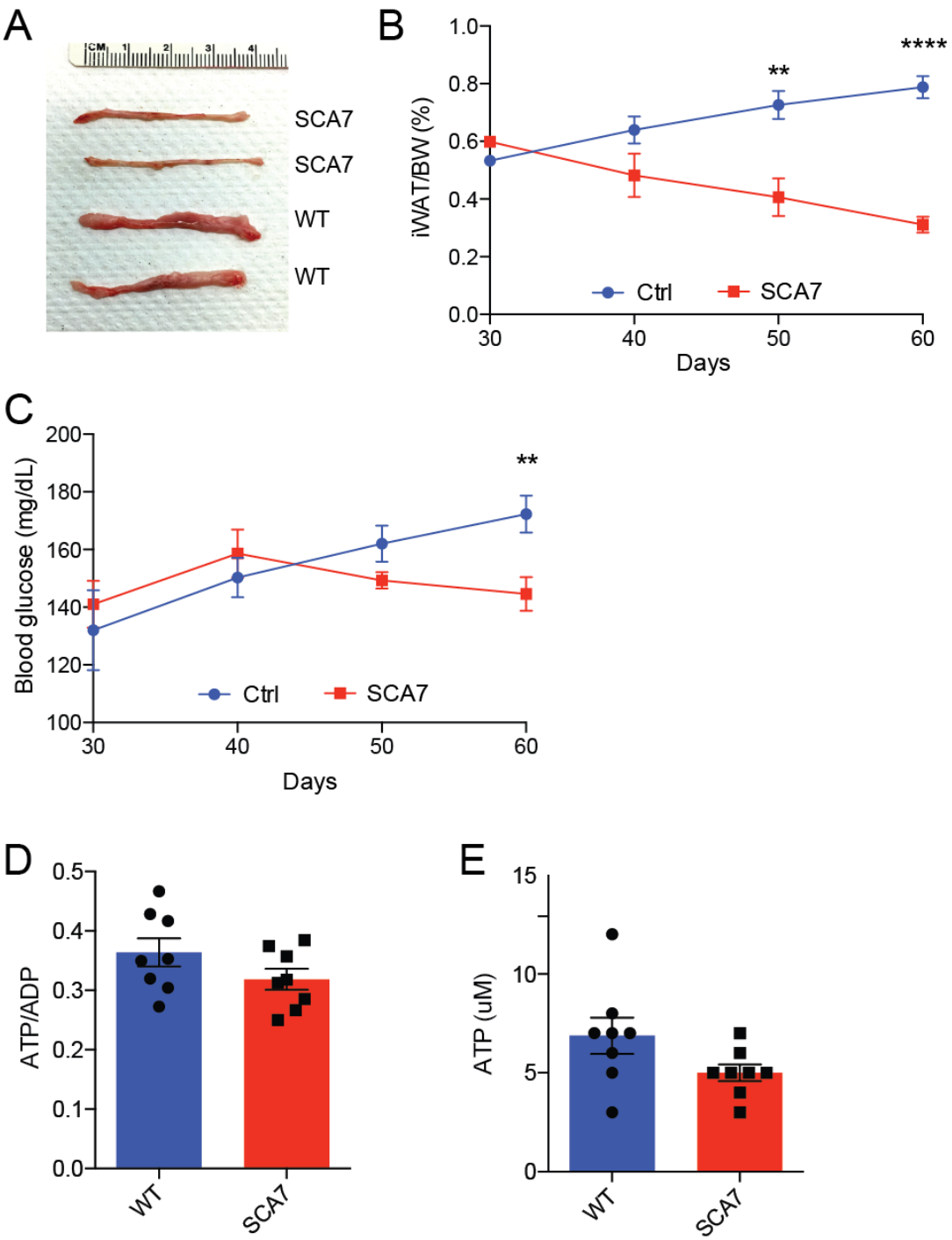

Figure 2.7 SCA7 mice exhibit decreased fat content and blood glucose. A Representative images of iWAT from WT and SCA7 mice. **B** iWAT was dissected and weighed as a proportion of body weight at different timepoints. **C** Blood glucose levels after 6 hr of fasting at different timepoints. **D** Quantification of ATP in proportion to ADP levels and **F** total ATP concentration in the cerebellum of 60-day-old WT and SCA7 mice. Each black point represents an individual mouse. Data are represented as mean ± SEM, *n* ≥ 5 mice per genotype, *P≤0.05, **P≤0.01, ****P≤0.0001.

Chapter 3:

Generation and Characterization of Mitochondrial Dysfunction in an SCA7 Stem Cell Model

Abstract

I generated a novel stem cell model of SCA7 to evaluate mitochondrial dysfunction in an applicable human system. I obtained patient and control fibroblasts and reprogrammed them into induced pluripotent stem cells (iPSCs). I used a CRISPR gene editing technique to knockout mutant ataxin-7 in patient cells and evaluate the effect of normal and pathogenic ataxin-7 expression in neural progenitor cells (NPCs). These cells demonstrate reduced mitochondrial network length, but exhibit no differences in mitochondrial membrane potential (MMP) and reactive oxygen species (ROS). Importantly, they have a significantly reduced oxygen consumption rate (OCR), an indicator of defective metabolic respiration. Coupled with results from SCA7 mice, these data demonstrate that mitochondrial dysfunction is an authentic feature associated with SCA7 pathogenesis.

3.1 Introduction

Induced pluripotent stem cells (iPSCs) have revolutionized the field of disease modeling. By merely expressing 4 transcription factors in human fibroblasts, it is possible to reprogram them to pluripotent cells that have the capacity to differentiate into any other cell type. This tool has turned out to be remarkably powerful for modeling diseases that lack appropriate mouse models or are difficult to recapitulate in a cell model. While the SCA7 field has benefitted from several different mouse models, not all have produced parsimonious conclusions about the biology of the disease. Additionally, using

iPSC technology in combination with mouse models gives further assurance that the results are not specific to one model system, but are broadly applicable to the disease itself. It is in this pursuit that I sought to generate a novel SCA7 stem cell model.

While adult-onset SCA7 primarily affects mature neuronal cell types such as Purkinje cells and retinal photoreceptors, infantile-onset SCA7 is a much broader form of disease. These patients present with symptoms very early, and in a wide variety of cell and tissue types. Hypotonia, muscle wasting, developmental delay, and congestive heart failure have all been observed in infantile-onset patients (reviewed in Whitney, et al. [15]). These cases invariably result in fatal multi-organ failure[15-17]. In fact, infantile-onset SCA7 is so severe that it could be considered a neurodevelopmental disorder.

Neural progenitor cells (NPCs) are multipotent stem cells that, in normal development, are able to differentiate into any cell of the neural lineage. These cells were first isolated from the mouse brain[30,31], but have more recently been derived from human pluripotent stem cells (hPSCs)[32]. Moreover, NPCs have even been shown to recapitulate disease-specific phenotypes associated with adult-onset neurodegenerative diseases[35-37], despite the fact that these cells are most prominent in neural development. In pragmatic terms, they are also very easy to grow in culture, proliferate quickly, and can be cryopreserved. With this in mind, I hypothesized that NPCs would be a particularly relevant system for interrogating mitochondrial dysfunction in infantile-onset SCA7.

One of the challenges of iPSC disease modeling is the sheer variability between different iPSC lines. This variability stems from a number of genetic, epigenetic, and environmental factors. In genetic disease modeling, it is best to compare several clonal iPSC lines from several patients and controls to ensure valid results, but the cell line variability can cause subtle phenotypes to get lost in the noise[24]. In response to these challenges, the advent of gene editing has been a boon for the field. The advent of Clustered Regularly Interspaced Short Palindromic Repeats (CRISPR) technology has made it inexpensive and straightforward to perform gene editing in a broad range of systems. When a CRISPR guide RNA is co-expressed with CRISPR associated protein 9 (Cas9), double strand breaks (DSBs) are targeted to a selected site in the genome. These DSBs can be resolved through homologous recombination (HR), which results in repair with a donor template, or through non-homologous end joining (NHEJ), which commonly results in a loss of function allele. Utilization of this technique therefore leads to changes in the targeted gene of interest, while the rest of the DNA is identical to the untreated cells—resulting in isogenic cell lines. While I began these studies by comparing many clonal lines from patients and controls, it became evident that the comparison amongst all of these lines made it difficult to determine if the observed effects were disease-specific or simply due to variation in the system. With this in mind, I designed a gene editing strategy with the goal to correct the CAG expansion mutation in patient cells to a normal, non-pathogenic length. I did not obtain any cell lines with such a rescue, but the

process did result in cell lines with a functional ataxin-7 knockout. I was able to use these cells to my advantage by re-expressing normal and mutant versions of ataxin-7 to compare isogenic lines of NPCs.

I thoroughly characterized these cells through the stages of reprogramming, CRISPR gene editing, and re-expression of ataxin-7, to ensure that this model would be appropriate to investigate mitochondrial dysfunction. I then performed an assessment of mitochondrial structure, and determined that NPCs expressing mutant ataxin-7 have more fragmented mitochondrial networks, as I observed in SCA7 mice. I also took advantage of the cellular model to investigate novel effects on mitochondrial membrane potential (MMP) and reactive oxygen species (ROS), but surprisingly found no disease-specific effect. However, in a metabolic assessment of oxygen consumption, I found that these cells suffer from a defect in metabolic respiration, similar to the effects observed in the SCA7 mice. Taken together with the studies described in chapter 2, I have found that SCA7 is a disease characterized by mitochondrial dysfunction. I further pinpoint this defect here, as the assessment of mitochondrial depolarization—a late stage marker of mitochondrial dysfunction—was not different from controls. This indicates a specific link between mitochondrial fragmentation and metabolic respiration in SCA7.

3.2 Results

Generation and characterization of iPSCs

I began by obtaining fibroblast samples from two different families consisting in total of 3 SCA7 patients, 1 relative with an intermediate allele length, and 2 related controls. A summary of patient details is included in Figure 3.1a. I reprogrammed all patient fibroblast lines to iPSCs (Figure 3.1b) and ensured that these cell lines exhibited key characteristics of pluripotent stem cells (Figure 3.1c-3.1e). My reprogramming efforts resulted in 2 to 8 clonal iPSC lines from each individual, as indicated in Figure 3.1a.

CRISPR gene editing knocked out *ATXN7*

Due to variability and limitations when comparing iPSC lines and derivatives[24], I also generated an isogenic model by using CRISPR/Cas9 to edit the mutant *ATXN7* gene in patient iPSCs. My primary goal was to, in effect, "contract" the repeats to a non-pathogenic length. I designed a guide RNA that would target a double strand break in proximity of the CAG repeat region within exon 3 of the human *ATXN7* gene (Figure 3.2a). When co-expressed with Cas9, this system introduced DSBs at high efficiency (Figure 3.2b). This did not occur when the guide RNA was co-transfected with a Cas9D10A nickase that only introduced single strand breaks (SSBs) (Figure 3.2b). After co-expressing Cas9 and the guide RNA in 65Q patient iPSCs (patient indicated by asterisk in Figure 3.1a), I obtained several clones with deletions large enough to be noticeable when the PCR amplicons were run on an agarose gel (Figure 3.2c). Upon more thorough sequencing analysis, 3 out of 4 of these clones did not retain the proper coding reading frame (Table 3.1).

Of the one that did, the deletion did not extend into the CAG repeat region. While I did not obtain any clonal lines that had a natural contraction to a non-pathologic number of CAG repeats while still maintaining a functional protein, I did obtain several clonal lines with small insertions or deletions (indels) predicted to cause a premature stop codon that would result in a functional knockout of the protein (Table 3.1). I further analyzed one clone that had small deletions in each allele (Figure 3.2d) and determined that polyQ-expanded ATXN7 protein was undetectable by immunoblotting (Figure 3.2e). To assess genome stability in these cells, I performed digital karyotyping via SNP array through hybridization to the Illumina Infinium HumanCoreExomeBeadChip. This analysis revealed that there were no large aberrations detected in either the unedited SCA7 patient iPSC line or the edited *ATXN7* knockout line derived from it. Additionally, through analyzing the absolute number of different single nucleotide polymorphism (SNP) genotype calls between these two lines, I found that there were zero out of the total 257,118 SNP probes that had any homozygous mutational differences, and only 10 probes that contained heterozygous mutational differences. This is similar to the mutational load observed when two different clonal lines are derived from a single individual's fibroblasts. In my hands, these mutations ranged from 2 to 17 heterozygous differences. Furthermore, these differences could be attributed to mutations accumulated through passaging not just CRISPR/Cas9 induced mutagenesis, as the edited cells had been passaged several times before analysis.

Characterization of isogenic model through lentiviral ATXN7 expression

While an *ATXN7* knockout line was not my primary goal, I decided to use these cells to my advantage by re-expressing either normal length or mutant ataxin-7. In this manner, I could specifically assess phenotypic differences caused by the presence of mutant ATXN7 independent of the variability of many different patient cell lines. I differentiated these iPSCs to neural progenitor cells (NPCs) then lentivirally expressed either normal length (10Q) or mutant (113Q) ataxin-7, along with EGFP separated by a 2A peptide as a marker of transduced cells (Figure 3.3a). I ensured that these NPCs expressed markers of the neural lineage (Figure 3.3b) and lentiviral transduction resulted in equivalent expression of normal and mutant ATXN7 (Figure 3.3c). Current work involves precisely measuring the lentiviral expression compared to endogenous expression in the patient line from which these cells were derived. Only the 113Q cell lysate was immunoreactive when probed with an antibody that recognizes expanded polyglutamine repeats (Figure 3.3c). I also detected polyglutamine-containing SDS-insoluble aggregates in cell lysate from the 113Q cells via filter trap assay (Figure 3.3d). The expression of both 10Q and 113Q reduced the overall proportion of live cells, which is unsurprising considering both versions of ATXN7 are being expressed at a higher level than endogenous (data not shown). However, there were significantly fewer live cells in the 113Q condition, indicating a polyQ dependent toxicity (Figure 3.4a and 3.4b). In addition to the isogenic model system, I also assessed the percentage of live cells in SCA7 patient

and control NPCs. Only the 65Q patient line exhibited a significant reduction in live, healthy cells (Figure 3.4c). This result could be attributed to variability or to the less severe endogenous mutations present in the patient cells.

Mitochondrial network length is decreased in SCA7 NPCs

Mitochondrial fragmentation is often associated with bioenergetic defects and decreases in metabolic respiration—as observed in the SCA7 mice. I was able to perform a very similar analysis to that performed in Purkinje cells of the mice, by measuring the average length of mitochondrial networks in the GFP+ NPCs, thereby specifically selecting those cells expressing ataxin-7, (example shown in Figure 3.5a). Mitochondria in 113Q cells were significantly decreased in length when compared to GFP empty or 10Q, indicating increased fragmentation (Figure 3.5b and 3.5c). I also assessed the average length of mitochondrial networks in SCA7 patient and control NPCs. While the 50Q and 65Q patient lines exhibited a trend towards decreased mitochondrial length, only the 70Q patient line was significantly reduced compared to controls (Figure 3.5d). I also generated primary cerebellar granule neurons (CGNs) from mice expressing 92Q ataxin-7[20], which likewise exhibited a trend towards decreased mitochondrial length, though not significant (Figure 3.5e). Taken together, these results indicate that mitochondrial fragmentation is not particular to a single model system, but a *bona fide* SCA7-associated phenotype. The patient NPCs and 92Q CGNs are models of a less severe version of SCA7, so it makes sense that there would

be a coordinate decrease in severity of the phenotype in these model systems.

Mitochondrial membrane potential is unchanged in SCA7 NPCs

I sought to take advantage of this cellular model to perform further *in vitro* studies to assess mitochondrial membrane potential (MMP). Proper MMP is maintained by the proton electrochemical gradient that is generated by the electron transport chain (ETC) in the inner membrane of the mitochondria. Collapse of this potential is indicative of late stage mitochondrial dysfunction and leads to cell death[83,84]. Subtler decreases in MMP have been associated with mitochondrial fragmentation[85,86], but the effects can also be independent of each other[87,88]. I used fluorescence-activated cell sorting (FACS) to select GFP+ cells and measure MMP using a rosamine-based dye, CMXRos, which accumulates in polarized mitochondria[89]. I normalized this to the total mitochondrial content of cells through Mitotracker Deep Red fluorescence (which does not accumulate in polarized mitochondria) to ensure that any differences in CMXRos fluorescence intensity would be specific to differences in mitochondrial polarization. There was no significant increase or decrease in the MMP in the 10Q or 113Q expressing cells compared to GFP empty controls (Figure 3.6a and 3.6b). Likewise, the patient NPCs showed no significant differences in this measurement, though there was more variability between these lines, as expected (Figure 3.6c). CGNs from 92Q mice also exhibited equivalent MMP compared to WT CGNs (Figure 3.6d). Since I also

selected for live cells (through forward scatter and side scatter gating), I did not expect to see a complete collapse of MMP, which quickly leads to cell death[83,84], but there does not seem to be any evident subtle difference either.

ROS levels are unchanged in SCA7 NPCs

I used a similar FACS technique to measure the abundance of reactive oxygen species (ROS) both at a total cellular level and specifically in mitochondria. CellROX is a dye that fluoresces upon ROS oxidation. MitoSOX targets to mitochondria and fluoresces specifically upon superoxide oxidation. As before, I selected the GFP+ cells and measured the median fluorescence intensity of both of these ROS markers. There was no apparent difference in either the total cellular ROS or mitochondrial ROS levels between GFP empty, 10Q, or 113Q cells (Figure 3.7a and 3.7b), which indicates that these cells were not undergoing excessive oxidative stress. One line of patient SCA7 NPCs had significantly elevated levels of cellular ROS and another line had elevated mitochondrial ROS (Figure 3.7e and 3.7f). Since the isogenic model did not exhibit this difference, these differences are most likely attributable to non-disease specific variability. CGNs from 92Q mice were likewise equivalent to WT cells (Figure 3.7g and 3.7h). As before, these levels were normalized to the total mitochondrial content to ensure that the signal was specific to changes in ROS levels and not mitochondrial content. As with the MMP, I specifically analyzed the live GFP+ cells, so it is possible that I was not able to

observe the cells with massive increases in ROS as this would quickly lead to cell death.

Mitochondrial protein levels are unchanged in SCA7 NPCs

I analyzed the protein levels of a panel of mitochondrial proteins in these cells to determine whether there was a significant difference in specific proteins important to mitochondrial function. By western blot, I detected no differences in overall protein levels of components of the mitochondrial outer membrane (VDAC1 and Tom20) or members of the ETC (CoxIV or CytC) (Figure 3.8). Though not exhaustive, this analysis of mitochondrial protein levels, in coordination with equivalent MMP and ROS levels, implies that the mitochondrial defects present in this system are not due to a significant loss in mitochondria or total collapse in mitochondrial function.

SCA7 NPCs exhibit bioenergetic defects

As the SCA7 mice exhibited such a marked and severe decrease in metabolic respiration, I was curious to see whether this model would likewise exhibit defects in bioenergetics. I performed a functional assessment of mitochondrial respiration in these cells via seahorse assay. The basal metabolic rate of each condition reveals that 113Q cells have a diminished oxygen consumption rate (OCR) and increased extracellular acidification rate, an indicator of glycolysis[90] (ECAR) (Figure 3.9a). This correlates with the indirect calorimetry measurements observed in the whole animal and indicates

an overall defect in metabolic respiration that is substantial enough to force the cells to rely heavily on glycolysis. With the treatment of an ATP synthase inhibitor (oligomycin), uncoupling agent (FCCP), or inhibitors of complex I and III (antimycin/rotenone), the 113Q cells all remained at a diminished OCR/ECAR ratio when compared to the 10Q cells (Figure 3.9b). I used this ratio as a readout, rather than total OCR, because of the decrease in live cells in the 113Q condition (see Figure 3.4). The ratio of OCR to ECAR accounts for the differences in total cell number. Nonetheless, decreases in OCR or increases in ECAR are reflections of dysfunctional metabolic respiration.

3.3 Discussion

To my knowledge, this is the first study that uses iPSCs to model SCA7. Heretofore, there has been a description of derivation of iPSCs and neurons from a single SCA7 patient, but no investigation of phenotypes[91]. While the variability associated with iPSC disease modeling is challenging, I was able to use an emerging tool in the form of CRISPR gene editing to generate an isogenic model of SCA7. It is not surprising that the patient cells exhibit more variability and less distinct phenotypes than the 113Q transduced cells. These cells have less severe expansions (50, 65, and 70 CAGs), and are expressed at endogenous levels. Moreover, my experiments were all performed in NPCs, but it may be more relevant to assess phenotypes from these less severe mutations in more mature differentiated neurons. In most

cases, the patient cells exhibited similar trends as the isogenic model, which I found encouraging.

Surprisingly, I did not observe any obvious phenotypes associated with knocking out ataxin-7 in the NPCs. The cells proliferate normally and maintain normal cellular morphology (data not shown). Recent work has indicated that atxn7 deficiency in zebrafish impairs embryonic development, and that even partial depletion prevents differentiation of retinal photoreceptors and specific cerebellar neurons[92]. However, ataxin-7 knockout mice do not exhibit any obvious defects, neurodegenerative or otherwise (personal communication, Huda Zoghbi). It is possible that these cells may lack differentiation capacity similar to the zebrafish, or like the mice, may have some compensatory ability to overcome the protein deficiency. There was a slight but non-significant increase in mitochondrial network length between knockout (GFP empty) and 10Q expressing NPCs (Figure 3.5c). It is possible that the presence of normal ataxin-7 could be beneficial for mitochondria. I will have to perform more precise experiments comparing the ataxin-7 knockout cells to non-pathogenic controls to assess this difference.

I was encouraged to see a recapitulation of the mitochondrial fragmentation effect in this cell model. Not only is this a less severe mutation than in the SCA7 mice, but it is also present in human cells, indicating that this is a physiologically relevant defect. Importantly, patient NPCs and cerebellar granule neurons (CGNs) derived from 92Q transgenic SCA7 mice also show a tendency towards decreased mitochondrial length. Interestingly, I did not

detect any observable differences in mitochondrial polarization or ROS levels coordinate with the increased fragmentation. There have been entire reviews written about the complicated cause and effect relationship between a variety of mitochondrial defects[88,93]. In fact, it has been shown that fragmented mitochondria have been associated with increases, decreases, and complete dissipations of MMP (reviewed in Galloway and Yoon [88]). Therefore it's not entirely surprising that this was unchanged in these cells despite the fact that they have more fragmented mitochondria. Using the FACS technique, I also selected for the live, healthy cells so it is likely this is the reason I did not observe severe depolarization or massively elevated ROS levels. There is one report of increased ROS production linked to increased ataxin-7 aggregation in a cell model of SCA7[94], but this system did not confirm this finding.

My initial motivation to perform the bioenergetics assay on these cells was to perturb individual complexes of the ETC in order to specify which complex might be the culprit of the metabolic defect. What I found was dysfunction in the basal metabolic rate. Perturbation with ETC modulators seemed to just maintain this reduced rate. In further work, I will isolate mitochondria from these cells to perform specific ETC complex activity assays to determine if a single complex is the culprit for this defect.

In these studies, I have generated and characterized a novel human cell model system of SCA7. I have also established mitochondrial fragmentation as a significant phenotype in a human model system. Likewise, reductions in metabolic respiration are evident. However, further work is

necessary to determine the exact link between polyQ ataxin-7 and these mitochondrial defects. Why and how this dysfunction occurs molecularly and how it is linked to the SCA7 mutation are still open questions. In the next chapter, I will describe the initial dive into exploring the mechanistic underpinnings of this dysfunction.

3.4 Experimental procedures

iPSC derivation

Fibroblasts were generated from dermal biopsies from SCA7 patients and controls indicated in Figure 3.1a, upon informed consent and in compliance with UCSD IRB protocols. Fibroblasts were cultured in Dulbecco's modified Eagle's medium (DMEM) with 10% FBS and 5% penicillin and streptomycin. Low passage fibroblast cultures were treated with the retroviral reprogramming factors Oct4, Sox2, Klf4, and c-Myc, as described previously[21,95]. Two days after transduction, fibroblasts were dissociated and plated on irradiated mouse embryonic fibroblasts (Chemicon) in human embryonic stem cell media consisting of DMEM, 10% KnockOut Serum Replacement (ThermoFisher), 0.5% non-essential amino acids (ThermoFisher), and 0.1 mM 2-mercaptoethanol. After 15-20 days, individual colonies with stem cell morphology were isolated and transferred to feeder free conditions on Matrigel (BD Bioscience) coated plates and grown in mTesr1 media (StemCell Technologies) as clonal lines. Thereafter, cells were

passaged manually by gently cutting colonies with a needle and scraping with a pipette tip under an EVOS inverted microscope (ThermoFisher).

RT-PCR

RNA was extracted from early passage fibroblasts and iPSCs using TRIzol reagent (Thermo Fisher), and DNase-treated with TURBO DNA-free kit (ThermoFisher) according to manufacturer's instructions. One microgram (ug) of RNA was reverse transcribed using the High-Capacity cDNA Reverse Transcription Kit (Applied Biosystems, Life Technologies) according to manufacturer's instructions. cDNA was then amplified using primers for *Oct4*, *Sox2*, *Nanog*, and *GAPDH* as described previously[95].

Guide RNA design and efficacy

The target sequence for the gRNA was designed and selected using the E-CRISP design site based on proximity to CAG repeat region and limited off-target effects (http://www.e-crisp.org/E-CRISP/). The target sequence (CGGGCCGCGGATGACGTCAGG) was incorporated into a synthesized GeneArt DNA String (Life Technologies), as described[26,96]. This fragment and the pUC57 expression vector were simultaneously digested with EcoR1 and Pst1 restriction enzymes, ligated together, and transformed into DH5α bacteria. Bacterial colonies were picked, and DNA was isolated and sequenced. To ensure function and specificity, this U6::gRNA vector and the CMV::Cas9-2A-EGFP vector were co-transfected into HEK293Tcells, which

were then harvested after 72 hours, or alternatively, selected for GFP expression by FACS on a BD influx and then harvested for DNA isolation (DNeasy, Qiagen). Surveyor nuclease assay was performed by PCR amplifying the region surrounding the putative cut site with the following primers: SCA73.1F 5'-GAGCGGAAAGAATGTCGGAGCG-3' and SCA73.327R 5'-CAGGAACTTTGGAAGCCTCAACCC-3'. The PCR product was hybridized and treated with Surveyor Nuclease S and Surveyor Enhancer S according to manufacturer instructions (Transgenomic, Inc.). Products were analyzed on an acrylamide gel and the relative amount of the resulting cleaved product was quantified using ImageJ.

CRISPR/Cas9 gene editing and screening

One clonal line of patient iPSCs was treated overnight with 5 uM ROCK inhibitor (Ri) (Tocris), then dissociated to single cells with Accutase (StemPro, ThermoFisher), and passed through a 40 um nylon mesh (BD Biosciences) to ensure single cells prior to transfection. Using hESC Kit 2 and Amaxa program B16 (Lonza), 2 x 10^6 cells were nucleofected with 9 µg of the CMV::Cas9-2A-EGFP vector or CMV::Cas9D10A-2A-EGFP (gifts from Kiran Musunuru; Addgene, #44719 and #44720) and 3 µg of the U6::gRNA vector. Transfected cells were plated in mTeSR supplemented with 5 µM Ri for 48 hours before FAC sorting. GFP expressing cells were selected using the BD influx at the UCSD Human Embryonic Stem Cell Core Facility and plated communally to recover for 48 hours with Ri. After 48 hours, cells were again dissociated to

single cells as described above, plated very sparsely (20000 – 80000 cells in a 10 cm dish), and allowed to grow out as clonal lines for 1-2 weeks. Isolated colonies were selected, expanded, and genomic DNA was extracted (DNeasy kit, Qiagen) for PCR and sequencing analysis. All clones were initially screened by PCR using the PCRx enhancer system (Invitrogen, Life Technologies) and the above 3.1F/3.327R primers. Several clonal lines were further investigated by TOPOcloning (ThermoFisher) the PCR product, selecting 10 resulting bacterial clones, isolating DNA (QIAprep kit, Qiagen), and sequencing (Eton Bioscience; San Diego, CA). One resulting clonal line with small deletions in each allele was selected for further studies.

Karyotyping

Standard G-banding chromosome analysis of iPSC clones was performed by Molecular Diagnostic Services (San Diego, CA). Digital karyotyping was performed by hybridization to the Illumina Infinium HumanCoreExomeBeadChip (module version 1.9.4) following manufacturer's instructions at the UCSD Institute of Genomic Medicine Genomics Center. Analysis was performed using Illumina's cnvPartition and gada R package[97] in addition to manual analysis.

NPC differentiation

NPCs were generated with STEMdiff Neural Induction Medium (NIM) (StemCell Technologies) according to manufacturer's monolayer culture

protocol instructions. Briefly, iPSCs were gently dissociated with Accutase (StemPro, ThermoFisher), pelleted, and resuspended in NIM at 1 x 10^6 cells/mL, then plated on Matrigel coated dishes. Cells were passaged one more time in NIM and plated in dishes coated with poly-L-ornithine (15 ug/mL) and laminin (10 ug/mL) (Sigma-Aldrich). Cells were thereafter passaged and expanded in STEMdiff Neural Progenitor Medium (NPM) (StemCell Technologies) on poly-L-ornithine/laminin-coated dishes.

Lentivirus generation and treatment

EGFP-2A-puroR-2A, EGFP-2A-puroR-2A-Atxn7cDNA (10 CAG), and EGFP-2A-puroR-2A-Atxn7cDNA (113 CAG) cassettes were cloned into pSico lentiviral constructs. Lentiviral particles were produced using standard techniques and titration was performed using limiting concentrations of the virus to ensure equivalent GFP expression by immunofluorescence. Lentiviral construct cloning and lentiviral production were performed at the University of Washington. NPCs were transduced with lentivirus and experiments were all performed after 48 to 72 hours.

Protein isolation and immunoblotting analysis

Cells were harvested in RIPA buffer (50 mM Tris, 0.1% SDS, 0.5% sodium deoxycholate, 1% triton X-100, 150 mM NaCl) supplemented with 1% protease inhibitor cocktail (Roche) and homogenized by passing 5 times through a 23-gauge needle. Lysate was then centrifuged at 10000 x *g* for 10

min at 4°C. Supernatant was quantified via BCA assay (Pierce; ThermoFisher). Fifteen ug of protein were separated on 4-12% Bis-Tris gels (Life Technologies), transferred to PVDF membranes (Millipore), and blocked with 3% Bovine Serum Albumin (Sigma-Aldrich) for at least 1 hour at room temperature. Membranes were then probed with rabbit anti-ATXN7 (Thermo, PA1-749) 1:1000, mouse anti-polyQ 1C2 (Millipore MAB1574) 1:1000, rabbit anti-Tom20 (Santa Cruz, SC11415) 1:1000, rabbit anti-CoxIV (Cell Signaling, 4850) 1:1000, mouse anti-cytochrome C (BD Pharmingen, 556433) 1:1000, mouse anti-VDAC1 (Millipore, MABN504) 1:1000, or mouse anti-beta actin (Abcam, ab8226) 1:10000 in 3% BSA in PBS overnight at 4°C. After 3 washes with 1x phosphate buffered saline supplemented with 0.1% Tween20 (PBS-T), membranes were incubated with HRP secondary antibodies (1:10000 Santa Cruz sc-2005 [anti-mouse], sc-2004 [anti-rabbit]) in PBS-T for 1 hour at room temperature. After treatment with enhanced ECL chemiluminescence (Upstate), the membranes were visualized by autoradiography. For the filter trap assay, cell pellets were resuspended in RIPA buffer, triturated as above with a needle, and then directly quantified by BCA. Thirty ug of protein was loaded in a PR-600 24 slot blot filtration manifold unit (Hoefer, Fisher Scientific) with a cellulose acetate membrane. Vacuum was applied until lysate had run through, membrane was blocked in 5% nonfat dried milk in PBS for 1 hour at room temperature, and then incubated in mouse anti-polyQ 1C2 (Millipore MAB1574) 1:1000 overnight at 4°C. Membranes were then

incubated in anti-mouse secondary antibody (1:5,000; Santa Cruz sc-2005) for 1 hour at room temperature, and visualized as above.

Immunostaining

Cells were grown in coated 96-well plates or chamber slides, fixed in 4% paraformaldehyde for 10 min, and permeabilized in 0.3% Triton X-100 in PBS for 10 min. Cells were then blocked with 5% BSA for at least 1 hour before incubation with chicken anti-GFP (Abcam, ab13970) 1:2000, rabbit anti-Tom20 (Santa Cruz, SC11415) 1:500, mouse anti-SSEA4 (Cell Signaling CS 4755) 1:500, mouse anti Tra-1-60 (Cell Signaling CS 4746) 1:500, mouse anti Tra-1-81 (Cell Signaling CS 4745) 1:500, rabbit anti-Pax6 (Covance, PRB-278P) 1:500, or mouse anti-Nestin (Abcam, ab6142) 1:1000 overnight at 4°C. Cells were washed 3 times with PBS, then incubated with AlexaFluor 488, AlexaFluor 555, and/or AlexaFluor 647 (Fisher) at 1:500 dilutions for 1 hour at room temperature. To stain nuclei, cells were incubated with 1:10000 Hoechst 33342 (Life Technologies) for 10 minutes in PBS, then washed twice more with PBS. Cells were preserved in Prolong Gold anti-fade reagent (Life Technologies) and imaged on a fluorescence microscope (Z1 Axio Observer Apotome, Zeiss). Mitochondrial length was quantified using an ImageJ mitochondrial morphometry plugin as described previously[64].

Flow cytometry analysis

Cells were incubated with 500 nM MitoTracker Red CMXRos, 10 uM MitoSOX Red, 5 uM CellROX Deep Red, or 250 nM MitoTracker Deep Red FM (all from ThermoFisher) for 1 hour at 37°C. Following a PBS wash, cells were dissociated with accutase then pipette triturated and analyzed on a BD Accuri C6 flow cytometer (BD Biosciences). Data was collected and analyzed using FlowJo single cell analysis software. GFP-expressing cells were gated based on a non-transduced control and the median fluorescence intensity from the appropriate detectors (CMXRos: FL3, MitoSOX: FL2, CellROX: FL4, MitoTracker Deep Red: FL4) was compared.

Cerebellar granule neuron (CGN) isolation and culturing

CGNs were isolated from 6- or 7-day-old 92Q SCA7 mice[20] as described[98]. Briefly, cerebella were dissected and dissociated through sequential trituration steps along with treatment with trypsin and DNase. CGNs are plated in Neurobasal A media supplemented with 1x B27, 20 mM KCl, and 0.5 mM L-glutamine on poly-D-lysine coated dishes. Cells were used for experiments after 10-14 days in culture.

Acknowledgements

Chapter 3, in part, will be part of a forthcoming manuscript being prepared for submission. Ward JM, Stoyas CA, Fan W, Evans R, Muotri AR, and La Spada AR. The dissertation author is the principal author of this work.

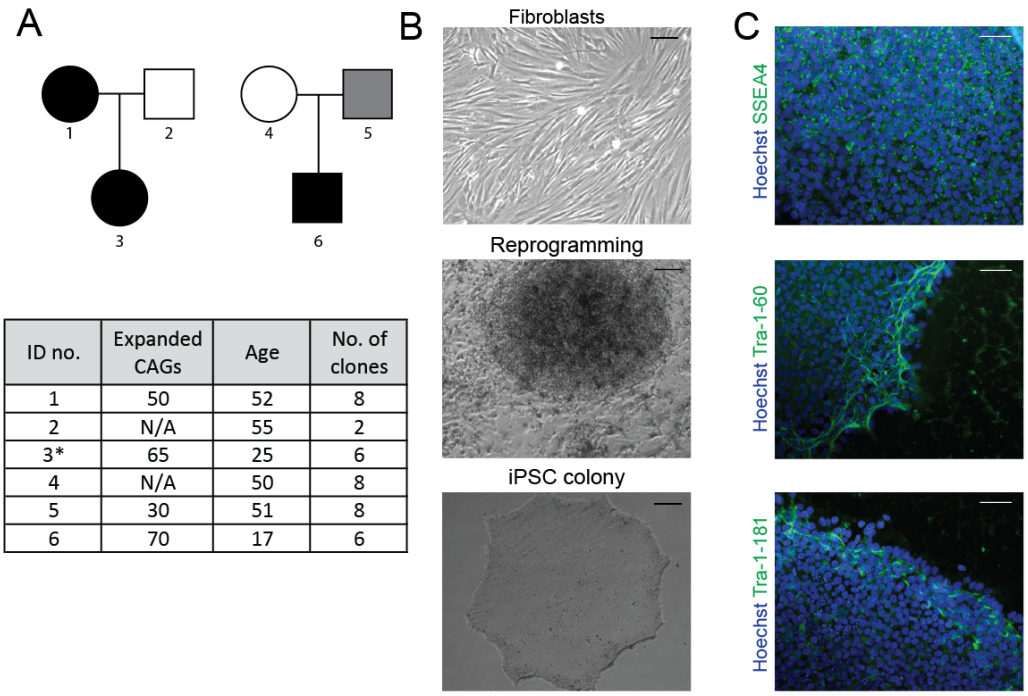

ID no.	Expanded CAGs	Age	No. of clones
1	50	52	8
2	N/A	55	2
3*	65	25	6
4	N/A	50	8
5	30	51	8
6	70	17	6

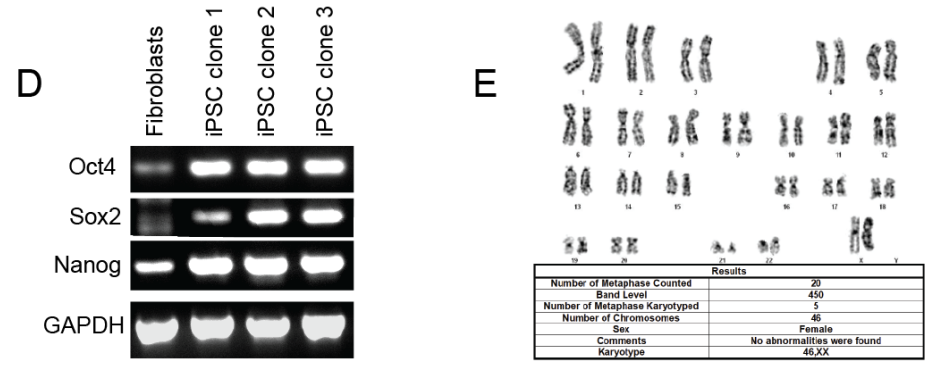

Results	
Number of Metaphase Counted	20
Band Level	450
Number of Metaphase Karyotyped	5
Number of Chromosomes	46
Sex	Female
Comments	No abnormalities were found
Karyotype	46,XX

Figure 3.1 iPSC derivation and characterization. **A** Pedigrees of SCA7 families. Circles represent females, squares represent males. Black shapes represent SCA7 patients with a pathogenic polyQ mutation, the gray shape represents an intermediate allele length, and unfilled shapes are unaffected controls. The numbers underneath each shape correspond with the identification number in the table below. This table indicates the length of the expanded CAG repeat (N/A, not applicable for control individuals), age (in years) when skin biopsy was taken, and number of clonal iPSC lines derived from fibroblast reprogramming. Asterisk indicates individual whose iPSC line were used for generating *ATXN7* knockout iPSCs. **B** Representative bright field images of fibroblasts (top), an iPSC colony arising on background of fibroblasts on day 19 of reprogramming (middle), and an iPSC colony at passage 10 (bottom). Scale bars, 200 um. **C** Representative images of iPSC colonies fixed and immunostained with antibodies to pluripotency markers SSEA4 (top), Tra-1-60 (middle), and Tra-1-81 (bottom). Scale bars, 40 um. **D** RNA was extracted from fibroblasts and different clonal lines of iPSCs, reverse transcribed to cDNA, and PCR amplified with primers against pluripotency genes Oct4, Sox2, and Nanog, with GAPDH as loading control. **E** Representative G-band karyotype analysis from one line of iPSCs.

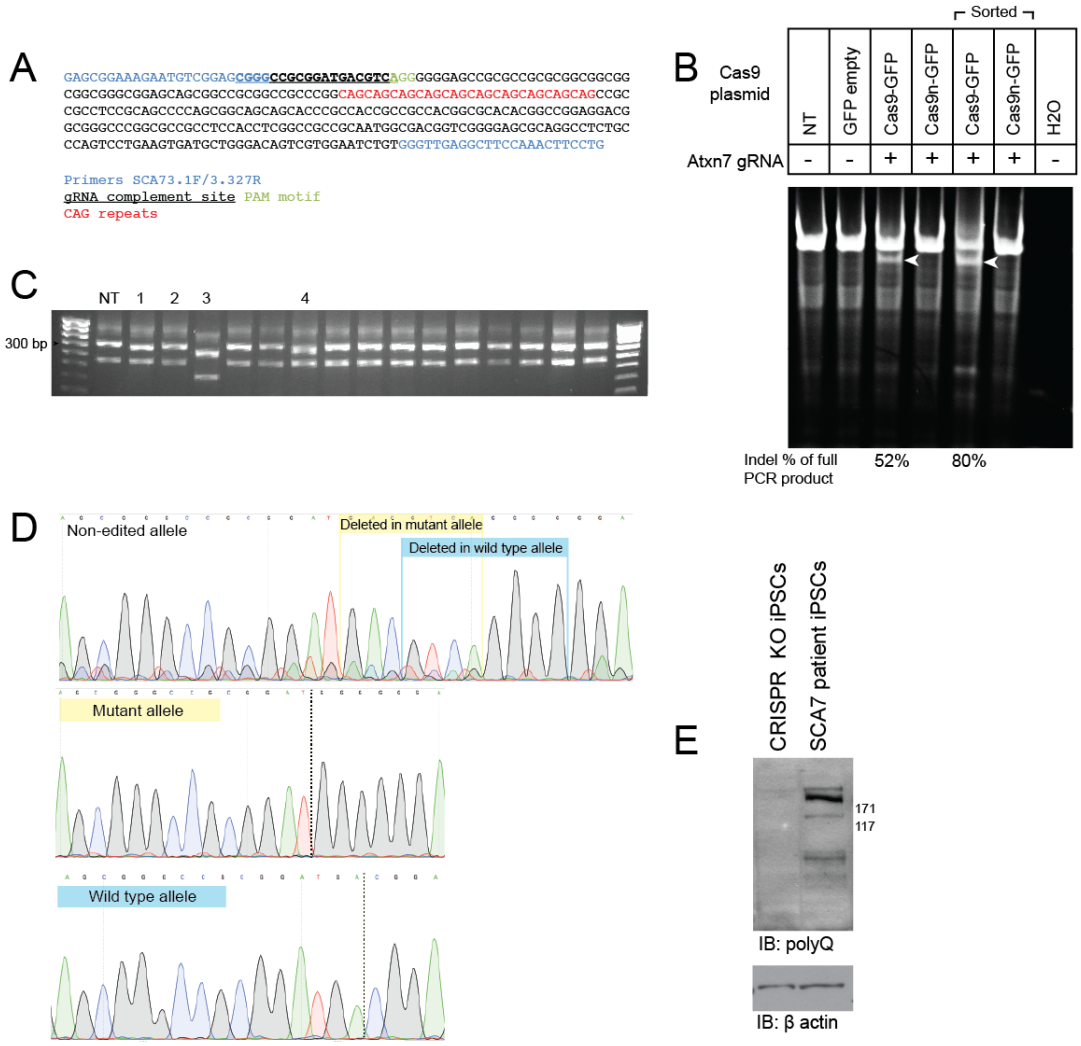

Figure 3.2 CRISPR/Cas9 *ATXN7* knockout characterization. A Diagram of a portion of the *ATXN7* gene amplified by primers in blue. gRNA is underlined and PAM motif is in green. Ten CAG repeats are indicated in red. **B** HEK cells were transfected with plasmids indicated in table above graph. Cells were selected for GFP expression using FACS (indicated above table), and all cells were collected and I performed a surveyor nuclease assay, products were run on an acrylamide gel. The prominent top band is the full length PCR product and white arrowhead indicates cleavage product. Percentage quantification of cleavage band to top band is indicated below gel. Cas9n is the Cas9D10A nickase. **C** Image of a set of PCR amplicons from individual clonal lines derived after guide RNA and Cas9 transfection that show small or large deletions in both alleles. NT, non-transfected; numbers of above certain wells correspond to the numbers in Table 3.1. **D** Chromatograms of normal and edited alleles in SCA7 patient iPSCs after CRISPR/Cas9 treatment. Top panel shows DNA sequence of a non-edited allele with overlays of deletions (in blue and yellow) caused by CRISPR/Cas9 shown in the panels below. Middle panel shows this same sequence in the 65Q allele following a 7 bp deletion (dotted line = yellow overlay above). Bottom panel indicates the same sequence in the 10Q allele with an 8 bp deletion (dotted line = blue overlay above). **D** Lysate from SCA7 patient iPSCs and those with deletion shown in C were immunoblotted with an antibody to polyQ, actin was used as loading control.

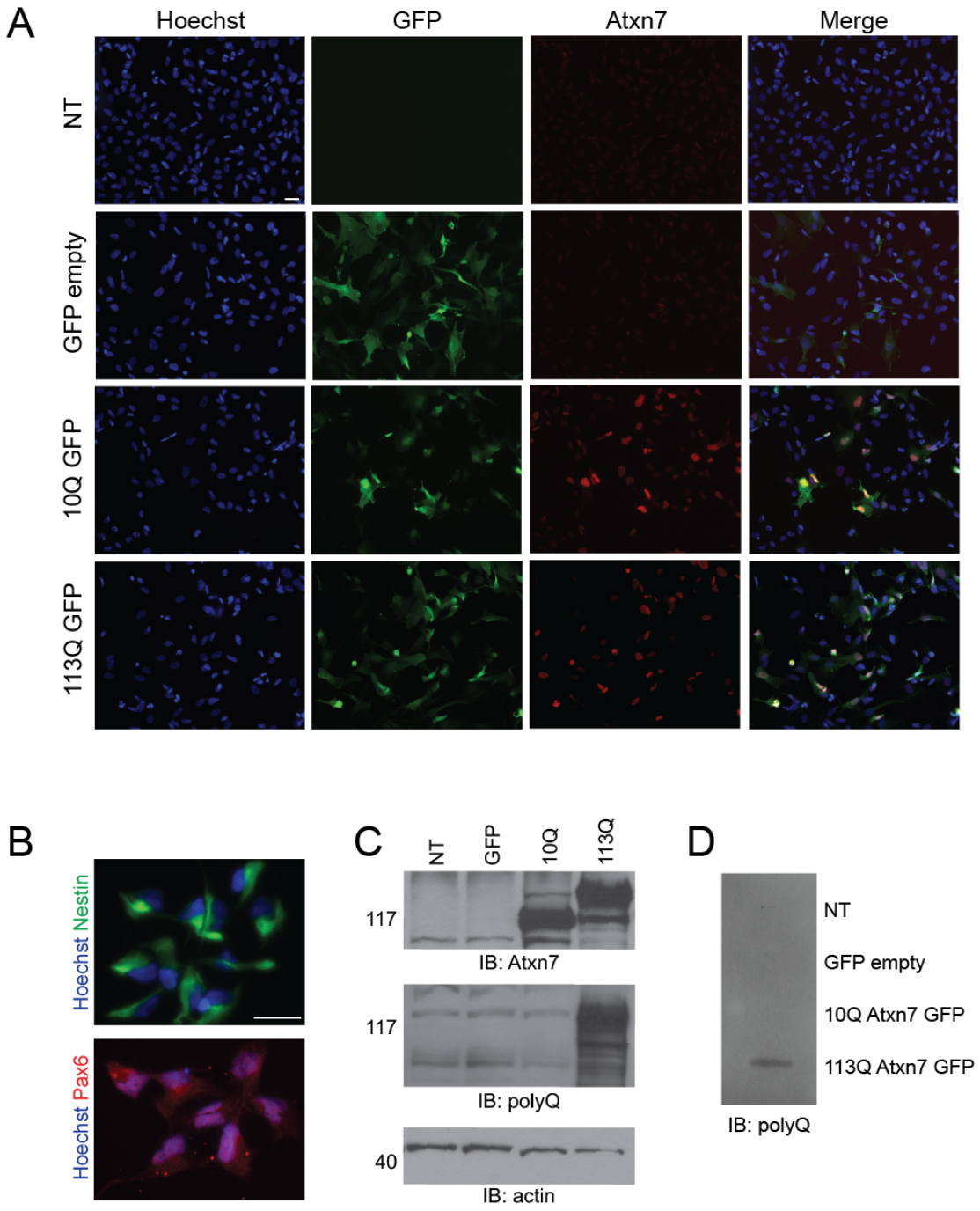

Figure 3.3 Characterization of transduced NPCs. A ATXN7KO NPCs were transduced with GFP empty, 10QATXN7-2A-EGFP, or 113QATXN7-2A-EGFP lentivirus. Non-transduced (NT) cells serve as control. After 48 hours, cells were fixed and immunostained with antibodies to GFP and ATXN7. **B** Representative image of NPCs immunostained with antibodies against Nestin and Pax6. Scale bar, 20 um. **C** Lysate from transduced cells was immunoblotted with antibodies to ATXN7 and polyQ. Beta actin was used as a loading control. **C** Lysates from transduced NPCs were run through a filter trap device, then immunoblotted with an antibody to polyQ.

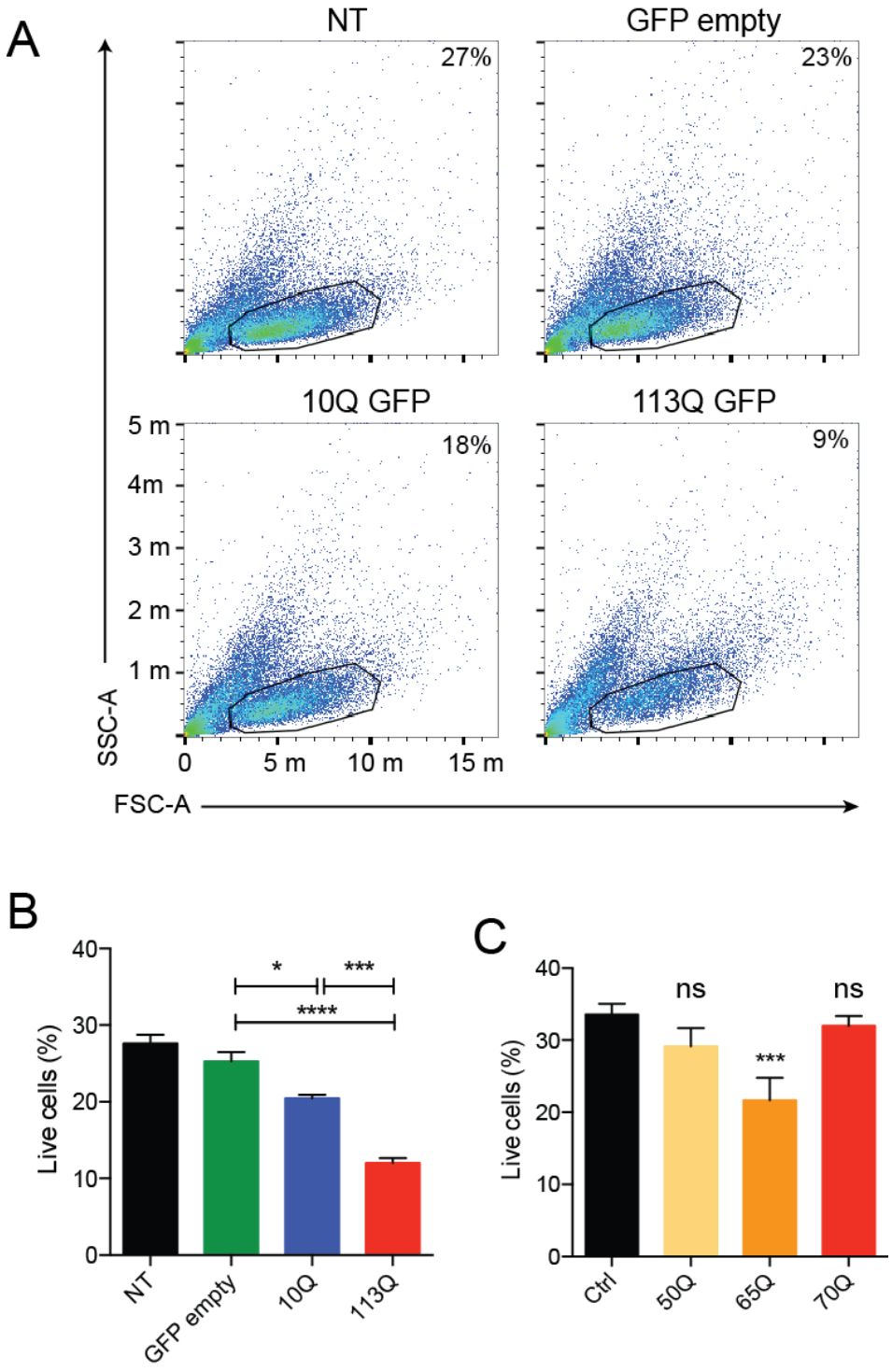

Figure 3.4 Decrease in live cells due to 113Q ATXN7 expression. A Representative plots of transduced NPCs that were analyzed by FACS for side scatter (SSC-A) and forward scatter (FSC-A). **B** Quantification of overall data as represented in **A. C** Quantification of live cells in patient NPC cultures. Data are shown as mean ± SEM, **P*≤0.05, ****P*≤*0*.001, *****P*≤0.0001, ns, not significant.

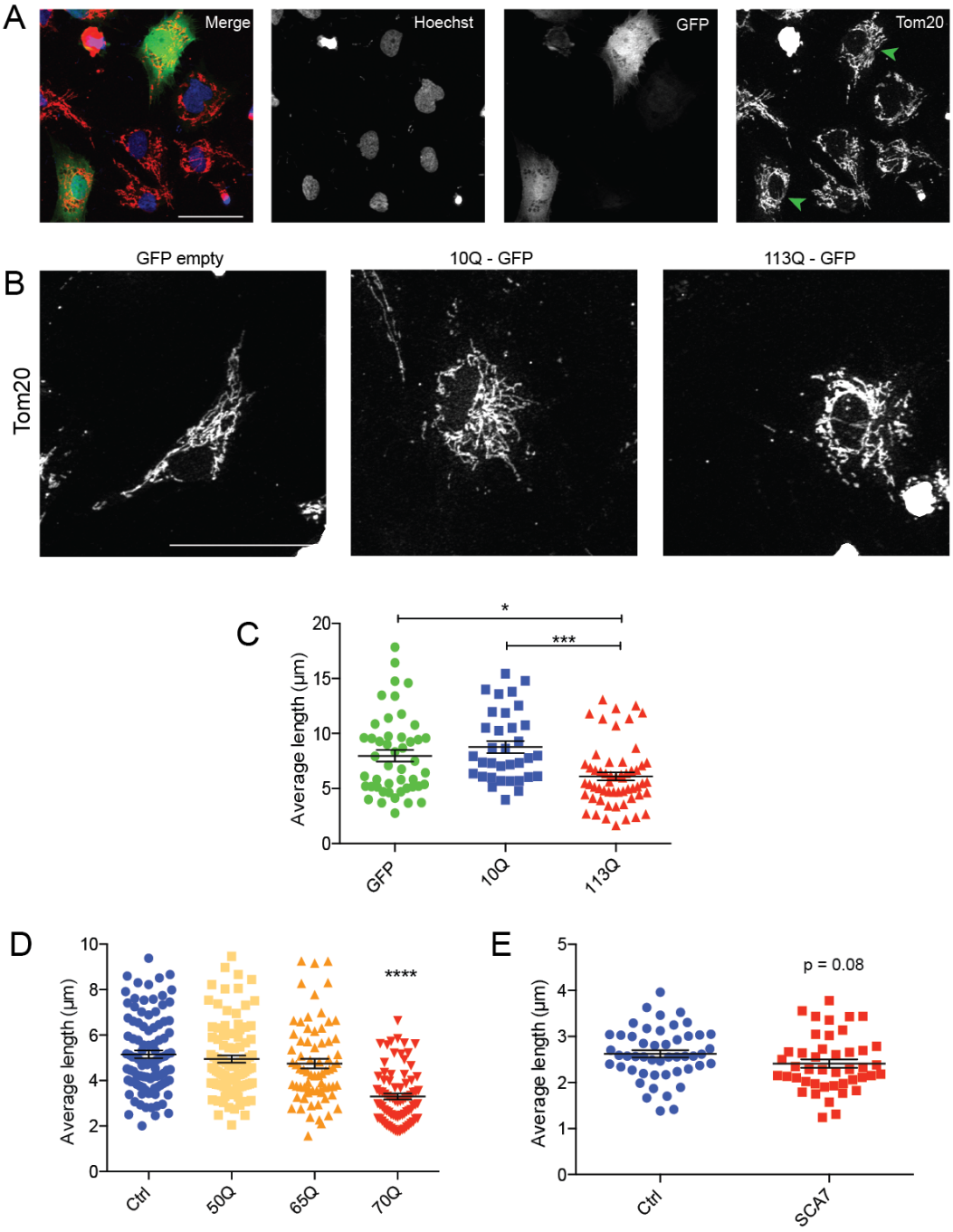

Figure 3.5 113Q NPCs have fragmented mitochondria. A Representative images of GFP expressing cells that were fixed and immunostained with antibodies to GFP and Tom20. Only GFP expressing cells were used in further quantification, as indicated by green arrowheads in last panel. **B** Representative mitochondrial Tom20 skeletonized signal in GFP empty, 10Q, or 113Q transduced NPCs. **C** Quantification of average mitochondrial length as represented in **B** based on ImageJ mitochondrial morphometry plugin. Quantification of average mitochondrial length of control and SCA7 patient NPCs (**D**) and cerebellar granule neurons (CGNs) derived from 92Q transgenic mice (**E**). Each dot represents an individual cell, data are represented as mean ± SEM, $n \geq 34$ cells per condition. *$P \leq 0.05$, ***$P \leq 0.001$. Scale bars, 20 um.

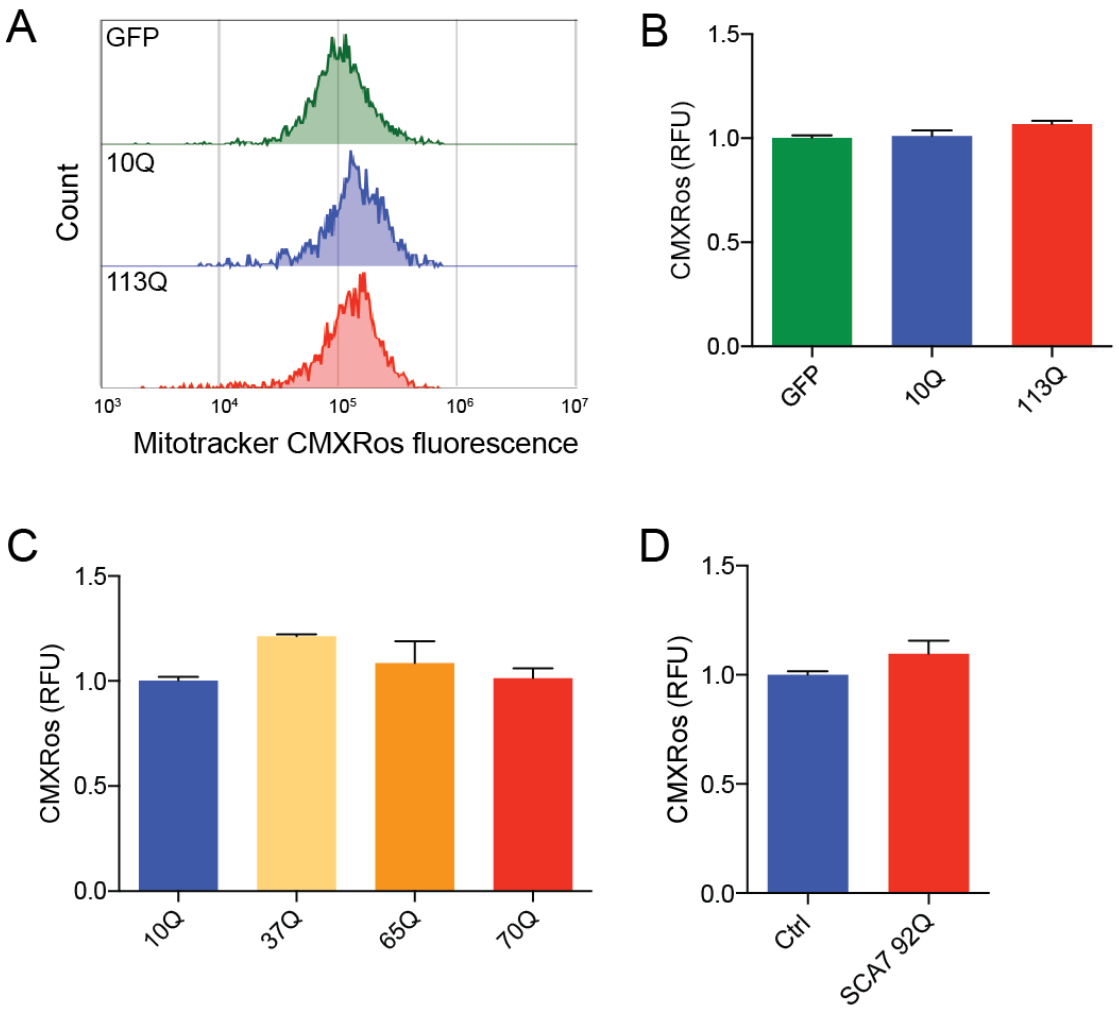

Figure 3.6 113Q NPCs do not differ in mitochondrial membrane potential. A Representative FACS plots of CMXRos fluorescence signal. Quantification of median fluorescence intensity of CMXRos stain in relative fluorescence units (RFU) from transduced NPCs (**B**), patient cells (**C**), and cerebellar granule neurons derived from 92Q transgenic mice (**D**)**.** Data are represented as mean ± SEM.

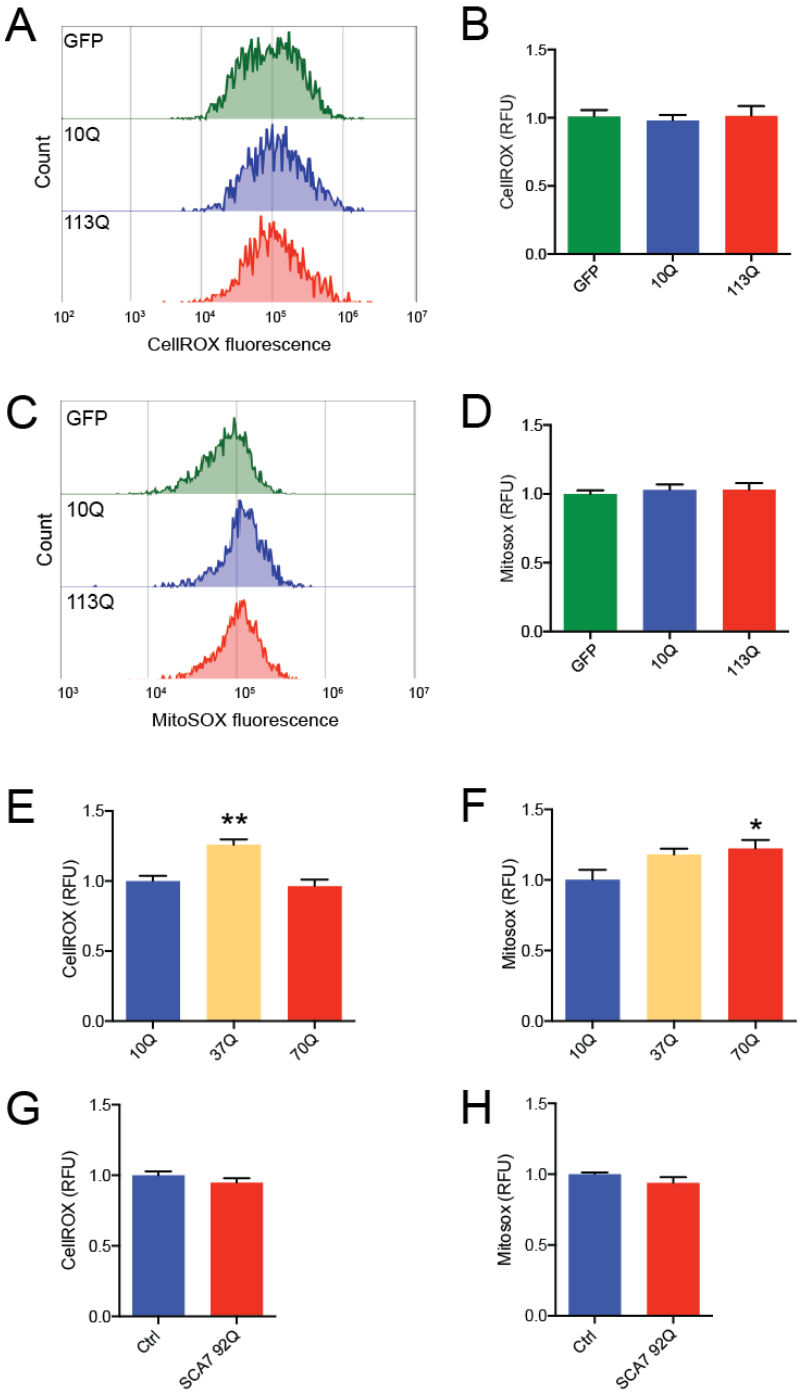

Figure 3.7 113Q NPCs show no difference in amount of reactive oxygen species. A Representative FACS plots of CellROX fluorescence signal. **B** Quantification of median fluorescence intensity of CellROX stain in relative fluorescence units (RFU) from transduced NPCs. **C** Representative FACS plots of MitoSOX fluorescence signal. **B** Quantification of median fluorescence intensity of MitoSOX stain in RFU from transduced NPCs. Quantification of median fluorescence intensity of CellROX stain and MitoSOX stain in patient NPCs (**E, F**, respectively) and cerebellar granule neurons derived from 92Q transgenic mice (**G, H**, respectively). Data are represented as mean ± SEM, *P≤0.05, **P≤0.01.

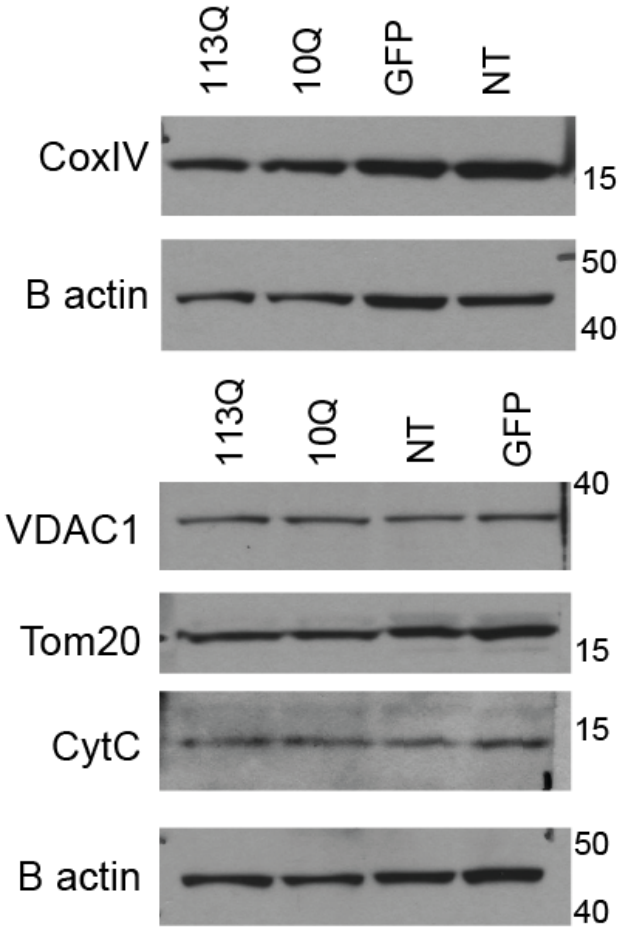

Figure 3.8 113Q NPCs do not differ in levels of mitochondrial proteins. Lysate from transduced NPCs were immunoblotted with antibodies against CoxIV, VDAC1, Tom20, and CytC. Beta actin was used as a loading control.

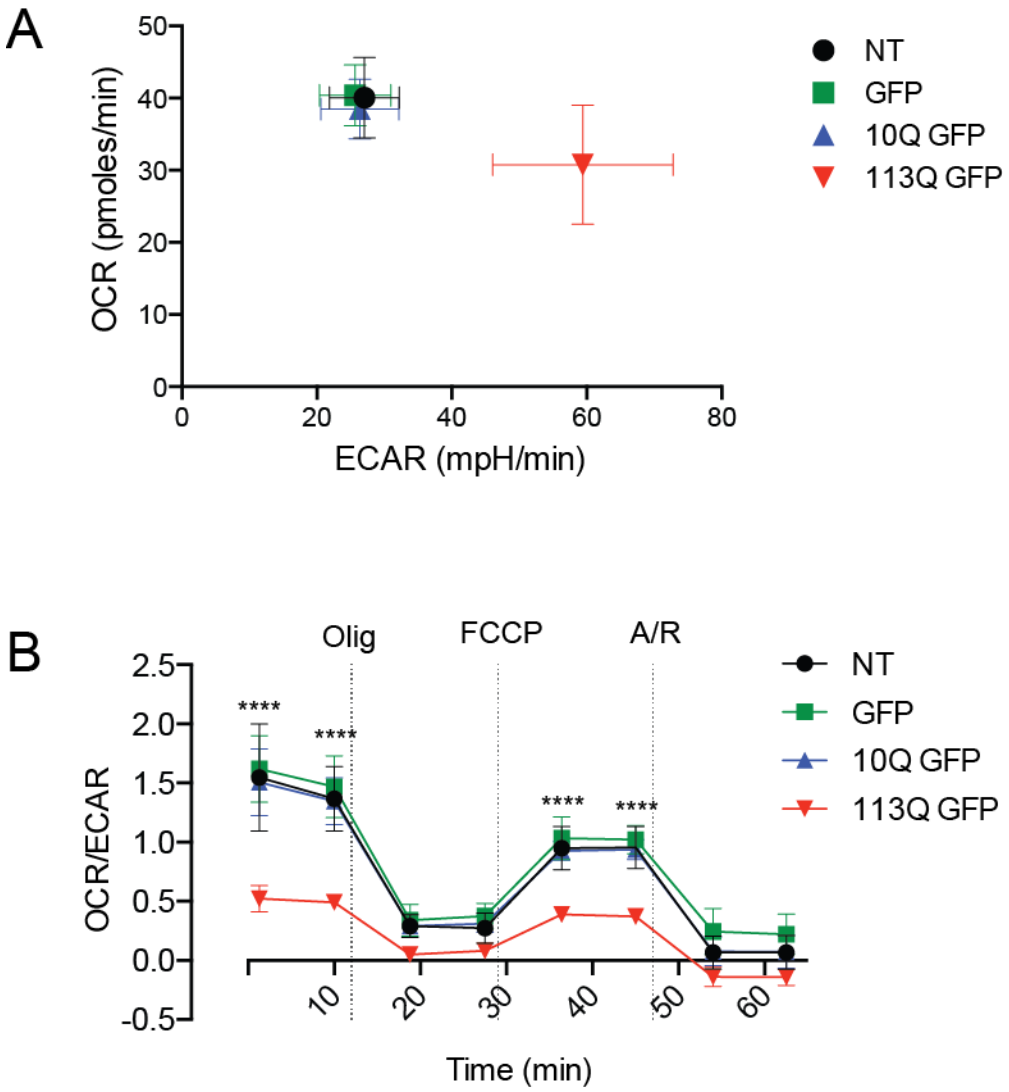

Figure 3.9 113Q cells exhibit decreased metabolic respiration. A Basal oxygen consumption rate (OCR) and extracellular acidification rate (ECAR) measurements of non-transduced, GFP empty, 10Q, or 113Q transduced NPCs, as assayed by Seahorse bioassay. **B** OCR to ECAR ratio of transduced NPCs with treatments of oligomycin, FCCP, or antimycin/rotenone (A/R) over time. Data are represented as mean ± SEM, ****$P \leq 0.0001$.

Table 3.1 Analysis of gene edited clonal lines. Clone number corresponds to bands shown in Figure 3.2c. Effect of induced mutations on protein predicted by http://sift.bii.a-star.edu.sg/index.html. Indel, insertion/deletion; AA, amino acid; NMD, nonsense mediated decay; KO, knockout.

Clone No.	Allele	Indel	Mutation type	NMD predicted?	Predicted effect at protein level
1	10 CAG	1 bp ins	Frameshift	Yes	Total KO
	65 CAG	40 bp del	Frameshift	Yes	
2	10 CAG	8 bp del	Frameshift	Yes	Total KO
	65 CAG	7 bp del	Frameshift	Yes	
3	10 CAG	121 bp del	Frameshift	Yes	Total KO
	65 CAG	67 bp del	Frameshift	Yes	
4	10 CAG	None	No change	No	Expression of WT protein
	65 CAG	60 bp del	AA deletion	No	Unknown effect on mutant protein

Chapter 4:

Transcriptional dysregulation of genes related to mitochondrial function in SCA7

Abstract

I have shown in both mouse and human cell models that mitochondrial dysfunction is a key feature of SCA7. However, the underlying the mechanism is not known. I hypothesized that mutant ataxin-7 causes transcriptional dysregulation of nuclear genes encoding proteins involved in mitochondrial function. To test this, I performed two separate bioinformatics analyses on microarray data from SCA7$^{266Q/5Q}$ and wild type (WT) mice cerebella. In the first analysis, I identified the most differentially expressed genes and performed pathway analysis on these genes. I found that there were no pathways significantly enriched in either the up- or down-regulated genes that were directly related to mitochondrial function. The second was to perform gene set enrichment analysis (GSEA), which takes a broader look at all of the genes on the microarray and analyzes the enrichment of a set of genes in one phenotype over another. Likewise in this analysis, I did not identify a gene set specific to mitochondrial function that was significantly enriched in the WT over the SCA7 data. While this hypothesis was not validated, I did find that the gene, Nicotinamide Nucleotide Adenylyltransferase 1 (*NMNAT1*), was downregulated. This led me to explore nicotinamide adenine dinucleotide (NAD) levels and has opened a new line of investigation. I propose further experiments to more specifically test transcriptional dysregulation and alternate hypotheses as well.

4.1 Introduction

Experiments in SCA7 mice and a human stem cell model have clearly associated mitochondrial dysfunction with SCA7 pathogenesis (Chapters 2 and 3). However, the underlying mechanism behind how polyQ ataxin-7 is interfering with mitochondria has yet to be elucidated. It is well established that ataxin-7 is a component of the human Spt3-Taf9-Ada-Gcn5 acetyltransferase (STAGA) complex[8,9]. STAGA is a transcriptional co-activator complex with histone acetyltransferase (HAT) and deubiquitinase (DUB) modules. Ataxin-7 plays a critical role in both of these epigenetic functions. It anchors the ubiquitin protease Usp22 to the rest of the complex[11], and its normal function is necessary for maintenance of the Gcn5-mediated HAT activity[9]. Both of these activities are important for transcriptional activation and when ataxin-7 contains a polyQ expansion these effects are abrogated.

There is no indication that ataxin-7 directly localizes to the mitochondria. Its nuclear function is well established, and there is evidence that it is also present to some extent in the cytoplasm[99,100]. I hypothesized that the most likely explanation for mitochondrial dysfunction would be due to transcriptional dysregulation of nuclear genes critical to mitochondria. The human mitochondrial genome contains 37 genes, but there are many more nuclear genes that are likewise critical to mitochondrial function. It is possible that the STAGA complex interacts with transcription factors critical to the transcription of these genes in order to promote mitochondrial function.

Alternatively, there could be a more indirect way in which STAGA, or its subunits, modify non-histone proteins that control mitochondrial gene transcription in their own right. One possibility is by modifying the activity of Sirt1. Sirt1 is a member of the sirtuin family of protein deacetylases that is modulated by levels of nicotinamide adenine dinucleotide (NAD). It has many functions, one of which is promoting mitochondrial biogenesis[101-103]. Indeed, Usp22 and Sirt1 have been shown to be direct interactors[104,105]. In Huntington's disease (HD), mitochondrial dysfunction is likewise linked to transcriptional dysregulation. In this case mutant huntingtin-induced transcriptional dysregulation is linked to PGC-1α, another transcriptional coactivator[42-44].

Regardless of mechanism, the goal of this work is to establish if transcriptional dysregulation is occurring at nuclear genes related to mitochondrial function. As described above, there are several avenues through which ataxin-7 dysfunction could control transcriptional regulation of these genes. These possibilities include STAGA's direct interaction with a transcription factor, or through non-histone interactions such as that with Sirt1. The purview of this work is to evaluate transcriptional dysregulation as an explanation for mitochondrial dysfunction. Further work will focus on establishing the protein interactions that are occurring. In order to establish if transcriptional dysregulation is occurring, I analyzed microarray data that had been acquired from the original SCA7$^{266Q/5Q}$ knock-in mice[106]. I performed two separate analyses on these data. The first was a pathway analysis of the most

differentially expressed genes, both downregulated and upregulated in SCA7. This was a stringent analysis of only those genes that were significantly different between the two sets of mice. The second analysis took a broader view through gene set enrichment analysis (GSEA). This method identifies whether a whole set of genes is enriched in one phenotype over another. It takes into account the entire data set of microarray probes, not those that are at the extremes of the expression list.

4.2 Results

Significantly differentially expressed genes

I obtained the normalized microarray data from 5 WT mice and 5 $SCA7^{266Q/5Q}$ knock-in mice through the National Center for Biotechnology Information (NCBI) Gene Expression Omnibus[106] (GEO) (no. GSE9914). This data was originally used to investigate the expression overlap of SCA1 and SCA7 mouse models[106]. The microarray was performed on RNA samples extracted from cerebella at a stage when the $SCA7^{266Q/5Q}$ mice are just beginning to exhibit symptoms (5 weeks). The first analysis consisted of analyzing the genes *most* upregulated and downregulated in the $SCA7^{266Q/5Q}$ mice compared to WT littermates. In brief, I selected the genes that were significantly ($p<0.05$) differentially expressed between the two conditions, and separated them based on upregulation or downregulation by fold change (Supplemental Tables 1 and 2). I then performed two different kinds of analyses: (1) Gene Ontology (Supplemental Tables 3 and 4) and (2)

Reactome Pathway analysis (Supplemental Table 5 and 6), to determine if any pathways related to mitochondria were significantly represented in these differentially expressed genes. The Reactome pathways that were identified as being significantly overrepresented ($p<0.05$) from the most differentially expressed genes are shown in Tables 4.1 and 4.2. Contrary to my hypothesis, none of the pathways identified through either method were directly linked to mitochondria. However, some of the top Reactome pathways that were significantly enriched in the downregulated genes in SCA7 are related to calcium handling (Cam-PDE1 activation, calmodulin induced events, CaM pathway, Ca-dependent events). Since mitochondria store calcium and regulate calcium signaling within the cell, this may indicate a specific pathway that could lead to mitochondrial dysfunction.

NMNAT1 is downregulated and cerebellar NAD+ is reduced in SCA7 mice

Another interesting finding is that the gene most downregulated in the SCA7 cerebellar samples was the nicotinamide nucleotide adenylyltransferase 1 (*NMNAT1*) gene. It encodes a protein critical in the biosynthesis of NAD, a cue for Sirt1. Interestingly, mutations in *NMNAT1* are associated with Leber's congenital amaurosis, a severe form of retinal degeneration[107]. I found that the SCA7 mice had significantly reduced NAD+ in their cerebellum (Figure 4.1a). There was a reduction in cortex, though not significant (Figure 4.1b) and no difference from WT in the liver (Figure 4.1c).

Gene set enrichment analysis

I posited that mitochondrial related genes might not be the most differentially expressed genes, but perhaps many genes related to mitochondria were slightly downregulated—leading to a combinatorial effect on mitochondrial function. To answer this question, I performed gene set enrichment analysis (GSEA), a method that identifies whether a given set of genes is enriched in one phenotype over another[108]. In brief, this type of analysis ranks all of the genes present on the microarray by phenotype. This list is then overlapped with a given set of genes (the "gene set") to determine if they are more represented in the top or bottom half of the list (compared to a randomly generated identical number of genes). I curated 27 gene sets (Table 4.3) from a variety of sources that were related to mitochondrial function in some way. There was one gene set, "REACTOME_RNA_POL_I_RNA POL_III_AND_MITOCHONDRIAL_TRANSCRIPTION", that was significantly enriched in WT over SCA7 ($p=0.0185$; more details provided in Supplemental Table 7). This gene set describes genes that are involved in RNA Polymerase I, RNA Polymerase III, and mitochondrial transcription. This gene set mainly represents gene products that are involved in transcribing rRNA, tRNA, and other small RNAs. Only 3 of the genes within the set are involved in mitochondrial transcription (TFAM, MTERF, POLRMT). Since this is the minority of the 97 genes within the set, the enrichment of these genes in WT over SCA7 implicates dysregulation of non-mRNA transcription more than it does genes important in the mitochondria.

4.3 Discussion

Based on this analysis it is not apparent that any specific set of genes with direct mitochondrial function are downregulated in the SCA7 cerebellum samples, contrary to my hypothesis[106]. It is important to keep in mind however, that the tissue used in this experiment was harvested from very early symptomatic mice. While I posited that mitochondrial gene transcriptional dysregulation would predate severe phenotypic effects, further studies should focus on transcriptional dysregulation of mice at later disease stages. However, the identification of calcium handling may signal an early effect that could lead to mitochondrial dysfunction. Calcium accumulation in mitochondria is a process relevant to intracellular calcium signaling (especially to the endoplasmic reticulum), but also metabolism and cell death[109]. Ongoing work in the lab is focused on functionally assessing calcium handling in SCA7 in relation to Sirt1, so it will be interesting to interrogate if this is intertwined with mitochondrial function.

While unexpected, the identification of NMNAT1 as being downregulated in SCA7 certainly leads me to consider some new connections between ataxin-7 and mitochondria. I observed that SCA7 mice have reduced cerebellar NAD+. I am currently working on verifying NMNAT1 transcript and protein levels in SCA7 mice and human NPCs. I expect that repression of the expression of this gene is likely responsible for reduced levels of NAD+. Less NAD+ could result in a number of consequences important to mitochondria. A model indicating the putative role of ataxin-7 and NMNAT1 is shown in Figure

4.2. In the nucleus, NAD+ is a direct cue for Sirt1. By decreasing Sirt1 activity, mitochondria could be affected through reduced activity of Sirt1 deacetylation targets such as PGC-1α and/or reduced mitophagy through Atg5/7 and the FoxO family of transcription factors[110]. Because the targets of Sirt1 are mostly transcription factors, I would still expect to see a downregulation of genes related to the mitochondria if these pathways were affected. But it is likely that the effect would not be obvious until later in SCA7 pathogenesis. This underscores the importance of performing transcriptional studies in older mice, which I plan to pursue. I am also currently pursuing rescue experiments to overexpress Sirt1 to see if the mitochondrial defects are, in fact, Sirt1 dependent.

NAD+ levels also have important implications directly in the mitochondria. NAD+ is a necessary component of the tricarboxylic acid (TCA) cycle, which reduces it to NADH. NADH is then fed in to the electron transport chain (ETC) to generate ATP. A reduction in levels of NAD+ would have direct consequences by diminishing the reducing equivalents used to generate ATP. NAD also serves as a cue for another sirtuin deacetylase in the mitochondria, Sirt3. Sirt3 has been shown to deacetylate and directly control the activity of complex I in the ETC[111]. Reduction in levels of cerebellar NAD+ would directly affect oxidative phosphorylation and the production of ATP in the mitochondria. What is less clear is how NMNAT1 may play a role in mitochondrial NAD+. Transcriptional downregulation of NMNAT1 would have direct effects on nuclear NAD+ levels and thereby on Sirt1. But mitochondria

have their own pool of NAD+, which can be made from its precursor, nicotinamide mononucleotide (NMN), by NMNAT3[112]. There is no indication that there is an NAD shuttle into the mitochondria[112]. It is possible that STAGA and ataxin-7 could affect transcription of all the NMNAT genes, including NMNAT3, which I am currently assessing. It is possible that the nuclear effects of NMNAT1 also affect NAD in the mitochondria, through an unidentified mechanism. The NAD analysis does not discriminate between different cellular pools of NAD+, but I think that mitochondrial NAD+ is most likely reduced due to the overall severity of the reduction (~35%). I am currently pursuing experiments to solidify this connection to NMNAT1 and ataxin-7.

Altogether, my analysis of transcriptional dysregulation of genes involved in mitochondrial function has yielded new avenues of investigation. Future studies will focus on performing this analysis in older mice as well as testing the involvement of NMNAT1 and Sirt1. These results have broadened the view of the possible mechanisms behind the mitochondrial dysfunction, and this could be occurring independent of direct transcriptional regulation of mitochondrial genes.

4.4 Experimental procedures

Differential gene expression analysis

Raw microarray was analyzed and normalized as indicated[106] and accessed through NCBI's Gene Expression Omnibus (accession number GSE9914, DataSet Record GDS3545). To determine significantly differentially

expressed genes, all the genes with a log2 expression value difference $p < 0.05$ were identified (596 total), and ranked based on fold change (SCA7/WT). Genes with fold change from 0.61 to 0.90 ("down" in SCA7) and 1.10 to 1.65 ("up" in SCA7) were submitted to Gene Ontology enrichment analysis (Gene Ontology Consortium, http://geneontology.org/page/go-enrichment-analysis) and Reactome pathway analysis (http://www.reactome.org/).

Gene set enrichment analysis

Gene set enrichment analysis (GSEA) was performed with 100 permutations by submitting all 22,690 (non-null) features from the normalized microarray values as a data set, in combination with 27 gene sets related to mitochondria (Table 4.3). Methods and invention of GSEA software is provided in Subramanian, et al. [108].

NAD analysis

Cerebellum, cortex, and liver tissue was harvested from 9 week old WT and SCA7 mice and snap frozen in liquid nitrogen. NAD+ levels were measured by HPLC as described previously[113].

Table 4.1 Reactome pathways identified in significantly downregulated genes in SCA7. Pathway identifier corresponds to number in the Reactome database. "#Entities found" are the number of genes submitted from the downregulated SCA7 genes represented in each pathway. "#Entities total" are the total number of genes involved in the pathway. FDR, false discovery rate. Asterisks indicate pathways related to calcium handling.

Pathway identifier	Pathway name	#Entities found	#Entities total	Entities ratio	Entities pValue	Entities FDR
R-HSA-111957	Cam-PDE 1 activation *	3	8	0.0007	0.0003	0.0271
R-HSA-1059683	Interleukin-6 signaling	3	16	0.0013	0.0024	0.0724
R-HSA-111933	Calmodulin induced events *	4	35	0.0029	0.0028	0.0724
R-HSA-111997	CaM pathway *	4	35	0.0029	0.0028	0.0724
R-HSA-111996	Ca-dependent events *	4	40	0.0033	0.0045	0.1116
R-HSA-1489509	DAG and IP3 signaling	4	45	0.0037	0.0067	0.1276
R-HSA-167021	PLC-gamma1 signalling	4	47	0.0039	0.0078	0.1403
R-HSA-212718	EGFR interacts with phospholipase C-gamma	4	47	0.0039	0.0078	0.1403
R-HSA-6783589	Interleukin-6 family signaling	3	32	0.0026	0.0161	0.2895
R-HSA-5654227	Phospholipase C-mediated cascade; FGFR3	4	60	0.0050	0.0176	0.3157
R-HSA-5654228	Phospholipase C-mediated cascade; FGFR4	4	61	0.0050	0.0186	0.3157
R-HSA-196819	Vitamin B1 (thiamin) metabolism	2	13	0.0011	0.0196	0.3297
R-HSA-112043	PLC beta mediated events	4	63	0.0052	0.0206	0.3297
R-HSA-112040	G-protein mediated events	4	64	0.0053	0.0217	0.3468
R-HSA-5654219	Phospholipase C-mediated cascade: FGFR1	4	64	0.0053	0.0217	0.3468
R-HSA-5654221	Phospholipase C-mediated cascade; FGFR2	4	67	0.0055	0.0251	0.3763
R-HSA-3108232	SUMO E3 ligases SUMOylate target proteins	5	103	0.0085	0.0281	0.4213
R-HSA-2990846	SUMOylation	5	111	0.0092	0.0369	0.5529
R-HSA-3108214	SUMOylation of DNA damage response and repair proteins	4	79	0.0065	0.0418	0.5807
R-HSA-1266695	Interleukin-7 signaling	2	20	0.0017	0.0431	0.5807
R-HSA-418457	cGMP effects	2	20	0.0017	0.0431	0.5807
R-HSA-2892247	POU5F1 (OCT4), SOX2, NANOG activate genes related to proliferation	2	21	0.0017	0.0470	0.5807
R-HSA-5683177	Defective ABCC8 can cause hypoglycemias and hyperglycemias	1	3	0.0002	0.0479	0.5807
R-HSA-5579020	Defective SLC35D1 causes Schneckenbecken dysplasia (SCHBCKD)	1	3	0.0002	0.0479	0.5807
R-HSA-5619107	Defective TRP may confer susceptibility towards thyroid papillary carcinoma (TPC)	1	3	0.0002	0.0479	0.5807

Table 4.2 Reactome pathways identified in significantly upregulated genes in SCA7. Pathway identifier corresponds to number in the Reactome database. "#Entities found" are the number of genes submitted from the upregulated SCA7 genes represented in each pathway. "#Entities total" are the total number of genes involved in the pathway. FDR, false discovery rate.

Pathway identifier	Pathway name	#Entities found	#Entities total	Entities ratio	Entities pValue	Entities FDR
R-HSA-264870	Caspase-mediated cleavage of cytoskeletal proteins	3	12	0.0010	0.0005	0.3919
R-HSA-3000171	Non-integrin membrane-ECM interactions	5	61	0.0050	0.0011	0.4363
R-HSA-2028269	Signaling by Hippo	3	22	0.0018	0.0028	0.4465
R-HSA-3000178	ECM proteoglycans	5	78	0.0064	0.0032	0.4465
R-HSA-3000170	Syndecan interactions	3	29	0.0024	0.0061	0.4465
R-HSA-1971475	A tetrasaccharide linker sequence is required for GAG synthesis	3	31	0.0026	0.0073	0.4465
R-HSA-1474244	Extracellular matrix organization	10	320	0.0264	0.0075	0.4465
R-HSA-1474228	Degradation of the extracellular matrix	6	145	0.0120	0.0104	0.4465
R-HSA-1442490	Collagen degradation	4	69	0.0057	0.0116	0.4465
R-HSA-8856828	Clathrin-mediated endocytosis	6	149	0.0123	0.0118	0.4465
R-HSA-111465	Apoptotic cleavage of cellular proteins	3	38	0.0031	0.0126	0.4465
R-HSA-157118	Signaling by NOTCH	6	153	0.0126	0.0133	0.4465
R-HSA-75035	Chk1/Chk2(Cds1) mediated inactivation of Cyclin B:Cdk1 complex	2	14	0.0012	0.0137	0.4465
R-HSA-390522	Striated Muscle Contraction	3	40	0.0033	0.0144	0.4465
R-HSA-3560782	Diseases associated with glycosaminoglycan metabolism	3	49	0.0040	0.0244	0.4465
R-HSA-216083	Integrin cell surface interactions	4	87	0.0072	0.0247	0.4465
R-HSA-6803207	TP53 Regulates Transcription of Caspase Activators and Caspases	2	20	0.0017	0.0266	0.4465
R-HSA-1912408	Pre-NOTCH Transcription and Translation	3	52	0.0043	0.0284	0.4465
R-HSA-3560801	Defective B3GAT3 causes JDSSDHD	2	21	0.0017	0.0291	0.4465
R-HSA-4420332	Defective B3GALT6 causes EDSP2 and SEMDJL1	2	21	0.0017	0.0291	0.4465
R-HSA-3560783	Defective B4GALT7 causes EDS, progeroid type	2	21	0.0017	0.0291	0.4465
R-HSA-75153	Apoptotic execution phase	3	55	0.0045	0.0327	0.4465
R-HSA-352238	Breakdown of the nuclear lamina	1	3	0.0002	0.0370	0.4465
R-HSA-2022090	Assembly of collagen fibrils and other multimeric structures	3	60	0.0050	0.0406	0.4465
R-HSA-194306	Neurophilin interactions with VEGF and VEGFR	1	4	0.0003	0.0490	0.4465
R-HSA-211736	Stimulation of the cell death response by PAK-2p34	1	4	0.0003	0.0490	0.4465

Table 4.3 Gene sets used in gene set enrichment analysis. These gene sets were curated from the molecular signatures database based on their connection to mitochondrial function.

GENE SET NAME	ORIGINAL SIZE	AFTER RESTRICTING TO DATASET
APOPTOTIC_MITOCHONDRIAL_CHANGES	19	18
BIOCARTA_MITOCHONDRIA_PATHWAY	44	34
GALLUZZI_PERMEABILIZE_MITOCHONDRIA	116	88
GALLUZZI_PREVENT_MITOCHONDIAL_PERMEABILIZATION	68	50
MITOCHONDRIAL_ENVELOPE	176	144
MITOCHONDRIAL_INNER_MEMBRANE	121	102
MITOCHONDRIAL_LUMEN	78	66
MITOCHONDRIAL_MATRIX	78	66
MITOCHONDRIAL_MEMBRANE	162	134
MITOCHONDRIAL_MEMBRANE_ORGANIZATION_AND_BIOGENESIS	33	22
MITOCHONDRIAL_MEMBRANE_PART	97	81
MITOCHONDRIAL_OUTER_MEMBRANE	40	31
MITOCHONDRIAL_PART	248	206
MITOCHONDRIAL_RESPIRATORY_CHAIN	53	44
MITOCHONDRIAL_RESPIRATORY_CHAIN_COMPLEX_I	33	28
MITOCHONDRIAL_RIBOSOME	35	30
MITOCHONDRIAL_SMALL_RIBOSOMAL_SUBUNIT	15	12
MITOCHONDRIAL_TRANSPORT	48	36
MITOCHONDRION	575	441
MITOCHONDRION_ORGANIZATION_AND_BIOGENESIS	98	77
MOOTHA_MITOCHONDRIA	847	653
PROTEIN_TARGETING_TO_MITOCHONDRION	20	17
REACTOME_MITOCHONDRIAL_FATTY_ACID_BETA_OXIDATION	20	19
REACTOME_MITOCHONDRIAL_PROTEIN_IMPORT	93	77
REACTOME_MITOCHONDRIAL_TRNA_AMINOACYLATION	26	12
REACTOME_RNA_POL_I_RNA_POL_III_AND_MITOCHONDRIAL_ TRANSCRIPTION	143	97
WONG_MITOCHONDRIA_GENE_MODULE	411	323

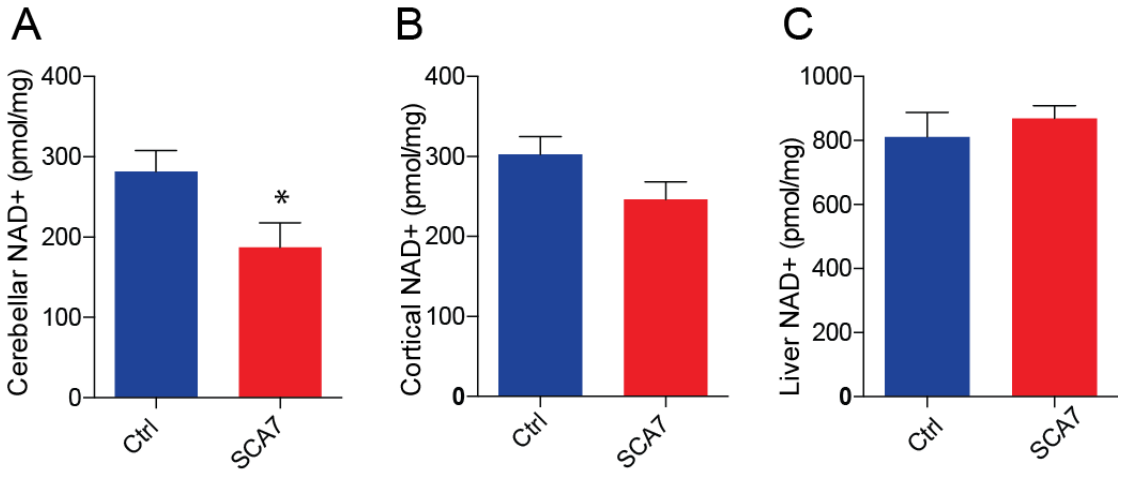

Figure 4.1 Cerebellar NAD+ is reduced in SCA7 mice. NAD+ was quantified from cerebellum (**A**), cortex (**B**), and liver (**C**) from control and SCA7 mice. Data are represented as mean ± SEM, *n* = 5 mice per genotype, *P≤0.05.

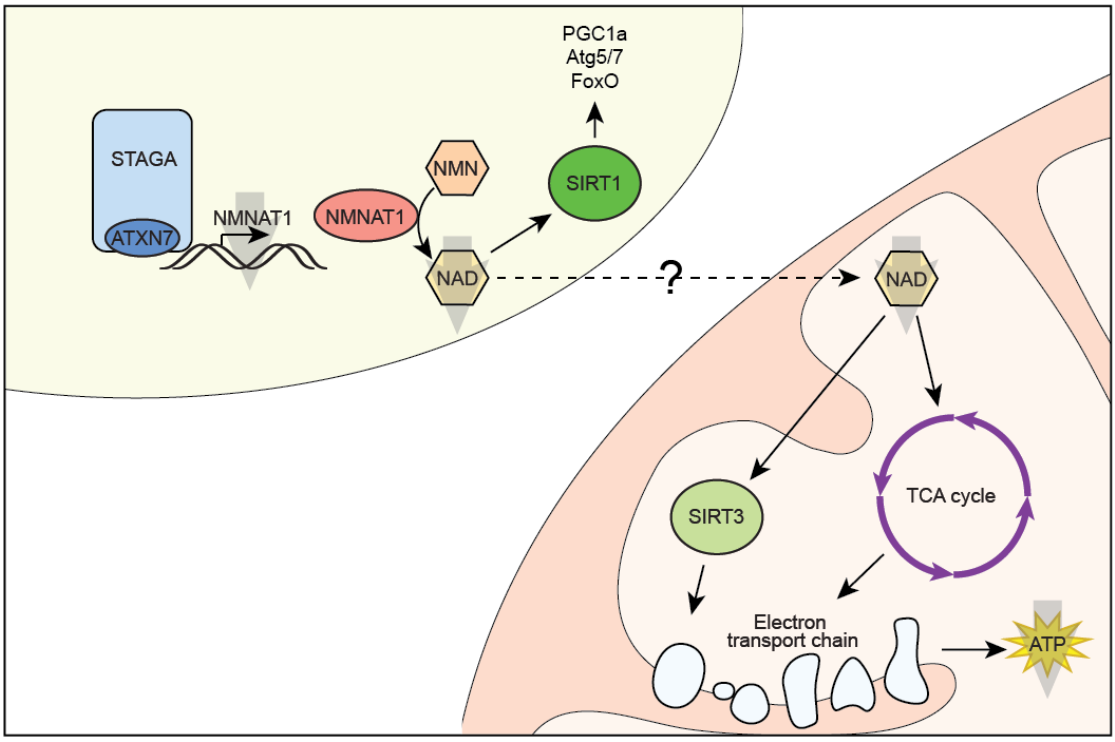

Figure 4.2 Model of potential effects of NMNAT1 downregulation and decreased NAD+ levels. This diagram depicts the putative role of ataxin-7 in *NMNAT1* transcription, its downstream effects, and the effects of reduced NAD+ levels. The transparent gray arrows indicate effects that I have observed in different models. I am in the process of testing the remaining processes. All abbreviations are defined within the text.

Chapter 5:

Summary and Future Directions

I have evaluated different models of SCA7 and established mitochondrial dysfunction as a novel feature in this disease. Using a new bioinformatics tool, I found that SCA7 clusters with and shares many clinical features of mitochondrial diseases. I found that Purkinje cells (PCs) from SCA7 knock-in mice have reduced mitochondrial content and more fragmented mitochondrial networks, as compared to control mice. Upon further interrogation of the mitochondrial ultrastructure, I observed an increase in larger individual mitochondria, which I speculate results from a compensatory response to make up for the decreased mitochondrial network length in the SCA7 mice. Functional analysis of these mice revealed that they have decreased metabolic respiration, a reduction in metabolic substrates, and lower ATP content in their cerebellum. The value of this work is a thorough description of mitochondrial and metabolic phenotypes in SCA7 mice. These mice have a very severe form of SCA7, similar to that seen in infantile-onset cases. Mitochondrial phenotypes are obvious here, as expected from the phenotypic features observed in the patients.

It remains to be determined whether these features are applicable to the more common adult-onset SCA7. In support of this possibility, liver and skeletal muscle biopsies from adult patients often have mitochondrial abnormalities[56-59], and the clinical presentation mimics that of some mitochondrial diseases[61]. I have begun performing studies on a 92Q mouse model, which exhibits a less severe form of the disease more specific to degeneration of the retina and cerebellum[20], to establish if these mice also

suffer from mitochondrial defects. A bacterial artificial chromosome (BAC) containing 92Q ataxin-7 was inserted into the translational start site of the murine prion protein (PrP) gene in these mice. Thus the expression is widespread throughout the central nervous system and select tissues in the periphery[20]. I have only begun these experiments, but an analysis of the glucose and adipose tissue in these 92Q mice indicate that there is not an obvious defect (data not shown). Since these mice are different both in mutation severity and expression, it is difficult to decouple what would cause these differences. It may be because mutant ataxin-7 is not expressed in all tissues as it is in the knock-in mice. I am coordinately pursuing follow-up studies in a novel model of SCA7 derived from the knock-in mice where a natural contraction was observed in a single mouse. This colony has been expanded and the mice exhibit an extension of lifespan is to 22-24 weeks. The mutation is estimated to be 210 CAGs, leading to a less severe form of SCA7. Through a combination of these approaches, I will gain a broader understanding of this dysfunction and can more specifically pinpoint whether mitochondrial dysfunction is a key feature of adult-onset SCA7.

To ensure that I am observing disease-specific effects, I used CRISPR gene editing to generate an isogenic system. My original goal was to rescue the mutation in patient cells through homologous recombination. While ideally I would introduce a double strand break (DSB) in the CAG repeat region, there are many CAG repetitive regions in the genome, and likely this would have generated many off-target effects. I designed and tested a guide RNA that is

as close to the CAG repeats as possible with the technology and information available at the time (2013). Now that gene-editing technology has advanced, it would be beneficial to revisit these experiments and pursue generating a mutation rescue in patient cells. This has been done through pure HR with Huntington's disease already[114].

Though my goal of contracting the CAG expansion in patient cells did not come to fruition, I was still able to use these cells to generate an isogenic model. I differentiated ataxin-7 knockout iPSCs to NPCs and then lentivirally expressed GFP empty, 10Q ataxin-7, or 113Q ataxin-7 to assess mitochondrial phenotypes. These cells had more fragmented mitochondrial networks, a trend I also observed in SCA7 patient NPCs. Mitochondrial fragmentation has been linked to defects in mitochondrial membrane polarization (MMP) as well. However, I did not observe any differences in MMP or reactive oxygen species (ROS) in transduced cells. This indicates that these effects are not always strictly intertwined. Mitochondrial fragmentation does directly link to metabolic respiration in this model, as the 113Q cells have a severely reduced rate of oxygen consumption. From multiple systems, it is becoming increasingly evident that fused mitochondrial networks are preferred during times of energy demand[66].

I am interested in investigating the role of mitophagy in this system as well. Mitochondrial fission is necessary for removal of damaged mitochondria through macroautophagy. If mitochondria are dysfunctional, it is possible that their fragmentation is an indicator of autophagic clearance of these damaged

organelles. I have obtained a reporter of *in vivo* mitophagy, a fluorescent mitochondrial-targeted reporter called mitoKeima, to express in NPCs to effectively assess mitophagy.

All of this work does lead to an open question: how, exactly, is mutant ataxin-7 causing mitochondrial dysfunction? My primary hypothesis, that mutant ataxin-7 leads to transcriptional dysregulation of genes critical to the mitochondria, was not unequivocally answered through analysis of microarray data from early symptomatic SCA7 mice. This does not entirely rule out transcriptional dysregulation, but I will have to dig deeper into these effects in late symptomatic mice. It is also possible that this type of analysis was not sensitive enough when the primary site of cerebellar dysfunction is the PCs. These cells constitute less than 1% of the cells in the cerebellum, whereas granule neurons make up the vast majority of cerebellar neuronal cells. To address these, I am considering laser capture microdissection to specifically isolate the PCs to perform RNA sequencing.

I also find it highly likely that these effects are related to Sirt1. Sirt1 is a converter of metabolic cues (NAD) into transcriptional output through deacetylating a vast array of other proteins—namely transcription factors and co-activators. NAD+ levels are reduced in the cerebellum, so this would provide a direct link for decreased Sirt1 activity. One of its pertinent targets is the regulator of mitochondrial biogenesis, PGC1α. There are many other Sirt1 targets that could result in mitochondrial dysfunction, including FOXO and PPAR family of transcription factors. I am pursuing experiments in SCA7 mice

crossed with Sirt1 overexpressing mice[115] to see if the observed mitochondrial defects are rescued in these bigenic mice. Again, these analyses will be performed at more symptomatic time points.

If, after a complete analysis, I do not find transcriptional dysregulation to be the culprit of mitochondrial dysfunction, then the explanation is inherently more complicated. Ataxin-7 is nuclear, and to some extent cytoplasmic[99,100], but there is no evidence that it directly localizes to the mitochondria and so it seems unlikely that it would directly be interfering with functions in this organelle. Another option to consider would be an aggregation of important mitochondrial proteins in polyQ aggregates, as has been seen in HD[116]. It is possible that these proteins are aberrantly localized to aggregates after being translated before they can appropriately shuttle to the mitochondria. Lastly, I am beginning to investigate the role of the mitochondrial unfolded protein response (mtUPR). Mitochondrial proteins are encoded both in the nucleus and the mitochondria. Chaperone proteins that assist in the proper folding and assembly of both sets of proteins are critical to proper mitochondrial function. There is also a recently elucidated connection between acute mitochondrial protein folding stress and reduced mitochondrial pre-RNA processing and translation of proteins localized to the mitochondrial matrix[117]. If the mitochondrial dysfunction is not transcriptional, it could be related to translation or protein folding stress caused by ataxin-7 polyQ aggregates.

I was very interested to observe that *NMNAT1* was the gene most significantly downregulated in SCA7 cerebellum. Interestingly, NMNAT1

deficiency leads to patients born with retinal dystrophy, and in some cases hypoplasia of the cerebellar vermis[118]. Ataxia is also observed in 10% of patients[119]. This could provide a link between polyQ expansion mutations in ataxin-7 repressing NMNAT-1 expression, which could lead to the reduction in NAD+ levels that I also observe. Reduced nuclear NAD+ would have direct effects on Sirt1 activity as outlined above. I am also interested in determining whether the NAD+ pool is reduced in the mitochondria. My current analysis measured total cellular NAD+ levels, but I could also specifically assess whether NAD+ is decreased in the mitochondria. I suspect this is the case, which would decrease Sirt3 activity as well as substrates necessary for the tricarboxylic acid (TCA) cycle, and thereby reduce activity of the electron transport chain and ATP production, as I have observed. While NMNAT1 does not directly control NAD+ levels in the mitochondria, it is possible that it could influence the mitochondrial pool through an unknown sensor mechanism. It is also possible that NMNAT3, the mitochondrial cousin of NMNAT1, is similarly affected by polyQ ataxin-7. I am currently in the process of testing and verifying these hypotheses. If this is the case, I could consider a genetic rescue of the SCA7 mitochondrial phenotypes with NMNAT1 overexpressing mice[120] or a pharmacological rescue with nicotinamide riboside (NR)[121], a precursor for NAD. The most salient rescue would be an amelioration of metabolic respiration—which could lead to a decrease in mitochondrial fragmentation.

In sum, my work here represents a significant step in understanding mitochondrial dysfunction as an important feature of SCA7. Both SCA7 mice and NPCs exhibit mitochondrial network fragmentation and decreased metabolic respiration. It is clear from ultrastructural analysis that SCA7 PCs have fewer mitochondria that are increased in size. My analysis of mitochondrial membrane potential and reactive oxygen species in cells indicated no obvious defect in this regard. There are still many questions remaining that need to be answered in pursuing this connection further, as outlined above. Ultimately, this link will add to our greater understanding of the biology of SCA7, as well as contribute to the greater neurodegenerative field. The importance of mitochondria in neurodegenerative disease is becoming more and more evident, and this work positions SCA7 within this burgeoning field. I am hopeful that the emerging trend of considering mitochondrial health as a neurodegenerative therapeutic target could ultimately extend to SCA7 in the future.

References

1 Martin, J. J., Vanregemorter, N., Krols, L., Brucher, J. M., Debarsy, T., Szliwowski, H., Evrard, P., Ceuterick, C., Tassignon, M. J., Smetdieleman, H., Hayezdelatte, F., Willems, P. J. & Van Broeckhoven, C. On an Autosomal-Dominant Form of Retinal-Cerebellar Degeneration - an Autopsy Study of 5 Patients in One Family. *Acta Neuropathol* **88**, 277-286 (1994).

2 Filla, A., Mariotti, C., Caruso, G., Coppola, G., Cocozza, S., Castaldo, I., Calabrese, O., Salvatore, E., De Michele, G., Riggio, M. C., Pareyson, D., Gellera, C. & Di Donato, S. Relative frequencies of CAG expansions in spinocerebellar ataxia and dentatorubropallidoluysian atrophy in 116 Italian families. *Eur Neurol* **44**, 31-36, doi:8189 (2000).

3 Storey, E., du Sart, D., Shaw, J. H., Lorentzos, P., Kelly, L., McKinley Gardner, R. J., Forrest, S. M., Biros, I. & Nicholson, G. A. Frequency of spinocerebellar ataxia types 1, 2, 3, 6, and 7 in Australian patients with spinocerebellar ataxia. *Am J Med Genet* **95**, 351-357 (2000).

4 David, G., Abbas, N., Stevanin, G., Durr, A., Yvert, G., Cancel, G., Weber, C., Imbert, G., Saudou, F., Antoniou, E., Drabkin, H., Gemmill, R., Giunti, P., Benomar, A., Wood, N., Ruberg, M., Agid, Y., Mandel, J. L. & Brice, A. Cloning of the SCA7 gene reveals a highly unstable CAG repeat expansion. *Nat Genet* **17**, 65-70, doi:10.1038/ng0997-65 (1997).

5 Stevanin, G., Durr, A. & Brice, A. Clinical and molecular advances in autosomal dominant cerebellar ataxias: from genotype to phenotype and physiopathology. *Eur J Hum Genet* **8**, 4-18, doi:10.1038/sj.ejhg.5200403 (2000).

6 Dion, V. & Wilson, J. H. Instability and chromatin structure of expanded trinucleotide repeats. *Trends Genet* **25**, 288-297, doi:10.1016/j.tig.2009.04.007 (2009).

7 David, G., Durr, A., Stevanin, G., Cancel, G., Abbas, N., Benomar, A., Belal, S., Lebre, A. S., Abada-Bendib, M., Grid, D., Holmberg, M., Yahyaoui, M., Hentati, F., Chkili, T., Agid, Y. & Brice, A. Molecular and clinical correlations in autosomal dominant cerebellar ataxia with progressive macular dystrophy (SCA7). *Hum Mol Genet* **7**, 165-170 (1998).

8 Martinez, E., Kundu, T. K., Fu, J. & Roeder, R. G. A human SPT3-TAFII31-GCN5-L acetylase complex distinct from transcription factor IID. *J Biol Chem* **273**, 23781-23785 (1998).

9 Palhan, V. B., Chen, S., Peng, G. H., Tjernberg, A., Gamper, A. M., Fan, Y., Chait, B. T., La Spada, A. R. & Roeder, R. G. Polyglutamine-expanded ataxin-7 inhibits STAGA histone acetyltransferase activity to produce retinal degeneration. *Proc Natl Acad Sci U S A* **102**, 8472-8477, doi:10.1073/pnas.0503505102 (2005).

10 Fry, C. J. & Peterson, C. L. Transcription. Unlocking the gates to gene expression. *Science* **295**, 1847-1848, doi:10.1126/science.1070260 (2002).

11 Zhao, Y., Lang, G., Ito, S., Bonnet, J., Metzger, E., Sawatsubashi, S., Suzuki, E., Le Guezennec, X., Stunnenberg, H. G., Krasnov, A., Georgieva, S. G., Schule, R., Takeyama, K., Kato, S., Tora, L. & Devys, D. A TFTC/STAGA module mediates histone H2A and H2B deubiquitination, coactivates nuclear receptors, and counteracts heterochromatin silencing. *Mol Cell* **29**, 92-101, doi:10.1016/j.molcel.2007.12.011 (2008).

12 McCullough, S. D., Xu, X., Dent, S. Y., Bekiranov, S., Roeder, R. G. & Grant, P. A. Reelin is a target of polyglutamine expanded ataxin-7 in human spinocerebellar ataxia type 7 (SCA7) astrocytes. *Proc Natl Acad Sci U S A* **109**, 21319-21324, doi:10.1073/pnas.1218331110 (2012).

13 Lan, X., Koutelou, E., Schibler, A. C., Chen, Y. C., Grant, P. A. & Dent, S. Y. Poly(Q) Expansions in ATXN7 Affect Solubility but Not Activity of the SAGA Deubiquitinating Module. *Mol Cell Biol* **35**, 1777-1787, doi:10.1128/MCB.01454-14 (2015).

14 Yoo, S. Y., Pennesi, M. E., Weeber, E. J., Xu, B., Atkinson, R., Chen, S., Armstrong, D. L., Wu, S. M., Sweatt, J. D. & Zoghbi, H. Y. SCA7 knockin mice model human SCA7 and reveal gradual accumulation of mutant ataxin-7 in neurons and abnormalities in short-term plasticity. *Neuron* **37**, 383-401 (2003).

15 Whitney, A., Lim, M., Kanabar, D. & Lin, J. P. Massive SCA7 expansion detected in a 7-month-old male with hypotonia, cardiomegaly, and renal compromise. *Dev Med Child Neurol* **49**, 140-143, doi:10.1111/j.1469-8749.2007.00140.x (2007).

16 van de Warrenburg, B. P., Frenken, C. W., Ausems, M. G., Kleefstra, T., Sinke, R. J., Knoers, N. V. & Kremer, H. P. Striking anticipation in spinocerebellar ataxia type 7: the infantile phenotype. *J Neurol* **248**, 911-914 (2001).

17 Ansorge, O., Giunti, P., Michalik, A., Van Broeckhoven, C., Harding, B., Wood, N. & Scaravilli, F. Ataxin-7 aggregation and ubiquitination in infantile SCA7 with 180 CAG repeats. *Ann Neurol* **56**, 448-452, doi:10.1002/ana.20230 (2004).

18 La Spada, A. R., Fu, Y. H., Sopher, B. L., Libby, R. T., Wang, X., Li, L. Y., Einum, D. D., Huang, J., Possin, D. E., Smith, A. C., Martinez, R. A., Koszdin, K. L., Treuting, P. M., Ware, C. B., Hurley, J. B., Ptacek, L. J. & Chen, S. Polyglutamine-expanded ataxin-7 antagonizes CRX function and induces cone-rod dystrophy in a mouse model of SCA7. *Neuron* **31**, 913-927 (2001).

19 Garden, G. A., Libby, R. T., Fu, Y. H., Kinoshita, Y., Huang, J., Possin, D. E., Smith, A. C., Martinez, R. A., Fine, G. C., Grote, S. K., Ware, C. B., Einum, D. D., Morrison, R. S., Ptacek, L. J., Sopher, B. L. & La Spada, A. R. Polyglutamine-expanded ataxin-7 promotes non-cell-autonomous purkinje cell degeneration and displays proteolytic cleavage in ataxic transgenic mice. *J Neurosci* **22**, 4897-4905 (2002).

20 Furrer, S. A., Mohanachandran, M. S., Waldherr, S. M., Chang, C., Damian, V. A., Sopher, B. L., Garden, G. A. & La Spada, A. R. Spinocerebellar ataxia type 7 cerebellar disease requires the coordinated action of mutant ataxin-7 in neurons and glia, and displays non-cell-autonomous bergmann glia degeneration. *J Neurosci* **31**, 16269-16278, doi:10.1523/JNEUROSCI.4000-11.2011 (2011).

21 Takahashi, K. & Yamanaka, S. Induction of pluripotent stem cells from mouse embryonic and adult fibroblast cultures by defined factors. *Cell* **126**, 663-676, doi:10.1016/j.cell.2006.07.024 (2006).

22 Takahashi, K., Tanabe, K., Ohnuki, M., Narita, M., Ichisaka, T., Tomoda, K. & Yamanaka, S. Induction of pluripotent stem cells from adult human fibroblasts by defined factors. *Cell* **131**, 861-872, doi:10.1016/j.cell.2007.11.019 (2007).

23 Papp, B. & Plath, K. Epigenetics of reprogramming to induced pluripotency. *Cell* **152**, 1324-1343, doi:10.1016/j.cell.2013.02.043 (2013).

24 Sandoe, J. & Eggan, K. Opportunities and challenges of pluripotent stem cell neurodegenerative disease models. *Nat Neurosci* **16**, 780-789, doi:10.1038/nn.3425 (2013).

25 Marraffini, L. A. & Sontheimer, E. J. CRISPR interference: RNA-directed adaptive immunity in bacteria and archaea. *Nat Rev Genet* **11**, 181-190, doi:10.1038/nrg2749 (2010).

26 Mali, P., Yang, L., Esvelt, K. M., Aach, J., Guell, M., DiCarlo, J. E., Norville, J. E. & Church, G. M. RNA-guided human genome engineering via Cas9. *Science* **339**, 823-826, doi:10.1126/science.1232033 (2013).

27 Cong, L., Ran, F. A., Cox, D., Lin, S., Barretto, R., Habib, N., Hsu, P. D., Wu, X., Jiang, W., Marraffini, L. A. & Zhang, F. Multiplex genome engineering using CRISPR/Cas systems. *Science* **339**, 819-823, doi:10.1126/science.1231143 (2013).

28 Marchetto, M. C., Brennand, K. J., Boyer, L. F. & Gage, F. H. Induced pluripotent stem cells (iPSCs) and neurological disease modeling: progress and promises. *Hum Mol Genet* **20**, R109-115, doi:10.1093/hmg/ddr336 (2011).

29 Han, S. S., Williams, L. A. & Eggan, K. C. Constructing and deconstructing stem cell models of neurological disease. *Neuron* **70**, 626-644, doi:10.1016/j.neuron.2011.05.003 (2011).

30 Temple, S. Division and differentiation of isolated CNS blast cells in microculture. *Nature* **340**, 471-473, doi:10.1038/340471a0 (1989).

31 Reynolds, B. A. & Weiss, S. Generation of neurons and astrocytes from isolated cells of the adult mammalian central nervous system. *Science* **255**, 1707-1710 (1992).

32 Zhang, S. C., Wernig, M., Duncan, I. D., Brustle, O. & Thomson, J. A. In vitro differentiation of transplantable neural precursors from human embryonic stem cells. *Nat Biotechnol* **19**, 1129-1133, doi:10.1038/nbt1201-1129 (2001).

33 Stein, J. L., de la Torre-Ubieta, L., Tian, Y., Parikshak, N. N., Hernandez, I. A., Marchetto, M. C., Baker, D. K., Lu, D., Hinman, C. R., Lowe, J. K., Wexler, E. M., Muotri, A. R., Gage, F. H., Kosik, K. S. & Geschwind, D. H. A quantitative framework to evaluate modeling of cortical development by neural stem cells. *Neuron* **83**, 69-86, doi:10.1016/j.neuron.2014.05.035 (2014).

34 Sterneckert, J. L., Reinhardt, P. & Scholer, H. R. Investigating human disease using stem cell models. *Nat Rev Genet* **15**, 625-639, doi:10.1038/nrg3764 (2014).

35 Cortes, C. J., Miranda, H. C., Frankowski, H., Batlevi, Y., Young, J. E., Le, A., Ivanov, N., Sopher, B. L., Carromeu, C., Muotri, A. R., Garden, G. A. & La Spada, A. R. Polyglutamine-expanded androgen receptor interferes with TFEB to elicit autophagy defects in SBMA. *Nat Neurosci* **17**, 1180-1189, doi:10.1038/nn.3787 (2014).

36 Consortium, H. D. i. Induced pluripotent stem cells from patients with Huntington's disease show CAG-repeat-expansion-associated phenotypes. *Cell Stem Cell* **11**, 264-278, doi:10.1016/j.stem.2012.04.027 (2012).

37 Cooper, O., Seo, H., Andrabi, S., Guardia-Laguarta, C., Graziotto, J., Sundberg, M., McLean, J. R., Carrillo-Reid, L., Xie, Z., Osborn, T., Hargus, G., Deleidi, M., Lawson, T., Bogetofte, H., Perez-Torres, E., Clark, L., Moskowitz, C., Mazzulli, J., Chen, L., Volpicelli-Daley, L., Romero, N., Jiang, H., Uitti, R. J., Huang, Z., Opala, G., Scarffe, L. A., Dawson, V. L., Klein, C., Feng, J., Ross, O. A., Trojanowski, J. Q., Lee,

V. M., Marder, K., Surmeier, D. J., Wszolek, Z. K., Przedborski, S., Krainc, D., Dawson, T. M. & Isacson, O. Pharmacological rescue of mitochondrial deficits in iPSC-derived neural cells from patients with familial Parkinson's disease. *Sci Transl Med* **4**, 141ra190, doi:10.1126/scitranslmed.3003985 (2012).

38 Lin, M. T. & Beal, M. F. Mitochondrial dysfunction and oxidative stress in neurodegenerative diseases. *Nature* **443**, 787-795, doi:10.1038/nature05292 (2006).

39 Jenkins, B. G., Koroshetz, W. J., Beal, M. F. & Rosen, B. R. Evidence for impairment of energy metabolism in vivo in Huntington's disease using localized 1H NMR spectroscopy. *Neurology* **43**, 2689-2695 (1993).

40 Gu, M., Gash, M. T., Mann, V. M., Javoy-Agid, F., Cooper, J. M. & Schapira, A. H. Mitochondrial defect in Huntington's disease caudate nucleus. *Ann Neurol* **39**, 385-389, doi:10.1002/ana.410390317 (1996).

41 Panov, A. V., Gutekunst, C. A., Leavitt, B. R., Hayden, M. R., Burke, J. R., Strittmatter, W. J. & Greenamyre, J. T. Early mitochondrial calcium defects in Huntington's disease are a direct effect of polyglutamines. *Nat Neurosci* **5**, 731-736, doi:10.1038/nn884 (2002).

42 Weydt, P., Pineda, V. V., Torrence, A. E., Libby, R. T., Satterfield, T. F., Lazarowski, E. R., Gilbert, M. L., Morton, G. J., Bammler, T. K., Strand, A. D., Cui, L., Beyer, R. P., Easley, C. N., Smith, A. C., Krainc, D., Luquet, S., Sweet, I. R., Schwartz, M. W. & La Spada, A. R. Thermoregulatory and metabolic defects in Huntington's disease transgenic mice implicate PGC-1alpha in Huntington's disease neurodegeneration. *Cell Metab* **4**, 349-362, doi:10.1016/j.cmet.2006.10.004 (2006).

43 Cui, L., Jeong, H., Borovecki, F., Parkhurst, C. N., Tanese, N. & Krainc, D. Transcriptional repression of PGC-1alpha by mutant huntingtin leads to mitochondrial dysfunction and neurodegeneration. *Cell* **127**, 59-69, doi:10.1016/j.cell.2006.09.015 (2006).

44 Tsunemi, T., Ashe, T. D., Morrison, B. E., Soriano, K. R., Au, J., Roque, R. A., Lazarowski, E. R., Damian, V. A., Masliah, E. & La Spada, A. R.

PGC-1alpha rescues Huntington's disease proteotoxicity by preventing oxidative stress and promoting TFEB function. *Sci Transl Med* **4**, 142ra197, doi:10.1126/scitranslmed.3003799 (2012).

45 Ranganathan, S., Harmison, G. G., Meyertholen, K., Pennuto, M., Burnett, B. G. & Fischbeck, K. H. Mitochondrial abnormalities in spinal and bulbar muscular atrophy. *Hum Mol Genet* **18**, 27-42, doi:10.1093/hmg/ddn310 (2009).

46 Riley, B. E. & Orr, H. T. Polyglutamine neurodegenerative diseases and regulation of transcription: assembling the puzzle. *Genes Dev* **20**, 2183-2192, doi:10.1101/gad.1436506 (2006).

47 Laco, M. N., Oliveira, C. R., Paulson, H. L. & Rego, A. C. Compromised mitochondrial complex II in models of Machado-Joseph disease. *Biochim Biophys Acta* **1822**, 139-149, doi:10.1016/j.bbadis.2011.10.010 (2012).

48 Yu, Y. C., Kuo, C. L., Cheng, W. L., Liu, C. S. & Hsieh, M. Decreased antioxidant enzyme activity and increased mitochondrial DNA damage in cellular models of Machado-Joseph disease. *J Neurosci Res* **87**, 1884-1891, doi:10.1002/jnr.22011 (2009).

49 Stucki, D. M., Ruegsegger, C., Steiner, S., Radecke, J., Murphy, M. P., Zuber, B. & Saxena, S. Mitochondrial impairments contribute to Spinocerebellar ataxia type 1 progression and can be ameliorated by the mitochondria-targeted antioxidant MitoQ. *Free Radic Biol Med* **97**, 427-440, doi:10.1016/j.freeradbiomed.2016.07.005 (2016).

50 Wang, Y. C., Lee, C. M., Lee, L. C., Tung, L. C., Hsieh-Li, H. M., Lee-Chen, G. J. & Su, M. T. Mitochondrial dysfunction and oxidative stress contribute to the pathogenesis of spinocerebellar ataxia type 12 (SCA12). *J Biol Chem* **286**, 21742-21754, doi:10.1074/jbc.M110.160697 (2011).

51 Simon, D. K., Zheng, K., Velazquez, L., Santos, N., Almaguer, L., Figueroa, K. P. & Pulst, S. M. Mitochondrial complex I gene variant associated with early age at onset in spinocerebellar ataxia type 2. *Arch Neurol* **64**, 1042-1044, doi:10.1001/archneur.64.7.1042 (2007).

52 Adinolfi, S., Iannuzzi, C., Prischi, F., Pastore, C., Iametti, S., Martin, S. R., Bonomi, F. & Pastore, A. Bacterial frataxin CyaY is the gatekeeper of iron-sulfur cluster formation catalyzed by IscS. *Nat Struct Mol Biol* **16**, 390-396, doi:10.1038/nsmb.1579 (2009).

53 Campuzano, V., Montermini, L., Lutz, Y., Cova, L., Hindelang, C., Jiralerspong, S., Trottier, Y., Kish, S. J., Faucheux, B., Trouillas, P., Authier, F. J., Durr, A., Mandel, J. L., Vescovi, A., Pandolfo, M. & Koenig, M. Frataxin is reduced in Friedreich ataxia patients and is associated with mitochondrial membranes. *Hum Mol Genet* **6**, 1771-1780 (1997).

54 Chinnery, P. F. in *GeneReviews(R)* (eds R. A. Pagon, M. P. Adam, H. H. Ardinger, S. E. Wallace, A. Amemiya, L. J. H. Bean, T. D. Bird, C. T. Fong, H. C. Mefford, R. J. H. Smith, & K. Stephens) (1993).

55 Scheibye-Knudsen, M., Scheibye-Alsing, K., Canugovi, C., Croteau, D. L. & Bohr, V. A. A novel diagnostic tool reveals mitochondrial pathology in human diseases and aging. *Aging (Albany NY)* **5**, 192-208, doi:10.18632/aging.100546 (2013).

56 Cooles, P., Michaud, R. & Best, P. V. A dominantly inherited progressive disease in a black family characterised by cerebellar and retinal degeneration, external ophthalmoplegia and abnormal mitochondria. *J Neurol Sci* **87**, 275-288 (1988).

57 Forsgren, L., Libelius, R., Holmberg, M., von Dobeln, U., Wibom, R., Heijbel, J., Sandgren, O. & Holmgren, G. Muscle morphology and mitochondrial investigations of a family with autosomal dominant cerebellar ataxia and retinal degeneration mapped to chromosome 3p12-p21.1. *J Neurol Sci* **144**, 91-98 (1996).

58 Han, Y., Deng, B., Liu, M., Jiang, J., Wu, S. & Guan, Y. Clinical and genetic study of a Chinese family with spinocerebellar ataxia type 7. *Neurol India* **58**, 622-626, doi:10.4103/0028-3886.68674 (2010).

59 Modi, G. Morphological abnormalities of hepatic mitochondria in two patients with spinocerebellar ataxia type 7. *J Neurol Neurosurg Psychiatry* **68**, 393-394 (2000).

60 Cancel, G., Duyckaerts, C., Holmberg, M., Zander, C., Yvert, G., Lebre, A. S., Ruberg, M., Faucheux, B., Agid, Y., Hirsch, E. & Brice, A. Distribution of ataxin-7 in normal human brain and retina. *Brain* **123 Pt 12**, 2519-2530 (2000).

61 Garden, G. in *GeneReviews(R)* (eds R. A. Pagon, M. P. Adam, H. H. Ardinger, S. E. Wallace, A. Amemiya, L. J. H. Bean, T. D. Bird, C. T. Fong, H. C. Mefford, R. J. H. Smith, & K. Stephens) (1993).

62 Ryu, S. W., Jeong, H. J., Choi, M., Karbowski, M. & Choi, C. Optic atrophy 3 as a protein of the mitochondrial outer membrane induces mitochondrial fragmentation. *Cell Mol Life Sci* **67**, 2839-2850, doi:10.1007/s00018-010-0365-z (2010).

63 Chen, H., McCaffery, J. M. & Chan, D. C. Mitochondrial fusion protects against neurodegeneration in the cerebellum. *Cell* **130**, 548-562, doi:10.1016/j.cell.2007.06.026 (2007).

64 Dickey, A. S. & Strack, S. PKA/AKAP1 and PP2A/Bbeta2 regulate neuronal morphogenesis via Drp1 phosphorylation and mitochondrial bioenergetics. *J Neurosci* **31**, 15716-15726, doi:10.1523/JNEUROSCI.3159-11.2011 (2011).

65 Knott, A. B., Perkins, G., Schwarzenbacher, R. & Bossy-Wetzel, E. Mitochondrial fragmentation in neurodegeneration. *Nat Rev Neurosci* **9**, 505-518, doi:10.1038/nrn2417 (2008).

66 Westermann, B. Bioenergetic role of mitochondrial fusion and fission. *Biochim Biophys Acta* **1817**, 1833-1838, doi:10.1016/j.bbabio.2012.02.033 (2012).

67 Filosto, M., Scarpelli, M., Cotelli, M. S., Vielmi, V., Todeschini, A., Gregorelli, V., Tonin, P., Tomelleri, G. & Padovani, A. The role of mitochondria in neurodegenerative diseases. *J Neurol* **258**, 1763-1774, doi:10.1007/s00415-011-6104-z (2011).

68 Mink, J. W., Blumenschine, R. J. & Adams, D. B. Ratio of central nervous system to body metabolism in vertebrates: its constancy and functional basis. *Am J Physiol* **241**, R203-212 (1981).

69 Mishra, P. & Chan, D. C. Metabolic regulation of mitochondrial dynamics. *J Cell Biol* **212**, 379-387, doi:10.1083/jcb.201511036 (2016).

70 Civiletto, G., Varanita, T., Cerutti, R., Gorletta, T., Barbaro, S., Marchet, S., Lamperti, C., Viscomi, C., Scorrano, L. & Zeviani, M. Opa1 overexpression ameliorates the phenotype of two mitochondrial disease mouse models. *Cell Metab* **21**, 845-854, doi:10.1016/j.cmet.2015.04.016 (2015).

71 Manczak, M., Sesaki, H., Kageyama, Y. & Reddy, P. H. Dynamin-related protein 1 heterozygote knockout mice do not have synaptic and mitochondrial deficiencies. *Biochim Biophys Acta* **1822**, 862-874, doi:10.1016/j.bbadis.2012.02.017 (2012).

72 Sykora, P., Misiak, M., Wang, Y., Ghosh, S., Leandro, G. S., Liu, D., Tian, J., Baptiste, B. A., Cong, W. N., Brenerman, B. M., Fang, E., Becker, K. G., Hamilton, R. J., Chigurupati, S., Zhang, Y., Egan, J. M., Croteau, D. L., Wilson, D. M., 3rd, Mattson, M. P. & Bohr, V. A. DNA polymerase beta deficiency leads to neurodegeneration and exacerbates Alzheimer disease phenotypes. *Nucleic Acids Res* **43**, 943-959, doi:10.1093/nar/gku1356 (2015).

73 Brunetti, D., Torsvik, J., Dallabona, C., Teixeira, P., Sztromwasser, P., Fernandez-Vizarra, E., Cerutti, R., Reyes, A., Preziuso, C., D'Amati, G., Baruffini, E., Goffrini, P., Viscomi, C., Ferrero, I., Boman, H., Telstad, W., Johansson, S., Glaser, E., Knappskog, P. M., Zeviani, M. & Bindoff, L. A. Defective PITRM1 mitochondrial peptidase is associated with Abeta amyloidotic neurodegeneration. *EMBO Mol Med* **8**, 176-190, doi:10.15252/emmm.201505894 (2016).

74 Hamilton, J., Pellman, J. J., Brustovetsky, T., Harris, R. A. & Brustovetsky, N. Oxidative metabolism in YAC128 mouse model of Huntington's disease. *Hum Mol Genet* **24**, 4862-4878, doi:10.1093/hmg/ddv209 (2015).

75 Houtkooper, R. H., Argmann, C., Houten, S. M., Canto, C., Jeninga, E. H., Andreux, P. A., Thomas, C., Doenlen, R., Schoonjans, K. & Auwerx, J. The metabolic footprint of aging in mice. *Sci Rep* **1**, 134, doi:10.1038/srep00134 (2011).

76 Betarbet, R., Sherer, T. B., MacKenzie, G., Garcia-Osuna, M., Panov, A. V. & Greenamyre, J. T. Chronic systemic pesticide exposure reproduces features of Parkinson's disease. *Nat Neurosci* **3**, 1301-1306, doi:10.1038/81834 (2000).

77 Benchoua, A., Trioulier, Y., Zala, D., Gaillard, M. C., Lefort, N., Dufour, N., Saudou, F., Elalouf, J. M., Hirsch, E., Hantraye, P., Deglon, N. & Brouillet, E. Involvement of mitochondrial complex II defects in neuronal death produced by N-terminus fragment of mutated huntingtin. *Mol Biol Cell* **17**, 1652-1663, doi:10.1091/mbc.E05-07-0607 (2006).

78 Poole, A. C., Thomas, R. E., Andrews, L. A., McBride, H. M., Whitworth, A. J. & Pallanck, L. J. The PINK1/Parkin pathway regulates mitochondrial morphology. *Proc Natl Acad Sci U S A* **105**, 1638-1643, doi:10.1073/pnas.0709336105 (2008).

79 Yang, Y., Ouyang, Y., Yang, L., Beal, M. F., McQuibban, A., Vogel, H. & Lu, B. Pink1 regulates mitochondrial dynamics through interaction with the fission/fusion machinery. *Proc Natl Acad Sci U S A* **105**, 7070-7075, doi:10.1073/pnas.0711845105 (2008).

80 Carpenter, S. & Schumacher, G. A. Familial infantile cerebellar atrophy associated with retinal degeneration. *Arch Neurol* **14**, 82-94 (1966).

81 Lim, S., Honek, J., Xue, Y., Seki, T., Cao, Z., Andersson, P., Yang, X., Hosaka, K. & Cao, Y. Cold-induced activation of brown adipose tissue and adipose angiogenesis in mice. *Nat Protoc* **7**, 606-615, doi:10.1038/nprot.2012.013 (2012).

82 Lazarowski, E. R., Tarran, R., Grubb, B. R., van Heusden, C. A., Okada, S. & Boucher, R. C. Nucleotide release provides a mechanism for airway surface liquid homeostasis. *J Biol Chem* **279**, 36855-36864, doi:10.1074/jbc.M405367200 (2004).

83 Marchetti, P., Castedo, M., Susin, S. A., Zamzami, N., Hirsch, T., Macho, A., Haeffner, A., Hirsch, F., Geuskens, M. & Kroemer, G. Mitochondrial permeability transition is a central coordinating event of apoptosis. *J Exp Med* **184**, 1155-1160 (1996).

84 Lemasters, J. J., Nieminen, A. L., Qian, T., Trost, L. C., Elmore, S. P., Nishimura, Y., Crowe, R. A., Cascio, W. E., Bradham, C. A., Brenner, D. A. & Herman, B. The mitochondrial permeability transition in cell death: a common mechanism in necrosis, apoptosis and autophagy. *Biochim Biophys Acta* **1366**, 177-196 (1998).

85 Legros, F., Lombes, A., Frachon, P. & Rojo, M. Mitochondrial fusion in human cells is efficient, requires the inner membrane potential, and is mediated by mitofusins. *Mol Biol Cell* **13**, 4343-4354, doi:10.1091/mbc.E02-06-0330 (2002).

86 Ishihara, N., Jofuku, A., Eura, Y. & Mihara, K. Regulation of mitochondrial morphology by membrane potential, and DRP1-dependent division and FZO1-dependent fusion reaction in mammalian cells. *Biochem Biophys Res Commun* **301**, 891-898 (2003).

87 Wu, S., Zhou, F., Zhang, Z. & Xing, D. Mitochondrial oxidative stress causes mitochondrial fragmentation via differential modulation of mitochondrial fission-fusion proteins. *Febs J* **278**, 941-954, doi:10.1111/j.1742-4658.2011.08010.x (2011).

88 Galloway, C. A. & Yoon, Y. Perspectives on: SGP symposium on mitochondrial physiology and medicine: what comes first, misshape or dysfunction? The view from metabolic excess. *J Gen Physiol* **139**, 455-463, doi:10.1085/jgp.201210771 (2012).

89 Pendergrass, W., Wolf, N. & Poot, M. Efficacy of MitoTracker Green and CMXrosamine to measure changes in mitochondrial membrane potentials in living cells and tissues. *Cytometry A* **61**, 162-169, doi:10.1002/cyto.a.20033 (2004).

90 Wu, M., Neilson, A., Swift, A. L., Moran, R., Tamagnine, J., Parslow, D., Armistead, S., Lemire, K., Orrell, J., Teich, J., Chomicz, S. & Ferrick, D. A. Multiparameter metabolic analysis reveals a close link between attenuated mitochondrial bioenergetic function and enhanced glycolysis dependency in human tumor cells. *Am J Physiol Cell Physiol* **292**, C125-136, doi:10.1152/ajpcell.00247.2006 (2007).

91 Luo, Y., Fan, Y., Zhou, B., Xu, Z., Chen, Y. & Sun, X. Generation of induced pluripotent stem cells from skin fibroblasts of a patient with olivopontocerebellar atrophy. *Tohoku J Exp Med* **226**, 151-159 (2012).

92 Yanicostas, C., Barbieri, E., Hibi, M., Brice, A., Stevanin, G. & Soussi-Yanicostas, N. Requirement for zebrafish ataxin-7 in differentiation of photoreceptors and cerebellar neurons. *PLoS One* **7**, e50705, doi:10.1371/journal.pone.0050705 (2012).

93 Brookes, P. S., Yoon, Y., Robotham, J. L., Anders, M. W. & Sheu, S. S. Calcium, ATP, and ROS: a mitochondrial love-hate triangle. *Am J Physiol Cell Physiol* **287**, C817-833, doi:10.1152/ajpcell.00139.2004 (2004).

94 Ajayi, A., Yu, X., Lindberg, S., Langel, U. & Strom, A. L. Expanded ataxin-7 cause toxicity by inducing ROS production from NADPH oxidase complexes in a stable inducible Spinocerebellar ataxia type 7 (SCA7) model. *BMC Neurosci* **13**, 86, doi:10.1186/1471-2202-13-86 (2012).

95 Marchetto, M. C., Carromeu, C., Acab, A., Yu, D., Yeo, G. W., Mu, Y., Chen, G., Gage, F. H. & Muotri, A. R. A model for neural development and treatment of Rett syndrome using human induced pluripotent stem cells. *Cell* **143**, 527-539, doi:10.1016/j.cell.2010.10.016 (2010).

96 Yang, L., Mali, P., Kim-Kiselak, C. & Church, G. CRISPR-Cas-mediated targeted genome editing in human cells. *Methods Mol Biol* **1114**, 245-267, doi:10.1007/978-1-62703-761-7_16 (2014).

97 Gonzalez, J. R., Pique-Regi, R., and Caceres, A. *gada: Genome Alteration Detection Algorithm (GADA). R package version 0.9-7.* , <http://www.creal.cat/jrgonzalez/software.htm#ancla-MAD> (2012).

98 Kramer, D. & Minichiello, L. Cell culture of primary cerebellar granule cells. *Methods Mol Biol* **633**, 233-239, doi:10.1007/978-1-59745-019-5_17 (2010).

99 Taylor, J., Grote, S. K., Xia, J., Vandelft, M., Graczyk, J., Ellerby, L. M., La Spada, A. R. & Truant, R. Ataxin-7 can export from the nucleus via a

conserved exportin-dependent signal. *J Biol Chem* **281**, 2730-2739, doi:10.1074/jbc.M506751200 (2006).

100 Nakamura, Y., Tagawa, K., Oka, T., Sasabe, T., Ito, H., Shiwaku, H., La Spada, A. R. & Okazawa, H. Ataxin-7 associates with microtubules and stabilizes the cytoskeletal network. *Hum Mol Genet* **21**, 1099-1110, doi:10.1093/hmg/ddr539 (2012).

101 Lagouge, M., Argmann, C., Gerhart-Hines, Z., Meziane, H., Lerin, C., Daussin, F., Messadeq, N., Milne, J., Lambert, P., Elliott, P., Geny, B., Laakso, M., Puigserver, P. & Auwerx, J. Resveratrol improves mitochondrial function and protects against metabolic disease by activating SIRT1 and PGC-1alpha. *Cell* **127**, 1109-1122, doi:10.1016/j.cell.2006.11.013 (2006).

102 Nemoto, S., Fergusson, M. M. & Finkel, T. SIRT1 functionally interacts with the metabolic regulator and transcriptional coactivator PGC-1{alpha}. *J Biol Chem* **280**, 16456-16460, doi:10.1074/jbc.M501485200 (2005).

103 Price, N. L., Gomes, A. P., Ling, A. J., Duarte, F. V., Martin-Montalvo, A., North, B. J., Agarwal, B., Ye, L., Ramadori, G., Teodoro, J. S., Hubbard, B. P., Varela, A. T., Davis, J. G., Varamini, B., Hafner, A., Moaddel, R., Rolo, A. P., Coppari, R., Palmeira, C. M., de Cabo, R., Baur, J. A. & Sinclair, D. A. SIRT1 is required for AMPK activation and the beneficial effects of resveratrol on mitochondrial function. *Cell Metab* **15**, 675-690, doi:10.1016/j.cmet.2012.04.003 (2012).

104 Armour, S. M., Bennett, E. J., Braun, C. R., Zhang, X. Y., McMahon, S. B., Gygi, S. P., Harper, J. W. & Sinclair, D. A. A high-confidence interaction map identifies SIRT1 as a mediator of acetylation of USP22 and the SAGA coactivator complex. *Mol Cell Biol* **33**, 1487-1502, doi:10.1128/MCB.00971-12 (2013).

105 Sowa, M. E., Bennett, E. J., Gygi, S. P. & Harper, J. W. Defining the human deubiquitinating enzyme interaction landscape. *Cell* **138**, 389-403, doi:10.1016/j.cell.2009.04.042 (2009).

106 Gatchel, J. R., Watase, K., Thaller, C., Carson, J. P., Jafar-Nejad, P., Shaw, C., Zu, T., Orr, H. T. & Zoghbi, H. Y. The insulin-like growth

factor pathway is altered in spinocerebellar ataxia type 1 and type 7. *Proc Natl Acad Sci U S A* **105**, 1291-1296, doi:10.1073/pnas.0711257105 (2008).

107 Koenekoop, R. K., Wang, H., Majewski, J., Wang, X., Lopez, I., Ren, H., Chen, Y., Li, Y., Fishman, G. A., Genead, M., Schwartzentruber, J., Solanki, N., Traboulsi, E. I., Cheng, J., Logan, C. V., McKibbin, M., Hayward, B. E., Parry, D. A., Johnson, C. A., Nageeb, M., Finding of Rare Disease Genes Canada, C., Poulter, J. A., Mohamed, M. D., Jafri, H., Rashid, Y., Taylor, G. R., Keser, V., Mardon, G., Xu, H., Inglehearn, C. F., Fu, Q., Toomes, C. & Chen, R. Mutations in NMNAT1 cause Leber congenital amaurosis and identify a new disease pathway for retinal degeneration. *Nat Genet* **44**, 1035-1039, doi:10.1038/ng.2356 (2012).

108 Subramanian, A., Tamayo, P., Mootha, V. K., Mukherjee, S., Ebert, B. L., Gillette, M. A., Paulovich, A., Pomeroy, S. L., Golub, T. R., Lander, E. S. & Mesirov, J. P. Gene set enrichment analysis: a knowledge-based approach for interpreting genome-wide expression profiles. *Proc Natl Acad Sci U S A* **102**, 15545-15550, doi:10.1073/pnas.0506580102 (2005).

109 Rizzuto, R., De Stefani, D., Raffaello, A. & Mammucari, C. Mitochondria as sensors and regulators of calcium signalling. *Nat Rev Mol Cell Biol* **13**, 566-578, doi:10.1038/nrm3412 (2012).

110 Sack, M. N. & Finkel, T. Mitochondrial metabolism, sirtuins, and aging. *Cold Spring Harb Perspect Biol* **4**, doi:10.1101/cshperspect.a013102 (2012).

111 Ahn, B. H., Kim, H. S., Song, S., Lee, I. H., Liu, J., Vassilopoulos, A., Deng, C. X. & Finkel, T. A role for the mitochondrial deacetylase Sirt3 in regulating energy homeostasis. *Proc Natl Acad Sci U S A* **105**, 14447-14452, doi:10.1073/pnas.0803790105 (2008).

112 Stein, L. R. & Imai, S. The dynamic regulation of NAD metabolism in mitochondria. *Trends Endocrinol Metab* **23**, 420-428, doi:10.1016/j.tem.2012.06.005 (2012).

113 Ramsey, K. M., Yoshino, J., Brace, C. S., Abrassart, D., Kobayashi, Y., Marcheva, B., Hong, H. K., Chong, J. L., Buhr, E. D., Lee, C., Takahashi, J. S., Imai, S. & Bass, J. Circadian clock feedback cycle through NAMPT-mediated NAD+ biosynthesis. *Science* **324**, 651-654, doi:10.1126/science.1171641 (2009).

114 An, M. C., Zhang, N., Scott, G., Montoro, D., Wittkop, T., Mooney, S., Melov, S. & Ellerby, L. M. Genetic correction of Huntington's disease phenotypes in induced pluripotent stem cells. *Cell Stem Cell* **11**, 253-263, doi:10.1016/j.stem.2012.04.026 (2012).

115 Firestein, R., Blander, G., Michan, S., Oberdoerffer, P., Ogino, S., Campbell, J., Bhimavarapu, A., Luikenhuis, S., de Cabo, R., Fuchs, C., Hahn, W. C., Guarente, L. P. & Sinclair, D. A. The SIRT1 deacetylase suppresses intestinal tumorigenesis and colon cancer growth. *PLoS One* **3**, e2020, doi:10.1371/journal.pone.0002020 (2008).

116 Wear, M. P., Kryndushkin, D., O'Meally, R., Sonnenberg, J. L., Cole, R. N. & Shewmaker, F. P. Proteins with Intrinsically Disordered Domains Are Preferentially Recruited to Polyglutamine Aggregates. *PLoS One* **10**, e0136362, doi:10.1371/journal.pone.0136362 (2015).

117 Munch, C. & Harper, J. W. Mitochondrial unfolded protein response controls matrix pre-RNA processing and translation. *Nature* **534**, 710-713, doi:10.1038/nature18302 (2016).

118 Nickel, B. & Hoyt, C. S. Leber's congenital amaurosis. Is mental retardation a frequent associated defect? *Arch Ophthalmol* **100**, 1089-1092 (1982).

119 Fazzi, E., Signorini, S. G., Uggetti, C., Bianchi, P. E., Lanners, J. & Lanzi, G. Towards improved clinical characterization of Leber congenital amaurosis: neurological and systemic findings. *Am J Med Genet A* **132A**, 13-19, doi:10.1002/ajmg.a.30301 (2005).

120 Sasaki, Y., Vohra, B. P., Baloh, R. H. & Milbrandt, J. Transgenic mice expressing the Nmnat1 protein manifest robust delay in axonal degeneration in vivo. *J Neurosci* **29**, 6526-6534, doi:10.1523/JNEUROSCI.1429-09.2009 (2009).

121 Canto, C., Houtkooper, R. H., Pirinen, E., Youn, D. Y., Oosterveer, M. H., Cen, Y., Fernandez-Marcos, P. J., Yamamoto, H., Andreux, P. A., Cettour-Rose, P., Gademann, K., Rinsch, C., Schoonjans, K., Sauve, A. A. & Auwerx, J. The NAD(+) precursor nicotinamide riboside enhances oxidative metabolism and protects against high-fat diet-induced obesity. *Cell Metab* **15**, 838-847, doi:10.1016/j.cmet.2012.04.022 (2012).